Department of Physics and Astronomy
University of Heidelberg

Master Thesis in Physics
submitted by

Luca Bayha

born in Stuttgart

2015

A Strongly Interacting Fermi Gas in a Two-Dimensional Optical Lattice

This Master Thesis has been carried out by Luca Bayha at the
Physikalisches Institut Heidelberg
under the supervision of
Prof. Selim Jochim

Abstract

This thesis summarizes our current studies of ultracold fermions in a two-dimensional optical square lattice.
In the first experiments the band structure of the lattice was investigated using a band mapping technique. Here, by tuning the filling of the lattice indication for a transition from a metallic to a band insulating state for non-interacting fermions in the two-dimensional lattice was observed.
The main experiments were performed with a strongly interacting sample of bosonic Feshbach-molecules close to a Feshbach resonance. The strong interactions in our anisotropic 2D lattice lead to the occupation of excited states in the lattice.
We successfully loaded a superfluid of these molecules in the two-dimensional lattice. To characterize the state of the system, its momentum distribution was studied as a function of the depth of the lattice potential, which was calibrated using matter wave diffraction. Loss of coherence was observed above a critical depth of the lattice potential. This hints towards a transition to an insulating state. We also found first evidence that this transition is interaction mediated and the insulating state should be of the Mott-insulator type.

Zusammenfassung

In dieser Arbeit präsentieren wir unsere Untersuchung von ultrakalten Fermionen in einem zwei-dimensionalen optischen Gitter.
In unseren ersten Messungen wurde die Bandstruktur des Gitters mithilfe einer Bandabbildungstechnik untersucht. Indem wir den Füllungsfaktor des Gitters veränderten konnten Hinweise auf einen Übergang von einem metallischen Zustand zu einem Bandisolator beobachtet werden.
Unsere Hauptexperimente wurden mit stark wechselwirkenden bosonischen Feshbach-Molekülen nahe einer Feshbach-Resonanz durchgeführt. Die starken Wechselwirkungen in diesem anisotropen System führen zu der Besetzung angeregter Zustände im Gitter.
Es gelang uns, eine Supraflüssigkeit dieser Moleküle in das Gitter zu laden und die Impulsverteilung als Funktion der Gittertiefe zu untersuchen. Dazu wurde die Tiefe des Gitterpotentials mithilfe von Materiewellenbeugung kalibriert. Wenn die Tiefe des Gitters einen kritischen Wert überschritt, wurde der Verlust der Kohärenz der Supraflüssigkeit beobachtet, was einen Übergang zu einem Isolator kennzeichnet. Darüber hinaus wurden erste Hinweise darauf gefunden, dass der Verlust der Suprafluidität von starken Wechselwirkungen verursacht wurde und der Isolator ein sogenannter Mott-Isolator ist.

Contents

1 Introduction

Scales play a crucial role in physics. There are absolute scales in nature, like the speed of light. Comparing a system to these absolute scales determines the framework, that has to be used to describe the system. For example, systems where the resolution of the phase space — the Planck constant h — becomes important are described by quantum mechanics.
In addition to these absolute scales, each system introduces its own relative (energy) scales. Most systems in nature have more than one single relevant scale. The state of these systems is given by the competition of the different energy scales. The often cited paradigm of the hydrogen atoms is one of the simplest of such systems, where the electron ground state is given by the competition between interaction energy, which favours localization of the electron, and kinetic energy, which favours delocalization of the electron, to minimize the total energy.
This competition of different scales is not only important for single particles systems, but also in many body systems. There, the competition of (energy) scales determines the state and phase of the system. A prime example for such a system are interacting particles in a periodic potential. Here, the interaction energy competes with the kinetic energy. Again, like in the case of the hydrogen atom, kinetic energy is increased by the localization of the particles, which in turn minimizes interaction energy. This competition of energies determines the state of the system. If the interaction dominates the particles are localized on single lattice sites and cannot move, whereas if the kinetic energy dominates the particles are delocalized over several lattice sites and can move freely. Such an interaction induced localization was first observed in NiO [Boe37]. This localization makes the system electrically insulating even though it should be conducting judging from its band structure. This was pointed out first by Mott [Mot37, Mot49]. Thus this type of insulator is called a Mott-insulator.
The simplest model containing the essential physics of the competition between interaction and kinetic energy is the Hubbard model. It describes particles in a single band of a periodic potential, which can tunnel between the sites and interact via an on-site interaction. Already this simple system model predicts a transition from a superfluid to a Mott-insulator, when the relative strength of the interactions is increased.
An ideal system to realize such simple models are ultracold quantum gases, as they offer incredible control over most of the relevant parameters. It is not only possible to control the external potential seen by the atoms, but also to tune the interaction strength by using so-called Feshbach resonances [Ino98]. This allowed to directly observe the quantum phase transition from a bosonic superfluid to a Mott-insulator, by tuning the relative strength of kinetic and interaction energy [Gre01].
However, these experiments with bosons are not suited for simulating the behavior

of fermionic electrons. The first realizations of fermionic superfluids of ultracold atoms were achieved close to a Feshbach resonance. There superfluidity of Feshbach molecules was observed in a bulk gas [Joc03, Gre03, Zwi03] and shortly afterwards superfluidity in the whole BEC–BCS crossover could be shown [Zwi05]. In theses systems, the use of a Feshbach resonance allows to tune from bosonic molecules to fermionic atoms. Later these strongly interacting fermionic systems were studied in a three dimensional optical lattice. Also in this system, a transition to an insulating state was observed when increasing the relative strength of interactions [Chi06].
In this master thesis, we extend the study of ultracold Feshbach molecules in a lattice to two-dimensional systems. The advantage of a two-dimensional system is that one can directly access the full density and momentum distribution, which allows to determine the phase of the system [Gre01]. In our group, a measurement of the momentum distribution was recently used to observe condensation and superfluidity in the two-dimensional BEC–BCS crossover in a bulk gas [Rie15, Mur15]. With the additional lattice beams, we extend this system to study the interesting physics of strongly interacting fermions or composite bosonic molecules in a two-dimensional lattice and to characterize the transition from a superfluid to an insulating state.
Furthermore, an insulator of molecules is an excellent starting point for studying even more complicated and interesting systems. For example, by dissociating the molecules, also the Fermi-Hubbard model can be realized, which has a much richer phase diagram. This is because of the additional degrees of freedom of the spin, which introduce another energy scale for spin ordering. Even though these systems have already been realized with cold atoms [Jör08, Sch08], the lowest temperatures reached so far were too high to observe long range spin ordering [Gre13, Har15]. This is partly due to the fact that these experiments started with fermions, which limits the minimal achievable temperatures. Here, cooling of bosonic molecules and subsequent dissociation of the Feshbach molecules makes it possible to reach much colder temperatures which will potentially allow to study spin ordering in such a system.
This thesis summarizes our current progress on loading a superfluid of molecules into a two-dimensional lattice and observing a transition to an insulating state.

Outline

This master thesis is structured in the following way. First, a short summary of the theory necessary to understand our experiment is given. Here we focus on the theory of particles in periodic potentials. In the next chapter, our experimental apparatus is briefly described. The calibration procedure of the new lattice setup is described in chapter four. The fifth chapter summarizes our results on the observation of a band insulator of non-interacting fermions. In the sixth chapter, the influence of interactions in the lattice on reaching the quasi-2D regime is investigated. Our main result of successfully loading a superfluid of molecules into a two-dimensional lattice is presented in chapter seven. There, also the first indications for a quantum phase transition to an insulting state in deep lattices are presented. This thesis concludes with a short summary and outlook on the next steps and interesting physics which we will study with this setup in the future.

2 Theory of Cold Atoms

In this section a brief introduction to the theory necessary to understand the experiments performed during this master thesis will be given. First, the influence of quantum statistics will be discussed. Second, a quick introduction to low energy scattering is given. Then the principle of optical trapping and how to create periodic potentials with laser beams are explained. Finally the properties of particles in such periodic potentials are discussed.

2.1 Quantum Statistics

At high temperatures the occupation of a single particle state with energy ε is given by the Boltzmann distribution

$$n_{Boltzmann}(\varepsilon, \mu, T) = \exp(-\beta(\varepsilon - \mu)), \tag{2.1}$$

where μ is the chemical potential[1] and $\beta = 1/k_B T$ is the inverse temperature. For large temperatures the chemical potential is large and negative and at fixed total particle number N the chemical potential increases for lower temperatures. However, at low temperatures where our experiments are performed, this does not properly describe the system. If the densities are such that the phase space density is large, the behavior of particles is strongly influenced by its quantum statistics and cannot be described by a Boltzmann distribution. There exist two types of particles: bosons and fermions. They differ by the symmetry of their wave function under exchange of identical particles, which is symmetric for bosons and antisymmetric for fermions. This leads to a different occupation of states of the system and thereby strongly influences the behavior of a many body system. Thus at low temperatures, the occupation of states must be described by the full quantum statistics discussed below.

2.1.1 Bosons

Since for Bosons the wave function is symmetric under the exchange of particles, several particles can occupy the same state and the average number of particles in a state of energy ε is given by the Bose-Einstein distribution

$$n_b(\varepsilon, \mu, T) = \frac{1}{\exp\left(\beta(\varepsilon - \mu)\right) - 1}. \tag{2.2}$$

[1] The chemical potential acts as a Lagrange multiplier to obtain the correct average total particle number.

From this it is clear, that for bosons the chemical potential must be always smaller than the ground state energy, as otherwise the occupation probability for this state would be negative, which is unphysical.
The fact that more than one particle can occupy a single state leads, for low enough temperatures, to the formation of a Bose-Einstein condensate (BEC), i.e. a macroscopic occupation of a single state. Let us consider particles in a 3D harmonic trapping potential

$$V(x,y,z) = 1/2m(\omega_x^2 x^2 + \omega_y^2 y^2 + \omega_z^2 y^2), \tag{2.3}$$

where m is the mass of the particles and ω_i the trapping frequency of the potential along the i-th direction. For an isotropic harmonic potential the total particle number N is given by

$$N = \sum_{n_x,n_y,n_z=0}^{\infty} \frac{1}{\exp(\frac{\hbar\omega(n_x+n_y+n_z+3/2)-\mu}{k_B T}) - 1}. \tag{2.4}$$

If one sets the chemical potential to its maximum value $3/2\hbar\omega$ for a given temperature T, the particle number in excited states is given by [Ket09]

$$N_{max} = \zeta(3)\left(\frac{k_B T}{\hbar\omega}\right)^3, \tag{2.5}$$

where ζ is the Riemann zeta function. If the particle number is further increased while the temperature is kept constant, then all added particles occupy the ground state of the system and form a BEC.

2.1.2 Fermions

Due to the antisymmetry of the wave function under exchange of identical particles, the Pauli principle holds and each state can at most be occupied by one fermion. The occupation of a state is given by the Fermi distribution

$$n_f(\varepsilon,\mu,T) = \frac{1}{\exp\left(\beta(\varepsilon-\mu)\right)+1}. \tag{2.6}$$

At zero temperature the Fermi distribution becomes a step function where all levels up to the Fermi energy $E_F = \mu(T=0)$ are filled with one fermion, whereas higher levels are unoccupied. For example for a 2D harmonic potential and N particles the Fermi energy is

$$E_F = \hbar\left(2N\omega_x\omega_y\right)^{1/2}. \tag{2.7}$$

This implies that, if only occupation up to a certain energy level is possible, the number of fermions in a system, even at zero temperature, is limited.

2.2 Ultracold Interactions

Adding interactions between particles can lead to a dramatic change of the properties of the system. For example it can result in the emergence of new behavior and phase transitions not possible in non-interacting systems, like the superfluid to Mott-insulator transition in a lattice.

2.2.1 Two Particle Scattering

The simplest case of interactions is the elastic scattering of two particles, which in relative coordinates is described by the following time-independent Schrödinger equation

$$\frac{\hbar^2}{2m}\nabla^2\Psi(\mathbf{r}) + V(\mathbf{r})\Psi(\mathbf{r}) = E\ \Psi(\mathbf{r}), \tag{2.8}$$

where m is the reduced mass of the particles and $E = \frac{\hbar^2 k^2}{2m}$ is a positive energy. Describing such a process is in general very complex. However for the low temperatures in our experiments, we have only to consider low energy scattering which is much simpler than solving the full problem.
In order to be in the quantum degenerate regime, the de-Broigle wavelength λ_{dB} has to be on the order of the interparticle spacing[2] of a few 100 nm. This is much larger than the short range Van-der-Waals potential, which falls off with distance as $V(r) \propto r^{-6}$ and has a finite effective range r_{eff} of the order of 60 Bohr radii. Hence, the low energy (large wavelength) scattering at this temperatures cannot resolve the details of the interaction potential and scattering is independent of the microscopic structure of the potential.
For these short range potentials, the wave function for large distances from the scatterer is simply given by the superposition of an incoming plane wave and a scattered spherical wave

$$\Psi(r) \propto e^{ikz} + f(k,\theta)\frac{e^{ikr}}{r}. \tag{2.9}$$

For our case of a spherical symmetric interaction potential, the scattering amplitude $f(k,\theta)$ only depends on the angle between ingoing and scattered wave. The outgoing particle flux is proportional to the square of the scattering amplitude and the cross-section is given by $\sigma(\theta) = |f(k,\theta)|^2$.
For a spherical symmetric potential, one can use the so-called partial wave expansion and rewrite the wave function as [Dal99]

$$\Psi(r) = \sum_{l=0}^{\infty} P_l(\cos(\theta))\frac{u_{k,l}(r)}{r}, \tag{2.10}$$

where $P_l(\cos(\theta))$ are the Legendre polynomials containing the angle dependence and the functions $u_{k,l}(r)$ are the solutions of the effective radial Schrödinger equation. Solving this Schrödinger equation for the scattering amplitude and cross-section gives [Sak94]

$$f(k,\theta) = \frac{1}{k}\sum_{l=0}^{\infty}(2l+1)e^{i\delta_l}\sin(\delta_l)\ P_l(\cos(\theta)), \tag{2.11}$$

$$\sigma_l = \sum_{l=0}^{\infty}\frac{4\pi}{k^2}(2l+1)\sin^2(\delta_l). \tag{2.12}$$

Since scattering in the spherical symmetric potential does not lead to mixing of the partial waves, each component just experiences a real phase shift δ_l at large

[2] For higher densities 3 body collisions would lead to large losses.

distances. These phase shifts scale as $\delta_l \propto k^{2l+1}$ for small k. Hence in the low (zero) energy limit only the $l = 0$ partial wave obtains a non-trivial phase shift and one is left with so-called s-wave scattering. Its contribution the so-called s-wave scattering amplitude is given by

$$f_0 = \frac{1}{k \cot \delta_0 - ik}. \tag{2.13}$$

Neglecting the effective range of the potential this can be approximated as [Ket08]

$$f_0(k) = \frac{a}{1 + iak}, \tag{2.14}$$

where the scattering length a was introduced, which is the single parameter effectively describing the low energy s-wave scattering. Hence the cross-section is simply given as

$$\sigma(k) = 4\pi \frac{a^2}{1 + k^2 a^2}. \tag{2.15}$$

For the limiting case of $ka \ll 1$ the cross-section can be approximated by $\sigma = 4\pi, a^2$ whereas for large scattering length the cross-section is unitary limited to $\sigma = 4\pi k^2$. As the physics of the scattering are all encoded in the single parameter a and the exact shape of the potential $V(\mathbf{r})$ is not important one can replace it by a contact interaction resulting in the same phase shift of the scattered particle. This is described by a (regularized) delta potential [Ket08]

$$V(\mathbf{r}) = \frac{4\pi\hbar^2}{m} a \; \delta(\mathbf{r}). \tag{2.16}$$

This means that in low energy scattering the shape of the potential is unimportant, as it cannot be resolved by the large wavelength particles. The only effect of the scattering is to shift the phase of the s-wave component. This phase shift is described by a single quantity — the scattering length a. The mapping on this pseudo potential makes the problem simple to describe theoretically, such that it can be solved, even if the real potential is very complicated.
On a mean field level the interaction is attractive for negative scattering lengths and repulse for positive scattering lengths, even though the underlying microscopic van-der-Waals interaction is always attractive for ground state atoms.

2.2.2 Scattering of Identical Particles

The discussion so far only considered scattering of distinguishable particles, where there is no symmetry of the wave function under exchange of particles. If two identical particles scatter their quantum statics become important, since the two scattering processes depicted in Figure (2.1) are indistinguishable and their amplitudes interfere.
Writing the relative wave function in the form (2.10) the odd l components are antisymmetric and even l components are symmetric. This means for identical fermions

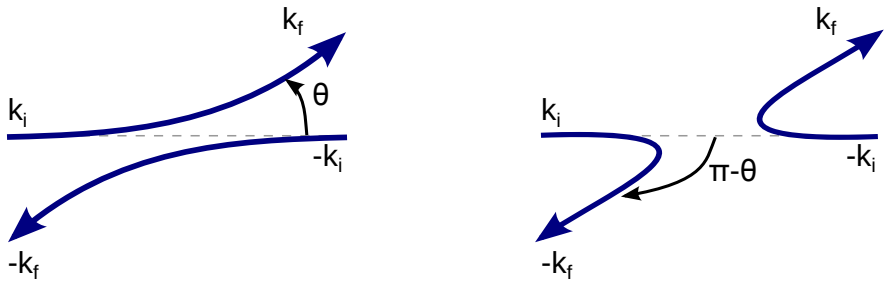

Figure 2.1: For identical particles the two scattering processes cannot be distinguished and the wave function has to be properly (anti-)symmetrized. Adapted from [Dal99].

no s-wave scattering is possible, since the even l components of the wave function are zero. Thus for low temperatures there is no scattering in a gas of identical fermions. This means that a two component Fermi gas is needed in order to have interactions and interesting physics at low temperatures. The interactions between the two components are crucial to even achieve these low temperatures as evaporative cooling relies on thermalisation of the cloud via scattering. For bosons the constructive interference of the two paths leads to s-wave cross-section which is twice as big, i.e.

$$\sigma(k) = 8\pi \frac{a^2}{1 + k^2 a^2}. \tag{2.17}$$

2.2.3 Bound States

So far we have only investigated the scattering of two interacting particles, i.e the behaviour at (small) positive energies. A closer look at the energy spectrum for small negative energies shows, that for a positive scattering length $a > 0$ there exists a two particle bound state. With a binding energy [Sak94]

$$E = \frac{\hbar^2}{2ma^2}. \tag{2.18}$$

This description is only valid, if the scattering length is much larger than the effective range r_{eff} of the potential. From the energy of the weakly bound state one can deduce, that its size must be of the order of the scattering length and thus much larger than the size of the interaction potential. Hence, these bound states are also called halo molecules.
At low temperatures and positive scattering length molecules are formed out of two distinguishable fermions. These are bosonic[3] and can form a molecular Bose–Einstein condensate (mBEC). For dimers of fermionic atoms one can calculate the dimer-dimer and dimer-atom scattering length [Pet04] which are

$$a_{dd} = 0.6a \quad \text{and} \quad a_{ad} = 1.2a, \tag{2.19}$$

[3]The fermionic nature of the constituents is unimportant as long as the binding energy is much larger than all other energy scales of the system.

respectively. Here a denotes the fermion–fermion scattering length. However, this bound state is the highest excited rovibrational state of the molecule and not the ground state. It can thus decay via inelastic collisions with another particle, which results in loss from the trap. However, the relaxation rates α_{rel} for inelastic collision to deeper lying states scale as $\alpha_{rel} \propto a^{-3.33}$ for atom-dimer and $\alpha_{rel} \propto a^{-2.55}$ for dimer-dimer scattering. Thus for large scattering lengths elastic collisions dominate over suppressed inelastic collisions and one can reach a stable many body state, without to much loss of particles.

2.2.4 Feshbach Resonances

A key feature of cold atom experiments is the possibility to tune the interactions to arbitrary values by means of so-called Feshbach resonances. Here a short summary of some basic properties, as described in [Chi10, Ket08], is given.
In order to understand a Feshbach resonance the internal structure of the scattering particles must be taken into account. A Feshbach resonance requires at least two coupled internal states. This coupling of a second internal state to the ingoing scattering state strongly affects the scattering process, if the energy level of the second state is close to the scattering state. At the end of the process the scattered particles must be in the same state since we are discussing elastic scattering. Hence the other channel must be a so-called closed channel, where the energy for large relative distances is bigger than the energy of the two particles and it cannot be populated permanently (see figure 2.2).
For concreteness take the ingoing (open) channel as a triplet and the closed channel as a singlet state. If there would be no coupling between the states the particle would just scatter in the open channel potential and obtain a phase shift, which is described by the background scattering length a_{bg}. If there is a hyperfine interaction at small distances the singlet and triplet states are not the eigenstates of the Hamiltonian if the particles are close to each other. This introduces a coupling between the two states. In case there is a bound state in the closed channel close to the energy of the scattering particles this leads to an additional phase shift of the outgoing wave and hence alters the scattering length. This is due to the fact that even a weak coupling strongly influences (nearly) degenerate states. As the closed and open channel have different magnetic moments one can tune the relative position of the bound state to the continuum scattering states of the open channel by changing the magnetic offset field. This changes the effective coupling and thus the scattering length. The resulting scattering length as function of the magnetic field B can then be approximated by

$$a(B) = a_{bg}\left(1 - \frac{\Delta}{B - B_0}\right), \tag{2.20}$$

where Δ and B_0 are the resonance width and position.
Hence using a Feshbach resonance allows to tune the interactions to negative scattering lengths where one obtains an attractive Fermi gas and to positive scattering lengths where one obtains a repulsively interacting Bose gas of molecules. The coupling of the two channels leads to an avoided crossing between the repulsive atomic and the attractive molecular branch, as sketched in figure (2.2 c). The Feshbach

resonance offers now two possibilities to create molecules. Either one can start in the repulsive branch (at positive scattering length) where the molecular bound state lies lower in energy. Then while evaporatively cooling down the sample molecules are formed by three body collisions of the atoms, where the third atom is needed to satisfy energy and momentum conservation. If the collision rate is sufficiently high, chemical equilibrium between forming and breaking up molecules is reached and as soon as the temperature becomes smaller than the binding energy the sample mainly consists of molecules. Even though these molecules are created by inelastic 3-body collisions they are themselves stable towards loss caused by inelastic collisions into lower lying molecular states if the scattering length is large enough as discussed in the previous section.
The other way to form molecules is by starting in the atomic ground state of the system in a magnetic field region, where the energy of the molecular state is higher than of the atomic state (right side of the crossing in figure 2.2 c). Then by slowly ramping the magnetic field across the resonance such that the system can adiabatically follow the ground state one can create a molecular sample.

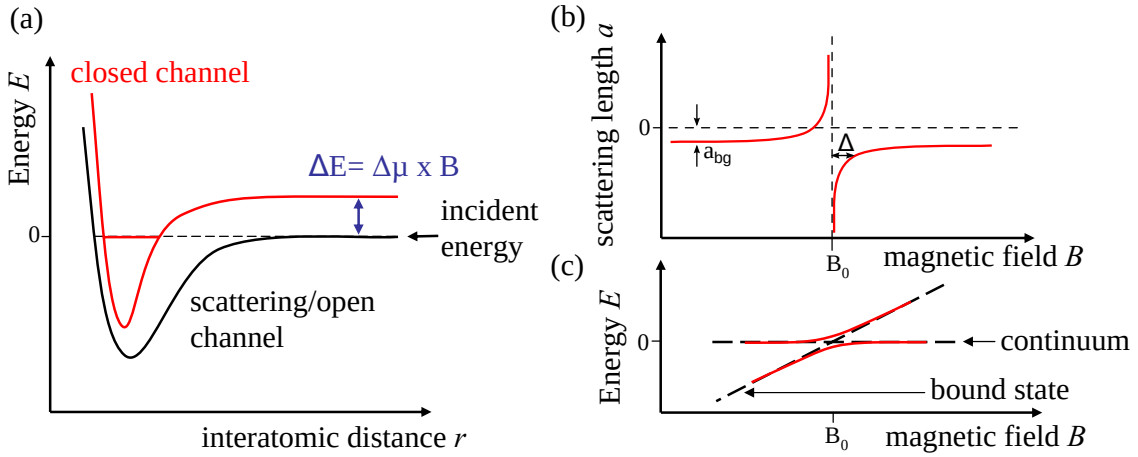

Figure 2.2: (a) Sketch of the potential of the open (black) an closed (red) channel as a function of inter atomic distance. By changing the magnetic field, the energy of the bound state of the closed channel can be tuned relative to the open channel. The Feshbach resonance occurs, if the energy of the bound state is equal to the energy of the ingoing particle. (b) Resulting scattering length as a function of the magnetic field. (c) Energy diagram of the bound and continuum state as function of the magnetic field. The coupling between the states results in an avoided crossing. Taken from [Wen08].

2.2.5 Hyperfine States and Feshbach Resonances of ^{6}Li

After these theoretical introductions to scattering, we have a closer look at lithium and shortly summarize its properties important for our experiment. More details can be found in [Geh03]. Lithium is an alkali atom and hence has only one electron in its outermost shell, which makes its level structure relatively simple. In the

electronic ground state the outermost electron is in the $2^2S_{1/2}$ state and has zero angular momentum. At low magnetic fields the nuclear spin I=1 of ^{6}Li couples to the electron spin S=1/2 resulting in a total spin F=1/2 doublet and F=3/2 quadruplet separated by 228.2 MHz (at zero magnetic field). In the high magnetic field region — where the experiments are performed — nuclear and electron spin are decoupled (Paschen–Back regime). This gives rise to the hyperfine spectrum of the electronic ground state shown in figure (2.3).

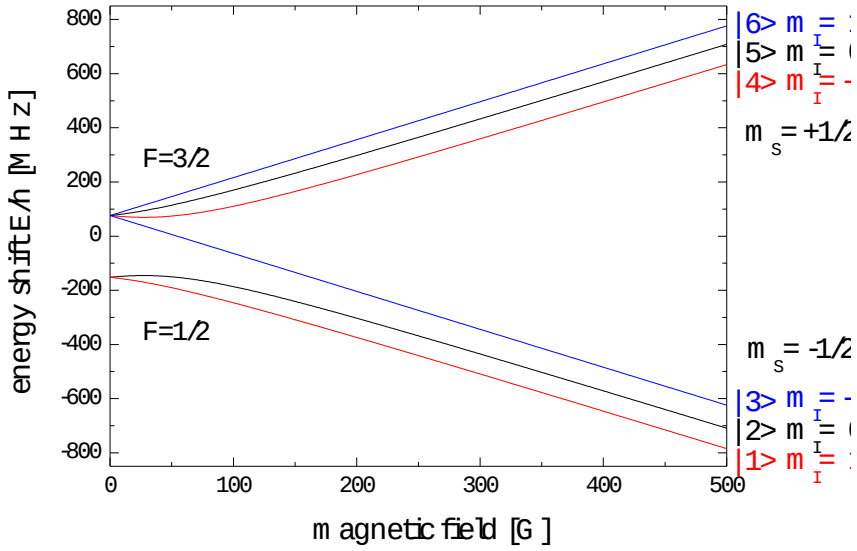

Figure 2.3: Hyperfine splitting of the ^{6}Lithium $2^2S_{1/2}$ electronic ground state as function of the magnetic offset field. Experiments are performed in the Paschen–Back regime (above 200 G) where the energy of the states scales linearly with magnetic field. Taken from [Nei13].

For our experiments we mainly use the two lowest lying hyperfine states — denoted by $|1\rangle$ and $|2\rangle$. These are collisional stable and cannot undergo spin changing collisions. Using these states we can use a broad Feshbach resonance at 832 G which has a width of 262 G and a large background scattering length of -2000 Bohr radii at high magnetic fields (1400 G) to tune the interactions [Zür12]. The resulting scattering length as function of the magnetic field is depicted in figure (2.4). Evaporative cooling of our sample is done close to the resonance (790 G), where the scattering rate is high allowing for effective evaporation. During evaporation molecules are created and a mBEC is obtained after cooling. Due to the large scattering length close to the resonance these molecules are stable towards 3-body loss for fields larger than roughly 730 G. This gives access to a wide range of interactions to investigate interesting physics, without being limited by 3-body loss.

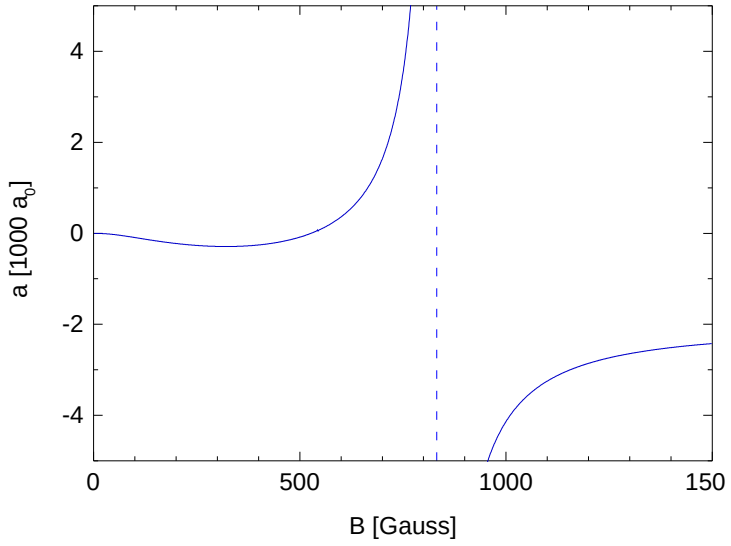

Figure 2.4: Scattering length between the states $|1\rangle$ and $|2\rangle$ as function of the magnetic field. The dashed line indicates the Feshbach-resonance at 832 G. Adapted from [Rie14].

2.3 Optical Dipole Traps

Experiments with cold atoms, require to trap them at a fixed spatial position. There are two main requirements for these trapping potentials. First, it should be the same for the different hyperfine states, since at least two different components are needed for interactions. Second, as we want to perform experiments at ultracold temperatures, the heating rates should be low. These requirements are fulfilled by trapping the atoms with far off-resonant light in a so-called optical dipole trap. The trapping of the atoms in the laser beam is due to the quadratic AC Stark shift. Here a short summary of the properties of these traps is given. More details can for example be found in [Gri00].
A neutral atom with (linear) polarizability α placed in an external electric field $\mathbf{E}$ oscillating with frequency ω gets polarized and has an induced dipole moment $\mathbf{p}$, which can be written as

$$\mathbf{E} = \hat{\mathbf{e}} E e^{i\omega t} + c.c. \tag{2.21}$$
$$\mathbf{p} = \hat{\mathbf{e}} \alpha(\omega) E e^{i\omega t} + c.c. \ . \tag{2.22}$$

The corresponding average dipole energy of the atom is given as

$$U_{dip} = -\frac{1}{2} < \mathbf{p} \cdot \mathbf{E} >, \tag{2.23}$$

where the factor $\frac{1}{2}$ is due to the fact that the dipole moment is induced and $< \cdots >$ denotes the time average over the oscillating fields. Rewriting the electric field in

terms of the intensity of the laser beam $I = 2\epsilon_0 c E^2$ yields

$$U_{dip} = -\frac{1}{2\epsilon_0 c}\Re(\alpha) I, \tag{2.24}$$

where $\Re(\alpha)$ it the real part of the polarizability, which is related to the energy shift the atom feels in an electric field. Photon scattering on the other hand is related to the imaginary part of the polarizability. Thus a large real part of the polarizability is wanted for creating a deep trapping potential, while the imaginary part should be small, as photon scattering causes unwanted heating of the gas. The resulting potential depths U_{dip} and scattering rates Γ_{sc} for the (position dependent) intensities are [Gri00]

$$U_{dip}(r) = \frac{3\pi c^2}{2\omega_0^3}\frac{\Gamma}{\Delta} I(r), \tag{2.25}$$

$$\Gamma_{sc}(r) = \frac{3\pi c^2}{2\hbar\omega_0^3}\left(\frac{\Gamma}{\Delta}\right)^2 I(r), \tag{2.26}$$

respectively. Here Γ is the decay rate of the excited level, ω_0 is the frequency of the atomic transition and $\Delta = \omega - \omega_0$ is the detuning of the light field from the atomic transition frequency. For red detuned laser beams ($\Delta < 0$), as used in our experiment, the potential is attractive, i.e. the energy of the atom is smaller for larger intensities and atoms are attracted towards the intensity maxima. Furthermore, as the potential depth scales as $\frac{\Gamma}{\Delta}$ and the photon scattering (heating) rate scales as $\left(\frac{\Gamma}{\Delta}\right)^2$ the detuning should be large to achieve a conservative potential and reduce heating. Thus we use 1064 nm light for the creation of the dipole traps, which is roughly 400 nm detuned from the atomic transition at 671 nm. Producing sufficient deep traps at this large detuning requires high intensities and thus high power lasers. In our experiment, the traps are produced by intersecting focused Gaussian laser beams. For the case of orthogonal polarization of the two beams no interference occurs and one simply obtains a potential which is the sum of the single beam potentials. If the atoms are trapped in a region close to the minima of the potential one can approximate the confining potential by a harmonic trap.
If the two beams have the same polarization and are coherent, the two electric fields interfere and create a periodic intensity and thus potential modulation in addition to the overall confinement. The spacing d of the potential maxima is

$$d = \frac{\lambda}{2\cos\phi}, \tag{2.27}$$

where λ is the wavelength of the light and the two beams cross under an angle of 2ϕ. This creates a periodic potential (lattice) along one direction. By adding a second (third) retro-reflected beam pair orthogonal to the first an array of coupled 1D tubes (zero-dimensional traps) can be created (see figure 2.5).
In our setup we create a 2D square lattice by using a set of two orthogonal Gaussian beams each retro-reflected under a small angle which create the following 2D potential

$$V(x,y) = -V_x e^{-2\frac{x^2}{w_x^2}} \sin^2\left(\frac{2\pi x\cos\phi}{\lambda}\right) - V_y e^{-2\frac{y^2}{w_y^2}} \sin^2\left(\frac{2\pi y\cos\phi}{\lambda}\right). \tag{2.28}$$

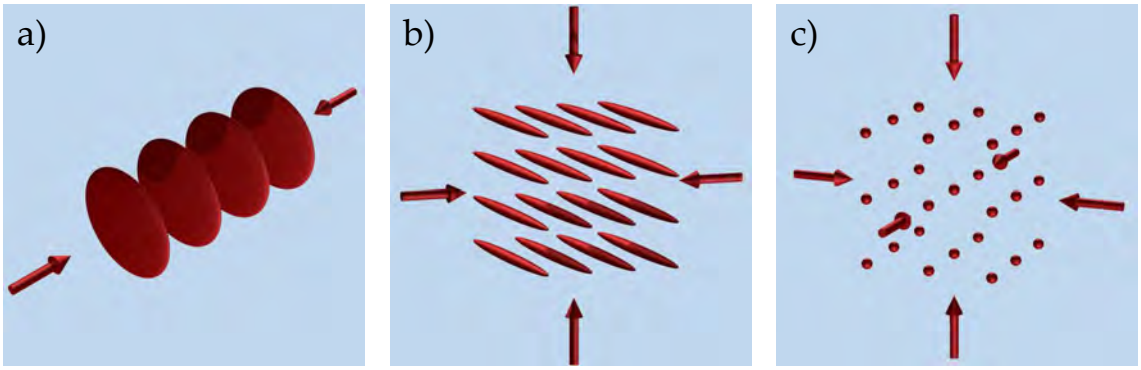

Figure 2.5: Trapping potentials created by retro-reflected interfering beams. (a) A single retro-reflected beam creates a array of 2D pancake shaped traps. (b) Adding a second lattice beam creates 1D tubes. (c) With three retro-reflected beams a 3D lattice of (zero-dimensional) traps is produced. Taken from [Boh12].

Here, the waist w is the $1/e^2$ size[4] of the laser beam orthogonal to its respective direction. Due to the position dependent intensity the depth V of the lattice potential is inhomogeneous and depends on position. Furthermore, a change in the central lattice depth changes the overall confinement, which can cause redistribution of atoms and thus heating. The lattice depth is often given in its 'natural' energy scale the recoil energy $E_r = \frac{\hbar^2 k^2}{2m}$, which is the energy gained by a particle when scattering a lattice photon. For the experimental setup with 1064 nm beams intersecting under an angle of $2\phi = 14°$ the lattice spacing is 536 nm. The recoil energy for this lattice spacing and lithium atoms and molecules are

$$E_{r,atom} = \text{h } 29.0\text{kHz} \qquad \text{and} \qquad E_{r,molecules} = \text{h } 14.5 \text{ kHz}. \tag{2.29}$$

2.4 Particles in Periodic Potentials

After discussing, how to create periodic potentials for ultracold atoms, the properties of particles in such potentials are summarized. For simplicity we will first consider a homogeneous system, without an additional trapping potential.

2.4.1 Non-Interacting Particles and Band Structure

For non-interacting particles, the periodic lattice potential simply modifies their motion. This results in a different dispersion relation compared to the homogeneous case [Ash76]. A particle in a 1D potential $V(x)$ with a periodicity d, i.e. $V(x+d) = V(x)$, is described by the following stationary Schrödinger equation

$$\left(\frac{\hat{p}^2}{2m} + V(x)\right)\psi = E\psi. \tag{2.30}$$

[4]This waist also depends on the position along the beam.

The periodic potential breaks the continuous translation symmetry of the free particle and replaces it by a discrete translational symmetry, where the Hamiltonian is invariant when shifted by the period of the potential. Hence the discrete translation operator and the Hamiltonian commute and there exists a common set of eigenstates of the Hamiltonian and the discrete translation operator. According to the Bloch theorem these eigenstates can be written as [Ash76]

$$\psi_{n,q}(x) = e^{iqx} u_{n,q}(x), \tag{2.31}$$

where the function $u_{n,q}(x) = u_{n,q}(x+d)$ is d-periodic and n is the band index for the n-th solution of the Schrödinger equation. Due to the periodicity, $u_{n,q}(x)$ can be written as a discrete Fourier series [Ash76]

$$u_{n,q}(x) = \sum_{l=-\infty}^{\infty} c_{n,q}^{(l)} e^{ilk_L x}, \tag{2.32}$$

$$\psi_{n,q}(x) = \sum_{l=-\infty}^{\infty} c_{n,q}^{(l)} e^{i(lk_L+q)x}, \tag{2.33}$$

where $k_L = 2\pi/d$ is the reciprocal lattice vector and the quasi-momentum q is restricted to a range $q \in \left(\frac{-k_L}{2}, \frac{k_L}{2}\right]$. Hence, the solutions for the wave function $\psi_{n,q}(x)$ in the lattice are just the sum of plane waves, whose momentum differs by a multiple of the lattice vector k_L. This is a simple consequence of the periodicity of $u_{n,q}(x)$.
For the 1D version of the periodic potential used in the experiment

$$V(x) = V \sin^2\left(\frac{\pi x}{d}\right) = \frac{1}{2} V\Big(1 - \cos\left(k_L x\right)\Big), \tag{2.34}$$

it is easy to numerically solve the Schrödinger equation in Fourier space [Lew12] by taking only a finite number of Fourier coefficients. This yields the band structure depicted in figure (2.6). As expected the lattice has the biggest effect on the dispersion for low energy particles, i.e. on the lowest band. Also the effect on the dispersion relation is strongest close to edges of the band, where some of the coupled plane waves, forming the Bloch states have the same energy. This results in an avoided crossing and the opening of the band gap [Ash76]. For energies inside the band gap the density of states is zero. Thus, if a band is completely filled with fermions and the higher lying bands are empty, the system becomes insulating as a finite energy (the band gap) is needed to create excitations. As the appearance of the insulator is caused by the band gap it is called a band insulator.
For deep potentials the band structure becomes flat as particle movement is strongly hindered by the lattice and the system becomes an array of weakly coupled single potential wells. Then one can treat the lattice wells as independent confining potentials[5]. To estimate the energy of the flat bands, the bottom of the wells can be approximated by a harmonic oscillator with frequency $\hbar\omega = 2\sqrt{VE_r}$. Note however, that this will always overestimate the energy, as the real potential is not harmonic and residual tunneling will always lower the energy.

[5] This approximation is not valid for higher bands where the tunneling rate can still be large.

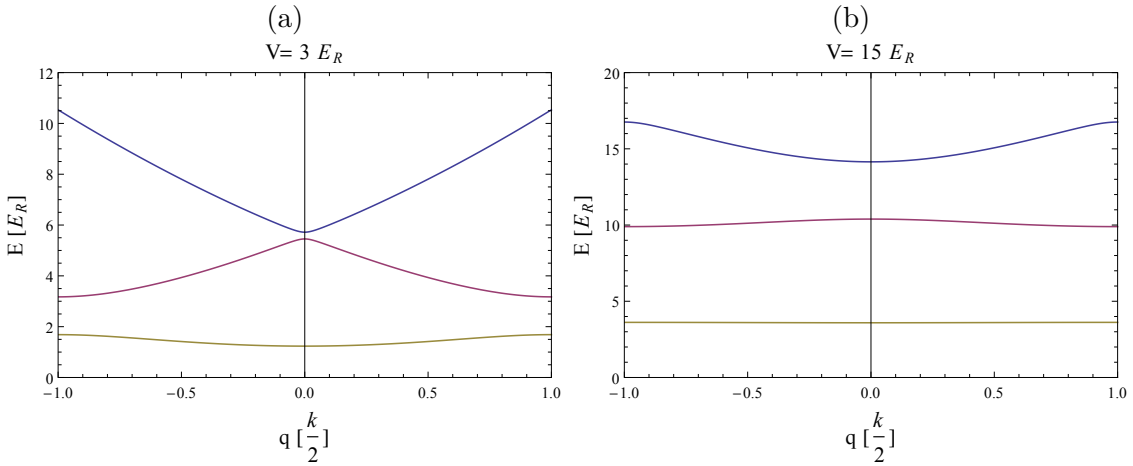

Figure 2.6: Band structure of a 1D lattice. Depicted are the lowest 3 bands for a (a) $V = 3\ E_r$ and (b) $V = 15\ E_r$ deep lattice. For deeper lattices the band gap becomes larger and the band flatter. The band structure was numerically calculated using Mathematica.

The above discussion is easily extended to a 2D square lattice since the problem is separable in the two dimensions and the dispersion relation is simply the sum of the dispersion relations of the 1D lattices along the two directions. However, in this 2D dimensional case higher bands touch each other as there are values for q_x, q_y where the solutions for $n_x = 1$ and $n_y = 2$ are degenerate to the solution for $n_x = 2$ and $n_y = 1$ (see figure 2.7). Thus there is no gap between the second and third band, while the gap between the lowest and the second band still remains [Gün07].

2.4.2 The Tight Binding Approximation

So far we have looked at infinitely extended Bloch waves, but as already discussed above for a deep lattice the picture of localized particles in coupled wells is more appropriate. A particle localized at lattice site x_i is described by a Wannier state [Wan37]

$$w_n(x - x_i) = \frac{1}{\sqrt{N}} \sum_q e^{-\imath q x_i} \psi_{n,q}(x), \tag{2.35}$$

where N is the number of lattice sites and n is the band index. For deep lattices the second band is separated form the first band by roughly the on-site trapping frequency $\hbar\omega_{on-site} = 2\sqrt{V E_r}$ which — for our system of a 2D lattice with additional harmonic confinement in the third direction — is on the order of tens of kHz for deep lattices and much larger than all other energy scales. Thus the particles in our experiment always stay in the lowest band of the 2D lattice. However, there are still excitations to higher states in the direction perpendicular to the lattice possible, where the trapping frequency is only on the order of ten kHz. The 3D wave function for a particle localized at a lattice site is given as the product of the wave function

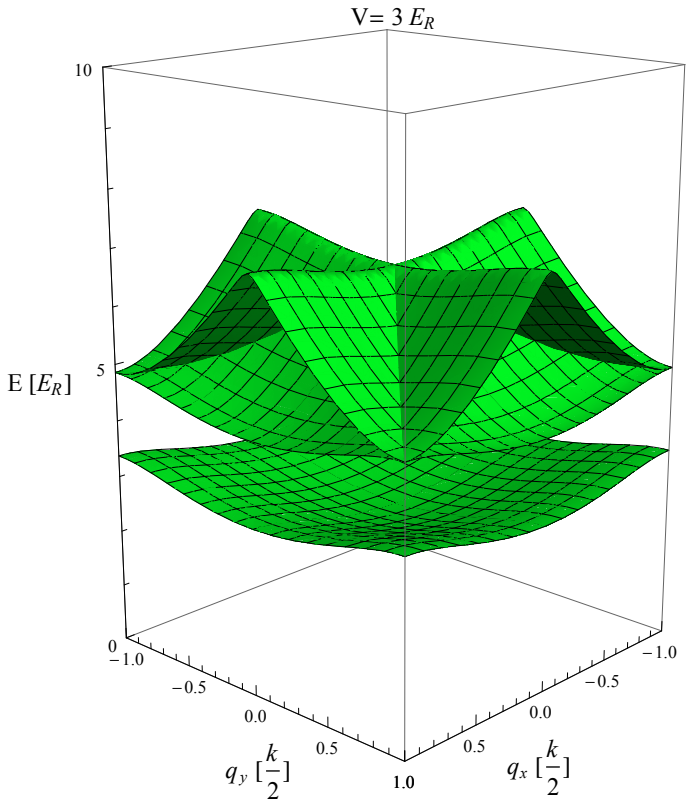

Figure 2.7: Three lowest band of a 2D square lattice, for a lattice depth of $V = 3\ E_r$. The second and third bands touch but the gap between the lowest band and higher bands still remains.

in the 3 directions

$$\Psi(x, y, z) = w_{x_i}(x) w_{y_j}(y) \phi(z), \tag{2.36}$$

where $\phi(z)$ is the wave function in the harmonic confining potential in z-direction, which for a non-interacting particle in the ground state would just be a Gaussian wave packet. Additionally, we dropped the band index for the Wannier state, as only the lowest band of the 2D lattice is considered. From the wave function one can construct a bosonic field operator

$$\psi^{(\dagger)}(\mathbf{r}) = \Psi(\mathbf{r}) a_i^{(\dagger)}, \tag{2.37}$$

where $a_i^{(\dagger)}$ is the operator annihilating (creating) a Boson at lattice site i. The $a_i^{(\dagger)}$ are bosonic operators fulfilling the usual commutation relations

$$[{a_i}^\dagger, a_j] = \delta_{i,j}, \qquad [{a_i}^\dagger, a_j^\dagger] = [a_i, a_j] = 0, \tag{2.38}$$

where $[a, b] = ab - ba$ is the commutator. The processes, which a particle located at a site can undergo are intuitively understood. First, it can change its position and tunnel to a different site. Second, when a contact interaction is present it can interact with another particle sitting at the same lattice site. As the interactions are short range their strength strongly depends on the wave function overlap between the

two particles. For the model taking into account only nearest neighbor tunneling and on-site interactions to give a good description of the system these must be large compared to off-site interaction and next-nearest neighbor tunneling. This can be simply estimated by comparing the size of the ground state wave function of a particle localized on a single site to the lattice spacing, as this gives a simple estimate for the wave function overlap of particles at different sites. This means the harmonic oscillator length of the single well $a_{\text{on-site}} = \sqrt{\hbar/(m\omega_{\text{on-site}})}$ must be much smaller than the lattice spacing. For our system this is reasonably satisfied for lattice depths above V $\approx$ 2.5 E_r. This is in good agreement for calculations of the next nearest neighbor tunneling and off-site interactions done in [Day05].

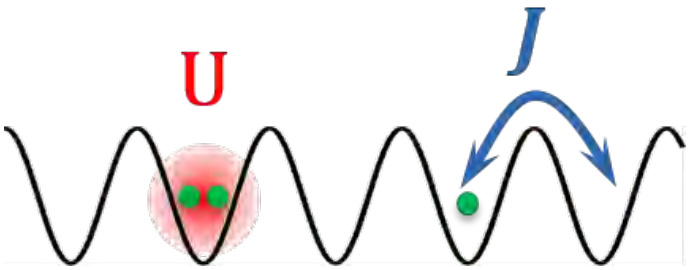

Figure 2.8: Sketch of particles in a periodic potential. There are two different processes the particles can undergo, either they tunnel to a different site with an amplitude J or, if two particles are on the same lattice site, they interact via a contact interaction U.

In the following we will take only the lowest band into account, which is justified if all other energies are (much) smaller than the band gap, which is the case for lattices deeper than V $\approx$ 2 E_r. Then, neglecting off-site interactions and next-nearest neighbor tunneling, this system can be described by the so-called Bose-Hubbard Hamiltonian

$$H = -J \sum_{<i,j>} a_i^\dagger a_j + U \sum_i n_i(n_i - 1) + \sum_i (\epsilon_i - \mu) n_i, \tag{2.39}$$

where the first term describes hopping of particles from one site to a neighboring site. The second term gives the interaction energy of particles sitting on the same site. The last term includes the energy offset ϵ_i of a site and the chemical potential μ. Here $n_i = a_i^\dagger a_i$ is the particle number operator on site i and the sum in the hopping term runs over the nearest neighbors. The tunneling probability J is given by [Wei09]

$$J = \int \mathrm{d}^3 r \; \Psi(\mathbf{r} - \mathbf{r}_i) \left(\frac{\hbar^2 \nabla^2}{2m} + V(\mathbf{r}) \right) \Psi(\mathbf{r} - \mathbf{r}_j). \tag{2.40}$$

This tunnelling element can also be calculated from the band structure as [Jak99]

$$J = \frac{E_0(q = k/2) - E_0(q = 0)}{4}, \tag{2.41}$$

with $E_0(q)$ denoting the energy of a particle with quasi-momentum q in the lowest band. The tunneling rates for Li_2 calculated in this way are shown in figure (2.9).

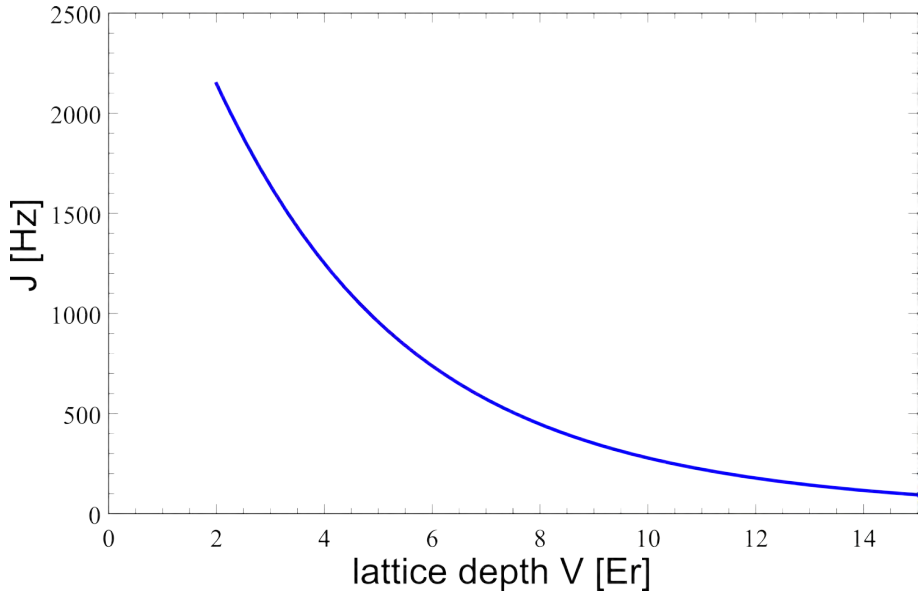

Figure 2.9: Tunneling rate J for Li_2 molecules as function of the depth of the lattice potential. The tunneling rate was calculated using equation (2.41) and the numerically obtained band structure.

The on-site interaction energy U is given by

$$U = \int \mathrm{d}^3 r \frac{4\pi\hbar^2}{m} a \, |\Psi(\mathbf{r})|^4. \tag{2.42}$$

In an inhomogeneous system each site i can have an energy offset ϵ_i. This is the case for a trapped system and for a harmonic confinement, this energy offset is given by $\epsilon_i = \frac{1}{2} m\omega_r^2 r_i^2$, where r_i is the distance from the trap center.
Even though this is a very simple model, it is still interesting as its ground state drastically changes with the relative strength between the interaction U and the hopping J. First, consider the ground state of a homogeneous system ($\epsilon_i = 0$) as a function of hopping and interaction. For small interactions $U \ll J$ it is energetically favorable for the particles to delocalize over the whole lattice and thereby minimizing their kinetic energy. Thus for zero interaction all bosons occupy the Bloch state with $q = 0$ and the system forms a superfluid condensate.
This condensate wave function has a fixed phase, which is the same for all sites as this minimizes the kinetic energy. Thus the number occupation of each lattice site fluctuates and system is described by the following wave function [Blo08]

$$|\psi_{SF}\rangle = \frac{1}{\sqrt{N!}} \left(\frac{1}{\sqrt{M}} \sum a_i^\dagger \right)^N |0\rangle, \tag{2.43}$$

where N is the particle and M the number of lattice sites. By increasing the interaction energy U, particle fluctuations on each site are suppressed because it becomes

energetically unfavorable to have more than one particle per site. Now the state of the system strongly depends on the filling. First, for the case of unity filling, i.e. 1 particle per site, and strong repulsive interactions $U \gg J$ the large interaction energy dominates over the kinetic energy needed to localize a particle on a lattice site. Thus each site is occupied by exactly one particle, with no fluctuations of the particle number. The system can then be described by the following wave function

$$|\psi_{MI}\rangle = \prod_{i=1}^{M} a_i^\dagger |0\rangle. \tag{2.44}$$

This system is in an insulating state — the so-called Mott-insulator — since a finite energy of U is needed to create a excitation (a particle–hole pair), which hinders transport. Since adding a second particle to a lattice site requires the interaction energy U, the system is incompressible, as squeezing of the system would lead to double occupancies. This can also be seen from the schematic phase diagram in figure (2.10), where the particle number is constant for a large range of chemical potentials in the insulating phase. This also implies zero compressibility, since the compressibility can be expressed as $\kappa = \partial n / \partial \mu$.

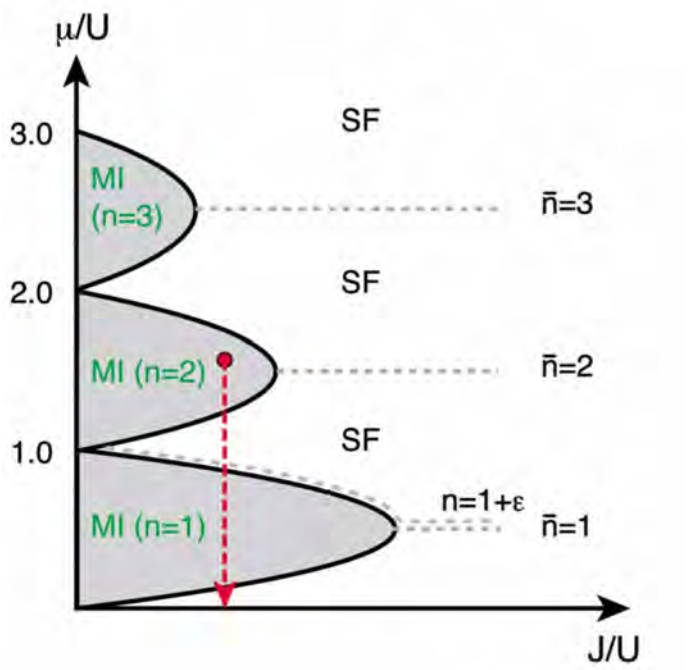

Figure 2.10: Zero temperature phase diagram of the Bose–Hubbard model. The different grey shaded regions depict the Mott-insulating phases of different filling. The average filling factor is set by the chemical potential. For strong repulsive interactions and integer filling the system is in the Mott-insulating state, whereas for small interactions the system is superfluid. Taken from [Blo08].

If the filling is not integer, the system is always in a superfluid state, since there are mobile particles on top of an insulating background of otherwise constant density.

This leads to the schematic zero-temperature phase diagram shown in figure (2.10). For unity filling the mean-field critical value for the transition from a superfluid to Mott-insulator state is $(U/J)_c = 5.8z$ [Zwe03], where z is the number of nearest neighbors. Thus from mean field theory the phase transition is expected to occur at a critical $(U/J)_c$ of 23.2 for a 2D square lattice. However, this value overestimates the critical value and from Quantum Monte Carlo simulations on a 2D square lattice one obtains $(U/J)_c = 16.2$ [Wes04].
By changing the power in the laser beams one can tune the lattice depth and thereby change the tunneling and on-site interaction such that it is possible to cross the transition from a superfluid to Mott-insulator in the experiment.
The problem of experimentally adjusting the density such that the lattice is exactly integer filled, is solved by the additional (harmonic) trapping potential leading to the energy offset ϵ_i in the Bose–Hubbard Hamiltonian (2.39). This leads to an effective chemical potential $\mu - \epsilon_i$ on each site. This variation of the effective chemical potential for different sites results in a variation of the average particle number for different sites. Hence, different local densities and thus phases are realized inside the trap and a single experimental realization probes a line of different μ/U in the phase diagram (red line in figure 2.10)[6]. The chemical potential in the trap center is maximal and decreases with distance from the center such that a ring like structure of different phases appears, where as a consequence of the incompressibility of the Mott-insulator the rings in the insulating phase have constant density, whereas in the superfluid and normal phases the density drops with distance from the center due to the decreasing local chemical potential.

[6]Since with distance from the center also the lattice depth changes the realized systems in the trap differ not only by μ/U, but for lower effective chemical potential at the edge of the trap also U/J is smaller.

3 Preparation and Probing of an ultracold Fermi gas

Performing experiments with ultracold quantum gases has several technical prerequisites. First, a hot gas has to be cooled down several orders of magnitude from room temperature to the nK region. Second, the atoms must be trapped and localized for performing the experiments. In these experiments one has to be able to manipulate the gas from outside, with out any physical contact. At the same time the gas must still be well isolated from the environment to reduce heating and loss. In this chapter the parts of our experimental apparatus required for the preparation of a quantum gas in an optical 2D square lattice are shortly summarized. More details on the different parts of the setup can be found in previous theses of the group.

3.1 Experimental Control and Feedback

The different parts of the experiment are controlled by a ADwin pro II real time control system, which has 16 analog outputs and 8 analog inputs, as well as 64 digital outputs. The digital outputs have an update rate of 1 μs, while the analog channels are slower and have only an update rate of 10 μs. The input channels can be used to provide feedback for the output channels and thus allow for regulated setting of parameters using a digital PID-control loop. The timing table for the channels is created via an external computer using LabView [Lom08].

3.2 The Vacuum Chamber and Resonant Pre-cooling

Having a quantum gas at low temperatures requires to limit collisions with fast particles from the background gas, as they would lead to loss and heating. Therefore our experiments are performed in an ultra high vacuum (see figure 3.2.1 for a drawing of the setup). Technical details of this vacuum system can be found in [Rie10]. In the main experimental chamber the pressure is at least as good as P=10^{-11} mbar resulting in a background collisions limited lifetime of the magneto optical trap (MOT) of approximate 23 min, which is much longer than the experimental cycle which takes roughly 12 s. Thus our experiments are not limited by collisions with the background gas.
The lithium vapor is produced in the oven camber, where a small piece of lithium is heated up to 350°C. This creates a sufficient flux of lithium atoms towards the experimental chamber for a reasonable MOT loading time, which in the current setup is roughly 3 s. When leaving the oven the atoms have a mean velocity of

roughly 1500 m/s. This is much higher than the capture velocity of our MOT of roughly 50 m/s, thus we have to slow down the atoms before trapping.

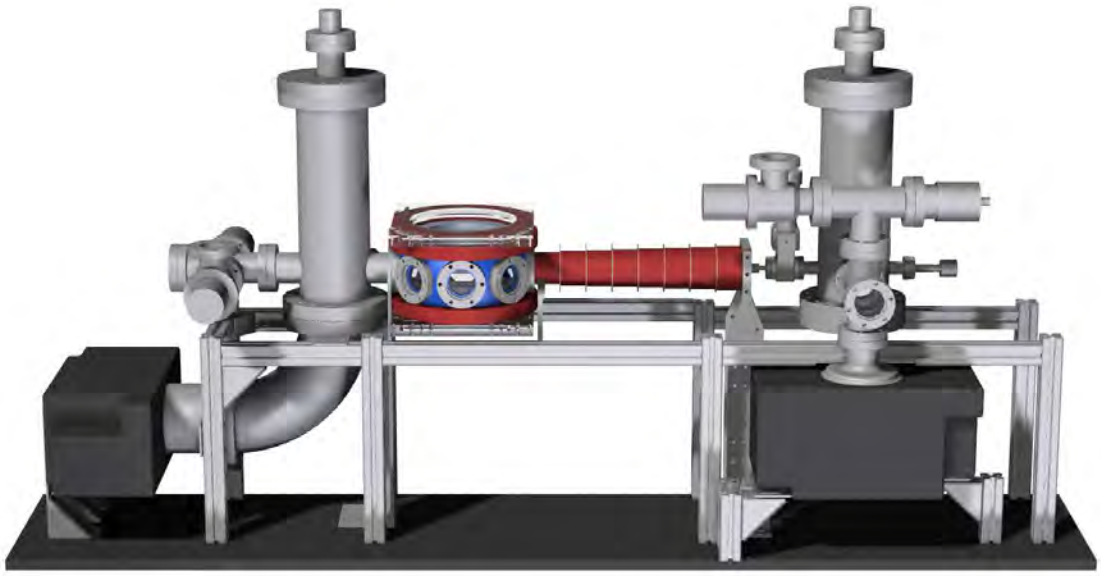

Figure 3.1: Drawing of the vacuum setup. The oven chamber on the right is connected via the Zeeman-slower (red coils), with the main experimental chamber (red octagon). The towers connecting the setup with the ion pumps and also serve as getter surfaces. Taken from [Rie10].

3.2.1 Zeeman-Slower

On the way to the experimental chamber the hot lithium atoms are slowed down by a Zeeman slower. This is done using light forces from a near resonant 671 nm laser beam to drive the D2 transition from the electronic ground state to the $2^2P_{3/2}$ state (see figure 3.2).
The 671 nm laser beam, which is red-detuned with respect to the atomic transition, is propagating in opposite direction to the atomic beam from the oven. By absorbing a photon the atom changes its momentum by the photon momentum $\mathbf{p}_\lambda$. When the excited state of the atom spontaneously decays it gains again a photon momentum. However, as emission from spontaneous decay is isotropic the average change of momentum from many emitted photons is zero[1]. Thus the atom in the resonant laser beam feels a net force

$$\mathbf{F}_{scatter} = \mathbf{p}_\lambda \Gamma, \tag{3.1}$$

which is proportional to the scattering rate Γ. This slows down the atom beam while moving towards the experiment chamber. However, the atoms initially resonant with the light field shift out of resonance as soon as they are slowed down due to the changing Doppler shift. This reduces the scattering rate and thus the force slowing

[1]This results in a random walk orthogonal to the propagation direction and the beam diverges.

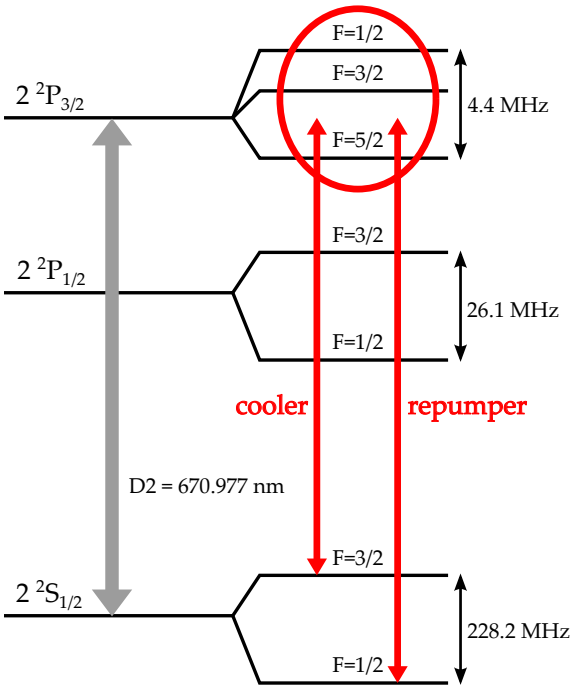

Figure 3.2: Level scheme of ^{6}Lithium. For our experiments we use the D2 line. Because at low magnetic fields there exists no closed transition we have to use two lasers labeled 'repumper' and 'cooler' to address atoms in both hyperfine states of the electronic ground state to avoid loss from dark states. The hyperfine splitting of the excited state is not resolved since it is smaller than the natural linewidth of 5.87 MHz. Adapted from [Geh03].

down the atoms. Thus one has to compensate for this change in the Doppler shift such that the atomic transition stays resonant with the laser light over the whole length of the Zeeman-slower. As the velocity of the atoms is position dependent the compensating shift has to vary along the atom trajectory.
For this purpose a spatially varying magnetic offset field along the tube connecting the oven and the experimental chamber is produced. The resulting Zeeman shift compensates the change in Doppler shift such that the atoms stay resonant with the laser beam. Thus they get effectively slowed down on their way to the experimental chamber and can be captured by the MOT. More on the theory of Zeeman-slowers can e.g. found in [Foo04], whereas the experimental implementation is explained in detail in [Sim10].

3.2.2 Magneto–Optical Trap

Cooling and trapping is done in a magneto–optical trap, which is described in more detail in many textbooks, e.g. [Foo04]. For dissipative cooling, red-detuned counter-propagating laser beams are used. Because of the Doppler shift and the red-detuning of the beams, the beam propagating in opposite direction to the atom is less detuned from the atomic resonance than the beam propagating in the same direction as the

atom. Thus more photons from the laser beam propagating in opposite direction will be absorbed. This leads to a net force, slowing down the atom. Using counter-propagating laser beams along all 3 major axes, the atoms can be slowed to zero average velocity. However, the atoms can not be cooled down to zero temperature, since at each scattering event the atom obtains an average kinetic energy of the recoil energy and a equilibrium is reached when this heating rate equals the cooling rate from the damping force. This puts a theoretical limit on the MOT temperature, the so-called Doppler-temperature which for the D2 line of lithium is $T_{\text{Doppler}} = 136$ μK.
The damping force discussed so far is only velocity and not spatially depended. Thus the atoms are not trapped in position space and can diffuse out of the trap. Confining the atoms is achieved by combining the lasers with magnetic field gradients. These magnetic field gradients lead to a position dependent splitting of the different sub levels of a hyperfine state. This allows for spatially dependent photon absorption and thus a restoring force.
The working principle of the MOT for an atom with a ground state of total angular momentum zero and excited state of total angular momentum one is depicted in figure (3.3). The laser beams are — as mentioned above — red-detuned so that at some distance the transition from the ground state to the $m_j = -1$ becomes resonant with the laser beam such that mostly σ_- polarized light will be absorbed. Here the polarization of the light is defined with respect to the local magnetic field direction. At the trap center the magnetic field has a zero and the magnetic field direction and thus the quantization axis for the spin changes direction. Thus the laser beam coming from the right (left) has σ_- polarization right (left) of the trap center and σ_+ polarization on the left (right) of the trap center. Thus on the right (left) side it drives a transition to the $m_j = -1$ state and on the left (right) side of the trap center it would drive a transition to the $m_j = +1$ state, which is detuned. Thus on the right side of the trap more light from the left propagating laser beam is absorbed leading to a restoring force towards the trap center, which traps the atoms near the field zero. Technical details of the laser and coil system of the MOT can be found in [Rie10].

3.3 The Optical Dipole Trap

To further cool the atoms below the Doppler temperature, they are transferred to an optical dipole trap (ODT). Producing a dipole potential deep enough to trap the hot[2] atoms from the MOT requires large intensities, as explained in section 2.3. Therefore we use a 1068 nm fiber laser which can output up to 200 W focused down to a waist of 100 μm $\times$ 20 μm. To further increase the trap depth and optimize the shape of the trap, the ingoing beam is intersected with the retro-reflected beam under an angle of 12° (red beam path in figure 3.4), where the polarization of the retro-reflected beam is rotated by 90° to avoid interference. This yields a sufficient trap depth of roughly 1.5 mK. The elliptical beams are used to produce a tighter focus and trap in vertical direction to improve later transfer to the final 2D confine-

[2]The final temperature of the atoms in our MOT is several 100 μK.

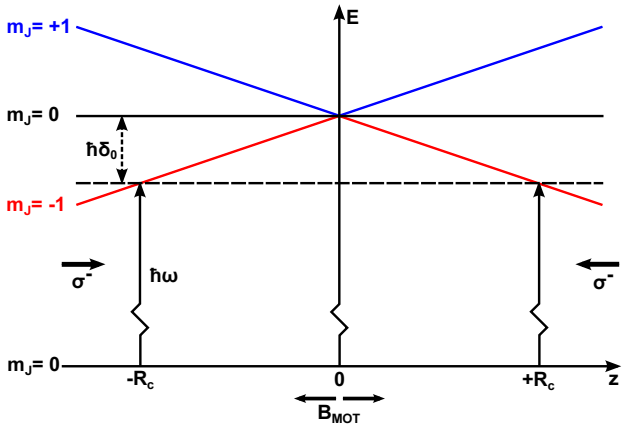

Figure 3.3: Sketch of the working principle of a MOT in 1D. Due to the change in magnetic field direction at the trap center the quantization axis changes. Thus the beam from the left can only drive a transition to $m_j = -1$ state on the left side of the center. Hence together with the red-detuning of the laser beams and the magnetic field gradient an atom on the left (right) of the trap center absorbs more photons from the laser beam propagating to the right (left). This results in a restoring force and trapping. Taken from [Rie10].

ment. This leads to a ratio of trapping frequencies $\omega_{\text{beam}} : \omega_{\text{horizontal}} : \omega_{\text{vertical}}$ of 1 : 9: 42. More details and a characterization of the setup can be found in [Boh12]. This setup allows for transferring roughly 10^6 particles in the lowest two hyperfine states to the ODT. By subsequently reducing the beam power, the gas is evaporatively cooled down to degeneracy. As efficient evaporative cooling relies on thermalization it is typically done at a magnetic offset field of 795 G (Thus this preparation scheme is called high-field evaporation.) close to the Feshbach resonance, where the scattering length is large and positive such that a molecular BEC[3] (mBEC) is produced during evaporation.

3.4 Feshbach Coils

Accessing the Feshbach resonance for effective evaporation and to change interactions during the experiments requires large magnetic fields up to 1400 G. In order to limit the current in the so-called Feshbach coils while still creating these high magnetic fields, the coils are placed as close to the vacuum chamber as possible. The small field region limits the energy stored in the field. The small inductance makes it possible to quickly ramp the magnetic field in a regulated way. Switching off the coils in a unregulated way by closing the FETs connecting the power supply with the coils is even faster and allows for ramp speeds of roughly 2700 G/ms, which can be used to quench the interactions near the Feshbach resonance. The two coils are placed slightly further apart than Helmholtz configuration. This leads to a

[3]The binding energy is on the order of 700 nK and thus much larger than the final temperature (≈100 nK).

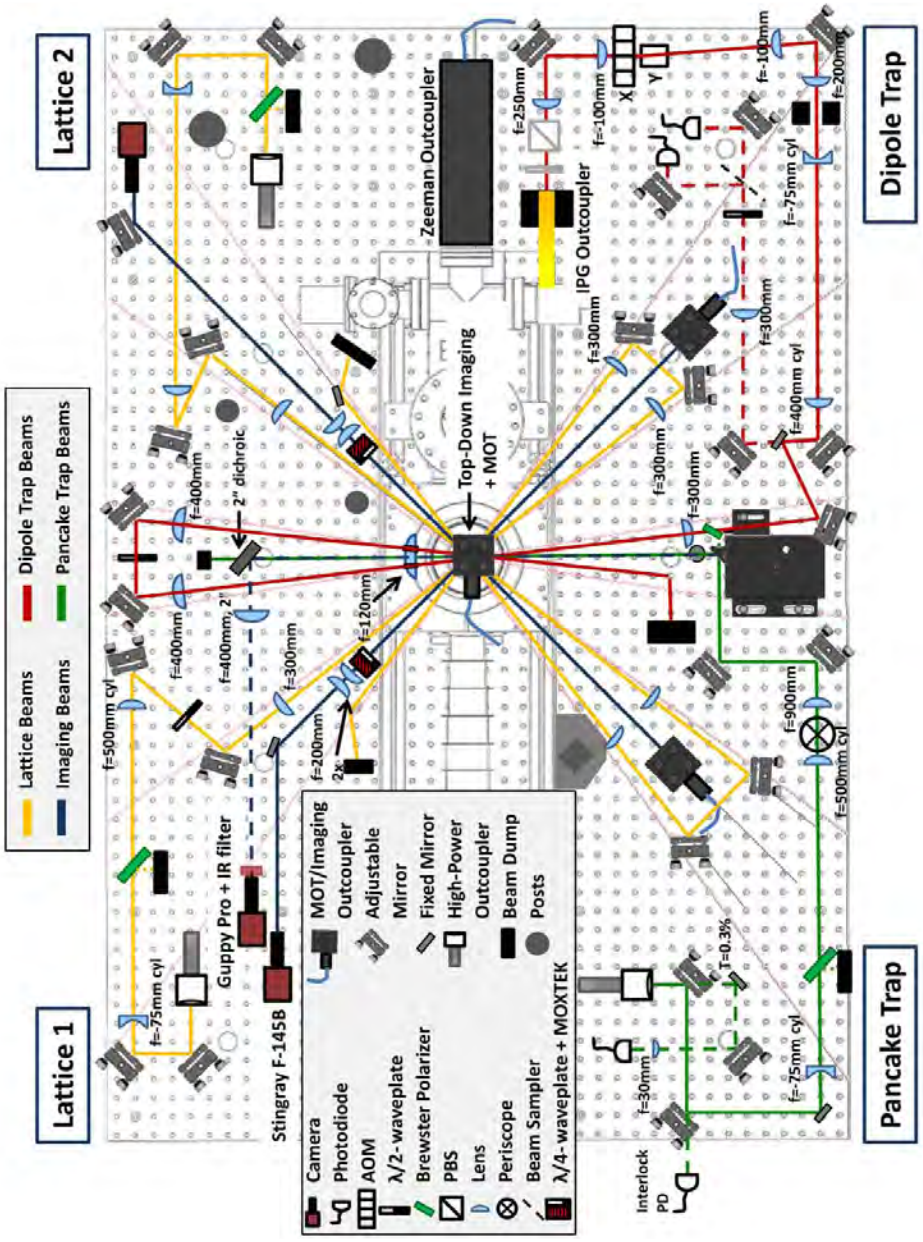

Figure 3.4: Drawing of the optical setup on the experiment table. Since the components of the two lattice setups are identical the optics of lattice 2 is not labeled. Taken from [Nei13].

magnetic field saddle such that the high field seeking states used in the experiment are anti-trapped in vertical direction and trapped by a small harmonic potential in the horizontal plane. More details on the coils can be found in [Wen13].

3.5 The RF Setup

Some of our experiments require to manipulate the internal states of the atoms. The transitions between the hyperfine states $|1\rangle$, $|2\rangle$ and $|3\rangle$ are driven by using radio frequency (rf) pulses. The coil creating these pulses is placed inside the vacuum chamber. The smaller distance to the atoms increases the achievable pulse power at the atom position. Thus this allows for more efficient transfer between the internal states compared to a coil outside the chamber. The performance of the coils and the detailed setup can be found in [Boh12, Heu11].

3.6 Loading the 2D Trap

In our experiments we want to access the quasi-2D regime. In a harmonic trap this regime is reached if all relevant energy scales, i.e. the chemical potential, temperature and the trapping frequencies in two spatial directions are (much) smaller than the trapping frequency in the third direction, such that the system is in the ground state along the tightly confined direction and motion along this axis is frozen out. Since the aspect ratio of the optical dipole trap is too small to reach the quasi-2D regime at reasonable particle numbers, we transfer the particles to the standing wave trap (SWT). To better match the shape of the ODT and the SWT during the transfer, we first compress the ODT by increasing its power. Furthermore to change the aspect ratio of the ODT which is roughly 1:5 in the horizontal plane, we modulate the beam position by quickly modulating the frequency of an AOM through which the beam passes. This modulates the pointing of the used first diffraction order such that the beam moves and creates a time averaged potential, which is much rounder and has an aspect ratio in horizontal direction of only 1: 1.5, better matching the round SWT. More details on this can found in [Rie14]. The SWT is created by two 1064 nm laser beams (green beam paths in 3.4) interfering under an angle of 14° producing a interference pattern in vertical direction. More details on the setup can be found in [Boh12, Nei13, Rie14]. The small angle results in a large spacing of roughly 4 μm between the maxima. This makes it possible to load only a single layer[4] with a mBEC [Rie14].
To reproducible load the single layer, a high stability of the interference pattern is required. Using a symmetric beam path makes the system relatively insensitive to small drifts in temperature or air pressure. Also the observed long term drift of the relative phase of the beams is less than $\pi/8$ over one week, such that the different maxima move by less than half a μm, with an even better short term (shot-to-shot) stability [Nei13], [Boh12].
Since the trapping potential is created by an interference pattern, the two beams must be coherent and a narrow frequency source is needed. We use a NUFERN SUB-1174-22 fiber amplifier, which can deliver up to 50 W, seeded by 1064 nm low noise single mode solid state laser (Innolight Mephisto-S 500 NE). More details on the (noise) characteristics of this setup can be found in [Nei13]. With this setup

[4] We can measure the fraction of particles in each maxima using a tomographic measurement [Nei13].

we can create an oblate trap with an aspect ratio of roughly 300 : 1 and nearly perfect radial symmetry, where the trapping frequency is $\omega_{vert} = 2\pi \times 5.83$ kHz along the tight confined vertical direction and $\omega_{hor} = 2\pi \times 18.2$ Hz along the horizontal directions for roughly 3 W beam power.
Further evaporation in the SWT allows us to produce a degenerate sample in the quasi-2D regime [Rie14].

3.7 The Lattice Setup

For our experiments in a 2D lattice we turn on the lattice beams after loading a single layer of the SWT. Each lattice arm is produced by a laser beams retro-reflected under a shallow angle close to 180° (see yellow beam paths in 3.4). Since lattice 1 and lattice 2 (adopting the notation from figure 3.4) form an angle of 90°, overlapping the SWT with the two lattice arms creates a 2D square lattice in each layer of the SWT. A sketch of the SWT and the lattice setup is shown in figure (3.5).

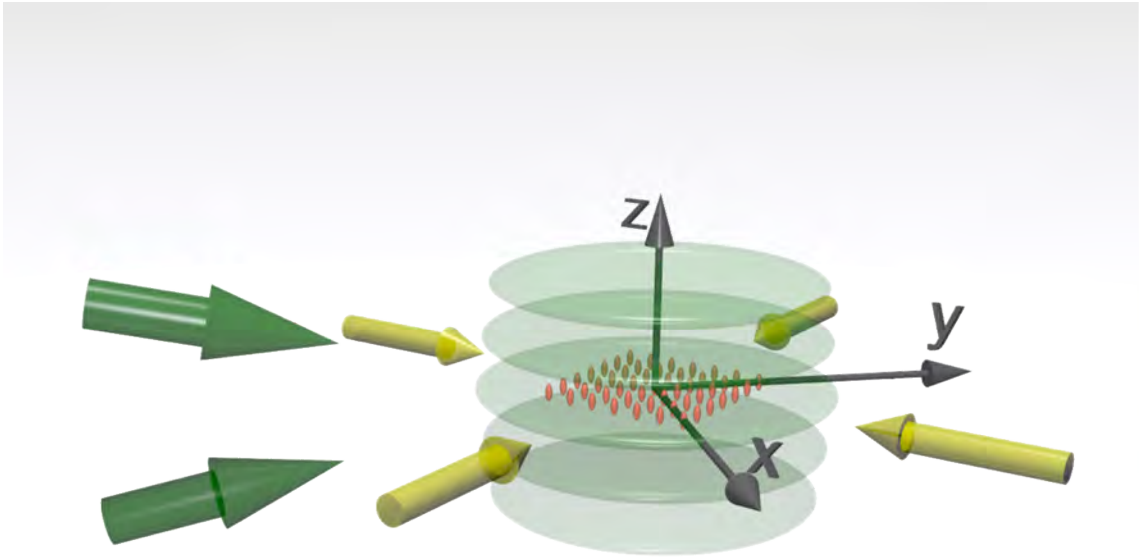

Figure 3.5: Sketch of the laser beams creating the SWT (green arrows) and the lattice (yellow arrows). The green disks illustrate the different pancake shaped traps created by the SWT. The red tubes show atoms localized at the lattice sites in the central layer of the SWT. The direction vertical to the lattice is taken to be the z-axis.

The used wavelength of 1064 nm produces a lattice spacing of $d = \frac{\lambda}{2\cos\phi} = 536$ nm. The light for creating the lattice is taken from the same laser as for the SWT. The

light for each beam is delivered by a high power optical fiber to the experimental table. Distributing the power from the laser to the different fibers is done on a separate breadboard, described in detail in [Bec13].
To avoid interference between the different lattice arms and the SWT they are detuned from the laser frequency by + 100 MHz (SWT), + 120 MHz (lattice 1) and - 100 MHz (lattice 2) using acousto-optic modulators (AOM) in front of each fiber. These AOMs are also used to switch and control the power of the beams, where the feedback signal is taken from a photodiode placed behind a mirror on the experiment table. To avoid interference between lattice 1 and the SWT, which are not far detuned from each other, the light creating lattice 1 is vertically polarized, while for lattice 2 and the SWT horizontally polarized light is used.
On the experimental table the setup for both lattice arms is (apart from one $\lambda/2$-waveplate in lattice 1 to turn the polarization) identical. After leaving the fiber the collimated beam has a Gaussian diameter of roughly 1.2 μm and passes trough a Brewster polarizer to clean the polarization.
Then the beam passes trough a cylindrical telescope built out of a f = -75 mm and f = 500 mm focal length cylindrical lens to expand the vertical beam size by a factor of approximately 6.7. Thus we can achieve a much smaller focal spot size in the vertical direction at the position of the atoms, reducing the laser power needed for the same intensity and trap depth. This we can safely do, since the confinement in vertical direction is mostly given by the SWT and we want to investigate only a lattice in a single layer of the SWT.
After the telescope the beams are focused down by a f = 300 mm lens onto the atoms yielding a focal spot size of 25 μm $\times$ 160 μm. On the other side of the chamber the beam is collimated using a f = 300 mm lens and then imaged on the atoms by another f=300 mm lens. The calibration of the trapping frequencies as a function of beam power is described in the next chapter.

3.8 Absorption Imaging

At the end of the experimental cycle, the sample has to be probed to obtain information about the state of the system. For this we use absorption imaging, where the atomic cloud is illuminated with resonant light. Absorption of light by the atoms results in a shadow behind the cloud which is imaged onto a camera and recorded. By taking a reference image without atoms one can calculate the fraction of absorbed light and thus the (integrated) column density of atoms. Since the imaging uses resonant light the sample gets heated and lost.
We can image the system from different directions (see cameras and blue lines in 3.4), either from the side to obtain information about the vertical distribution or from the top to obtain the distribution in the radial plane. The resolution of all imaging systems is worse than approximately 3 μm such that single lattice sites cannot be resolved. For more information on our imaging system see [Lom08, Nei13, Bec13].
One can obtain two kinds of information. First, by imaging the atoms inside the trap one obtains the in-situ density distribution.
Second, by switching off the trap and letting the cloud expand freely before taking

the image one can access the momentum distribution of the cloud, as the freely expanding atoms move according to their initial velocity and thus if the final size is much larger than the initial size the density distribution reflects the in trap velocity distribution. Here the free expansion of the atoms is crucial, as interactions and scattering would lead to a redistribution of the initial particle momenta.
Also, to obtain the true momentum distribution and to be able to completely neglect the effect of the initial density distribution one has to wait infinitely long, which is experimentally not feasible as the signal to noise ratio decreases for longer expansion times, which go along with a large size and small density of the expanding cloud.

3.8.1 Matter-Wave Focusing

Hence, for obtaining the momentum distribution we use the so-called matter-wave focusing technique, as described in [Mur14]. When switching off the optical trap the sample is not expanding freely but in the magnetic potential of the saddle point of the offset field, which is to a very good approximation harmonic. The trajectory $x(t)$ of a classical particle moving in a harmonic potential is given by

$$x(t) = x_0 \cos(\omega t) + \frac{p_0}{m\omega} \sin(\omega t), \tag{3.2}$$

where m is the mass of the particle, ω the trapping frequency and x_0 and p_0 are the initial position and momentum, respectively. Obviously, after a quarter of a period, at $T = \frac{2\pi}{4\omega}$, the initial momentum has been mapped onto the position and vice versa. Thus the in-situ density distribution is obtained after a finite time of flight in a harmonic potential using the T/4-imaging technique. Our magnetic potential has a trapping frequency of $\omega_{mag} \approx 2\pi \times 10$ Hz, resulting in a 25 ms time of flight for the momentum focusing technique.
Like conventional time of flight imaging this technique relies on ballistic expansion of the sample without scattering, in stark contrast to our strongly interacting sample with a large scattering length. Part of this problem is solved by the system geometry. Due to the tight confinement in vertical direction, the sample quickly expands along this axis after switching of the trap, reducing the density and thus the scattering rate. Additionally, interactions are quenched by quickly ramping the offset field to 527 G, i.e. close to the zero crossing of the scattering length shortly before the release of the atoms from the optical trap. This is done in approximately 150 μs such that the many-body wave function cannot react and is mostly unaffected.
Combining the fast expansion with the magnetic field ramp leads to a nearly ballistic expansion of the sample, where only less than 10 percent of the atoms are scattered and redistribute their momentum during the expansion [Mur14].
Note, that when imaging along the vertical (tightly confined) axis the full information of the 2D system is obtained, since the density distribution along the tight confined direction, which is integrated out during the imaging process, is trivial. This is not the case for a 3D system, where by imaging along an axis the density distribution along this axis is integrated and only the column density is obtained. There some further image processing has to be done in order to obtain the true density distribution.

3.8.2 Stopping Pulse

While the fast vertical expansion is useful to quench interactions it also cause some problems. During the 25 ms long time of flight the sample significantly expands and has a final Gaussian width of several hundred micron, which is larger than the depth of focus and thus blurs the image and decreases the signal. The axial expansion is slowed down by pulsing on the painted ODT 100 μs after releasing the sample from the trap. This free expansion time is such that the sample is already dilute enough to significantly reduce scattering. By pulsing on the ODT for a quarter period of its vertical trapping frequency, where the particles reach their classical turning point and thus have no energy, we stop the expansion of the cloud (see figure 3.6a). For the trapping frequency of $\omega_{vert} \approx 2\pi \cdot 200$ Hz this correspond to a stopping pulse duration of 1.25 ms. This does not significantly alter the matter wave focusing in radial direction as the estimated trapping frequency of the painted ODT is on the order of $\omega_{radial} \approx 2\pi \cdot 10$ Hz. Thus also distortion due to the non-harmonicity of the painted ODT should only have a negligible effect on the momentum distribution. Further expansion of the cloud after the stopping pulse (see figure 3.6b) is due to imperfections of the stopping pulse and the axial anti-confinement of the magnetic offset field. The smaller vertical cloud size during imaging significantly increases the signal, allowing to image smaller atom numbers. More detail can be found in [Rie14] and [Mur14].

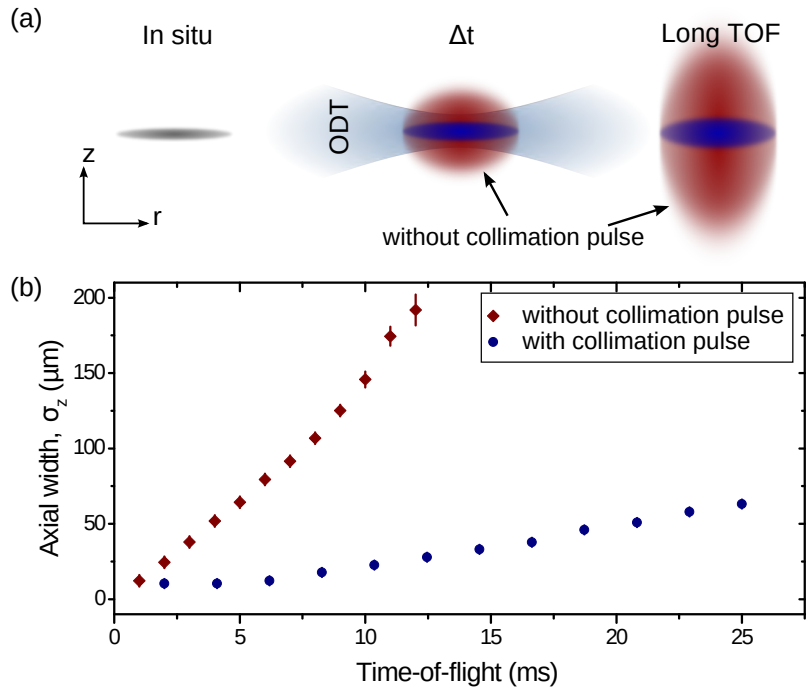

Figure 3.6: (a) Sketch of the vertical expansion of the cloud with and without stopping pulse. (b) Vertical cloud size as a function of time of flight. With stopping pulse the cloud size is much smaller, minimizing distortions during imaging. Taken from [Mur14].

4 Characterization of the Lattice

The state of a system in a periodic potential strongly depends on the depth V of this lattice potential. Thus it is crucial to know its exact depth, to be able to perform senseful experiments. So in a first step we calibrated the lattice setup and measured its depth V and overall confinement for different laser powers (for a sketch see figure 4.1). In the following all parameters are given as a function of the voltage on the photodiodes used by the experimental control, where 1 V roughly corresponds to 1 W of power in the lattice beam.

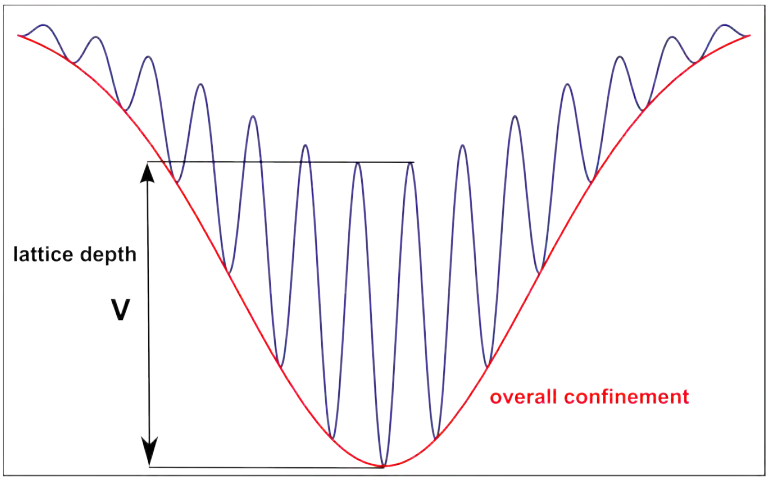

Figure 4.1: Sketch of the confinement provided by the lasers. The red line indicates the overall confinement due to the Gaussian shape of the beams, whereas the blue line shows the periodic modulation of the lattice potential with a central depth V. The periodicity of the lattice is not to scale and much smaller in reality.

4.1 Calibration of the Lattice Depth

The depth V of the periodic potential is especially important as the tunneling rate as well as the on-site interaction strength depend on this parameter. Hence by tuning this parameter the ground state of the system can be changed from a superfluid to a Mott-insulator. The calibration of the periodic potential V is done by means of Kapitza–Dirac scattering, whose details are explained in the following.

4.1.1 Kapitza–Dirac Scattering

From the particle–wave duality of quantum mechanics it is clear that similarly to the diffraction of light on a grating, the roles can be reversed and particles can be diffracted on a standing light wave. This diffraction of matter on a standing light wave is known as Kapitza–Dirac scattering. Kapitza and Dirac originally proposed to diffract electrons on a standing light wave [Kap33]. Due to the weak (ponderomotive) coupling of free electrons to light this requires high power (pulsed) lasers [Fre01]. However, diffraction of atoms on a standing light wave is much easier because of the larger coupling of the polarizable atoms to the light-field. This not only lead to the much earlier observation of the Kapitza–Dirac effect for atoms [Gou86], but also enables us to use the effect to calibrate the depth of our lattice potential.
The diffraction process can be thought of as absorption of a photon from one of the beams creating the standing light wave followed by stimulated emission of a photon to the beam propagating in the other direction. Thus for counter-propagating beams two times the photon momentum is transferred to the atom.
Instead of using a propagating beam of matter passing through a standing light wave, as originally proposed, we pulse on the standing wave for a short time on our static condensate. Thus the interaction time is not given by the transverse atom velocity and beam diameter, but by the time the lattice beams are turned on.
Neglecting interactions, the time evolution of the condensate wave function ψ can be described by [Fre02, Gad09]

$$i\hbar\partial_t\psi = \Big[-(\hbar^2/2m)\partial_z^2 + V\cos^2(kz)\Big]\psi, \tag{4.1}$$

where $k = 2\pi/\lambda$ denotes the wave vector of the light. Note that this is the same Hamiltonian as discussed in the theory section (see equation2.30). Here we are not interested in the static properties of the system, but in the time evolution, if the potential is turned on for a short time. Since only discrete momenta — multiple of the lattice momenta k_L — can be transferred to the atoms it is again convenient to Fourier expand the wave function. This leads to the following coupled differential equations for the coefficients of the different diffraction orders

$$i\partial_t c_n = \left(\frac{2\hbar k^2 n^2}{m} + \frac{V}{2\hbar}\right) c_n + \frac{V}{4\hbar}(c_{n+1} + c_{n-1}). \tag{4.2}$$

Depending on the strength of the potential V compared to the two photon recoil energy $E_r^{(2)} = (2k\hbar)^2/(2m)$ — the kinetic energy gained by a single scattering event[1] — different regimes can be distinguished (more details can be found in [Fre02], [Gad09] and [Bec13]):

- If the potential dominates over the kinetic energy, i.e. $V \gg E_r^{(2)}$, the kinetic energy (for low diffraction orders) can be neglected. This is the so-called diffraction or Raman-Nath regime, where the occupation probability of the different orders after a time t is given by $|c_n| = J_n^2(Vt/\hbar)$ with the n-th Bessel

[1] Absorption of a photon from one beam and subsequent stimulated emission in the other beam.

function J_n. Here one sees, that many different orders can be occupied. This is a consequence of the broad frequency spectrum of the short pulses. Thus the absorbed and emitted photon might have slightly different frequencies (energies) which compensates for the change of kinetic energy of the diffracted and thus accelerated atoms and total energy is conserved.

- For the case of a shallow lattice $V \approx E_r^{(2)}$, the number of diffraction orders is limited, since at most all of the potential energy can be converted to kinetic energy. This gives a maximal diffraction order $n_{max} = V/E_R^{(2)}$. Thus only a finite set of coefficients are non-zero and the 2 $n_{max} + 1$ coupled differential equations can be solved. For example for the case of $1 \leq n_{max} < 2$ the coefficients are given by [Gad09]

$$|c_{\pm 1}|^2 = C^2 \sin^2\left(t\frac{1}{2\hbar}\sqrt{\frac{V^2}{2} + (E_r^{(2)})^2}\right), \tag{4.3}$$

$$|c_0|^2 = 1 - 2|c_{\pm 1}|^2. \tag{4.4}$$

Here C^2 is the maximal fraction of atoms transferred to the first order, which depends on the coupling strength and the energy difference (detuning) between the first and zero order. It is always smaller than 1/2 as in each first order can be at most half of the atoms. In this effective 2-level system undergoes Rabi-oscillations and the population of atoms oscillates back and forth between the zero and the two first orders.

In both regimes the population of the different orders oscillates as a function of the pulse area $\frac{V}{\hbar}t$. Since we want to calibrate the lattice depth by observing the oscillation of occupation between the orders, we decided to work in the shallow lattice regime, where the population oscillates more slowly between the orders. In this regime the oscillation can be resolved with our limited timing resolution of 1 μs (see chapter 3.1).

4.1.2 Calibration of the lattice depth

For the calibration measurement, we produce a molecular condensate at a magnetic field of 692 G in a single layer of the SWT. This lower magnetic field reduces the interaction energy, compared to higher fields. The relative short lifetime is not a problem for this measurement, as the atoms are not hold in the trap for a long time. Then the trap is turned off and one lattice beam is pulsed on for a variable time t between 1 and 30 μs. The intensity of the laser beam of roughly 200 mW is chosen such that only the first diffracted order is populated. Afterwards the cloud expands for 5 ms in the harmonic potential of the saddle point of the magnetic offset field to separate the diffraction orders (see figure 4.2 a). We extract the fraction of atoms in the first orders by fitting a Gaussian to each of them. The fraction of atoms in the first order oscillates according to equation (4.3), with a frequency $f = \frac{1}{h}\sqrt{\frac{V^2}{2} + (E_r^{(2)})^2}$. Due to inhomogeneities of the beams the oscillations are not perfect but damped

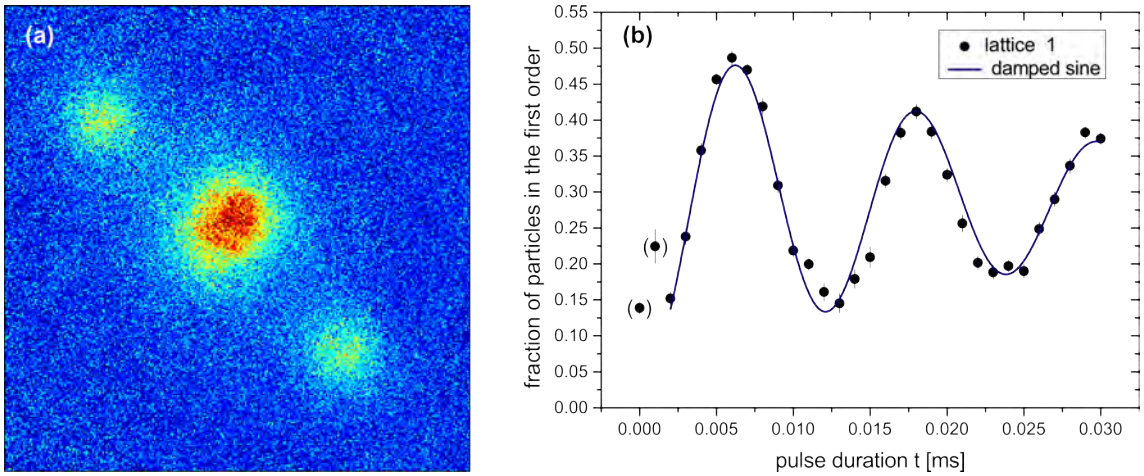

Figure 4.2: (a) Kapitza-Dirac scattering of a condensate using lattice beam 1. The picture is the average of 14 single images. After the pulse the particles expand in the external magnetic potential until they are separated. This allows to extracting the fraction of atoms in the first orders. This quantity is plotted in (b) as a function of pulse duration for the same lattice depth. The population oscillates between the first and the zeroth order as a function of pulse duration.

as a function of pulse duration[2] (figure 4.2 b). From the frequency we calibrate the lattice depth in units of the molecular recoil energy[3] as defined in equation (2.29) for a given control voltage. The resulting depths are summarized in table 4.1. Since the potential depth is proportional to the intensity (power in the beam) this allows us to calculate the lattice depth as a function of control voltage.

lattice	control voltage [mV]	lattice depth V [kHz]	lattice depth V [E_r]
1	236	113	7.75
2	195	212	14.5

Table 4.1: Calibration of the lattice depth V as a function of the control voltage. The potential energy of the lattice is not sufficient to populate higher orders. Because of the quadratic dispersion relation populating the second order would require a potential depth of V = 16 E_r.

We can use this method to calibrate the relative strength of both lattice arms. This enables us to produce a square lattice with the same depth in both directions. In

[2]That this is true can be seen from latter measurements with a larger beam, where the damping of the oscillation is smaller.

[3]Since we use Kapitza–Dirac scattering only as a tool to calibrate the lattice we give the energy in terms of the single photon recoil energy as it is done in lattice experiments and not in units of the two photon recoil energy, which is the natural energy scale for Kapitza–Dirac scattering.

the following only the control voltage of lattice 2 is given and the control voltage of lattice 1 is set accordingly such that the central lattice depth V is equal in both directions.
Note however, that this calibration might have some error due to the size of the atom cloud, which is comparable to the size of the beams. Thus the intensity and hence lattice depth is not constant over the whole cloud. This might lead to errors, since in different parts of the cloud the population of the orders oscillates with different frequency, resulting in errors of the lattice depth calibration.
More importantly, this measurements should have been repeated for several powers to fit the lattice depth as a function of beam power and obtain a more reliable result. Hence, this measurement can only give a very rough estimate of the lattice depth. Form a current measurement with different powers ,but a slightly changed setup, we estimate the error of the here obtained lattice depth to be on the order of 20 %.

4.1.3 Calibration of the Matter-Wave Focusing

Using Kapitza-Dirac scattering, we have a tool to transfer well defined and large momenta to a part of the cloud. This can be used to calibrate our setup with high accuracy. By changing the time of flight after pulsing on the lattice, we probe the evolution of the peaks in the radial confinement created by the saddle point of the magnetic offset field. This is shown for a condensate diffracted on lattice 1 in figure (4.3).
This method allows not only to calibrate the matter-wave focusing technique, but also the magnification of the imaging system. In the harmonic potential created by the magnetic offset field the particles oscillate and after a quarter of the period the density distribution reflects the initial momentum distribution [Mur14]. At this time T/4 the position of a particle $x_{T/4}$ is connected to the initial momentum by $p_0 = m\omega x_{T/4}$. Since the transferred lattice momentum during the Kapitza–Dirac scattering is much larger than the momentum spread of the condensate we observe distinct peaks after a quarter of a period in the external potential. Thus experimentally, after a quarter of a period the distance between the peaks is maximal. From this a matter wave focusing time[4] $T/4 = 24.6$ ms and a corresponding trapping frequency of $\omega_{mag} = 2\pi \times 10.2$ Hz are obtained (see figure 4.4).
These results also allow for a precise characterization of the magnification of the camera, as the transferred momentum $p_L = \hbar k_L$, the frequency of the magnetic offset field potential and the distance of the peaks on the camera are known. The so calculated magnification of the camera in the up-down (z-)direction is $M = 2.14 \pm 0.04$, roughly 10 % larger than the old value of 1.96. Which was obtained in a less precise measurement, where the expansion in the harmonic potential was neglected.

4.2 Trapping Frequencies of the Lattice

The lattice beams also change the overall confinement seen by the atoms. Since this can influence important quantities like the dimensionality of the sample, we

[4]Including the expansion in the stopping pulse.

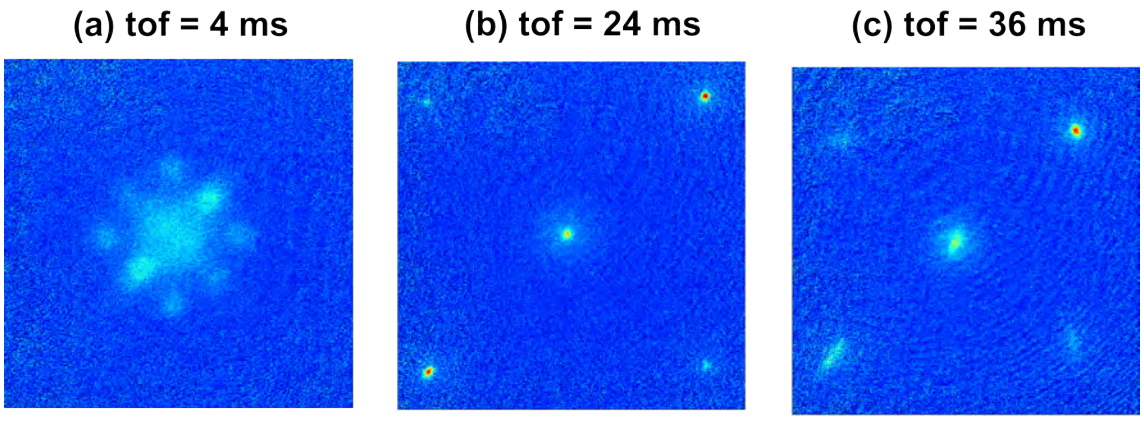

Figure 4.3: Kapitza-Dirac scattering of a condensate using both lattice arms. The different images correspond to different evolution times of (a) 4 ms, (b) 24 ms and (c) 36 ms in the magnetic offset field. For 4 ms expansion time also the mixed orders, where a photon of lattice arm 1 is absorbed and emitted into lattice arm 2, are visible inside the imaging region. Note that after a quarter of a trap period (b) the peaks are focused and have minimal width reflecting the narrow momentum distribution of the condensate. For expansion times longer than T/4 (c), the atoms return towards the center of the magnetic potential as expected for particles propagating in a harmonic trap. Also the peaks get blurred over time due to the expansion in vertical direction. Each picture is the average of roughly 40 images.

measured the overall confinement including the lattice beams. In order to perform this measurement nicely we first have to slightly change our experimental setup and place $\lambda/2$-waveplates in the retro-reflected lattice beams. These are used to rotate the polarization of the beams by 90° such that they are not interfering with the ingoing lattice beams. This is done to avoid effects due to the optical standing wave, i.e. a different effective mass of particles moving in a lattice. Since in the end a two dimensional lattice is investigated, we measured the confinement of the full potential including the SWT and both lattice arms. This is done by measuring the trapping frequencies of the confinement, which allows to characterize the harmonic part of the potential.
The trapping frequencies are measured by exciting the so-called breathing mode, where the cloud changes its size with twice the trapping frequency. The measurement was done with a single component and thus non-interacting Fermi gas[5] in order to avoid any interaction effects on the oscillation frequency [Ket09].
The Fermi gas is produced by loading a mBEC in a single layer of the SWT and afterwards adiabatically ramping the magnetic field to the BCS side of the resonance. There the molecules are transferred into weakly interacting fermions. To remove one component a light pulse resonant to state $|1\rangle$ is applied and the atoms in this state are 'kicked' out of the trap. This, of course, heats the remaining component, but

[5]Due to Pauli pressure the cloud of non-interacting fermions is much bigger than the mBEC but is still smaller than the approximately harmonic region of our potential.

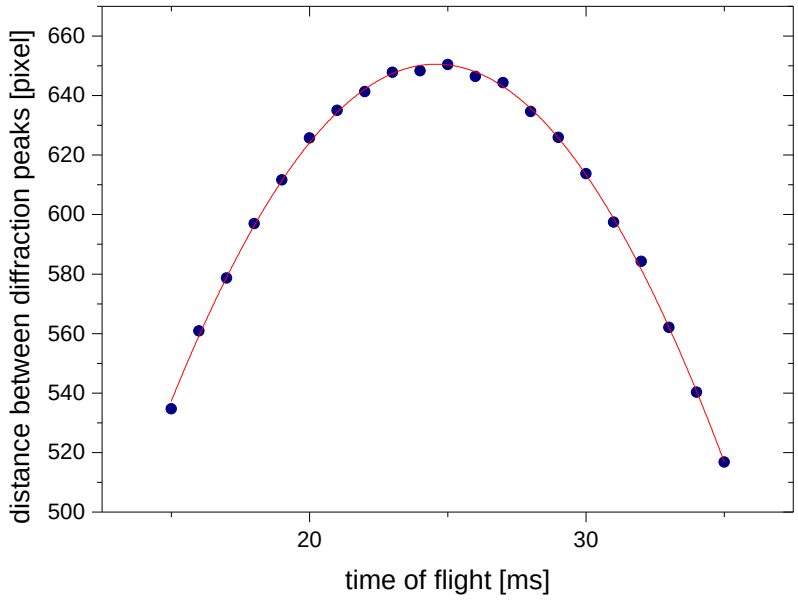

Figure 4.4: Distance of the first order peaks of Kapitza–Dirac scattering in pixels as a function of expansion time. To find the turning point of the motion in the harmonic potential, the distance between the peaks as function of expansion time was fitted with a sine. Note that the atoms return to their initial position after half a period of evolution in the harmonic potential.

one obtains a single component and thus non-interacting Fermi gas in a single layer of the SWT trap.
The breathing mode is excited by rapidly changing the power in the lattice beams to the final value[6]. The density distribution cannot follow this rapid change in trap depth and a breathing mode is excited. This can then be detected by measuring the cloud size for different wait times after the excitation.
In figure (4.5), the cloud size as a function of the hold time is depicted for a control voltage of $V_{control} = 0.1$ V. The cloud size along the lattice directions shows a damped oscillation as a function of the hold time after quickly changing the lattice beam powers. The damping of the oscillation is due to dephasing of the atoms.
All of these trap frequency measurements were done at a magnetic offset field of 730 G and at a SWT power of roughly 3 W, which already provides a harmonic confinement with a trapping frequency of approximately 18.2 Hz. The trapping frequency along the tightly confined z-direction was not measured for different lattice depths. The confinement provided by the lattice beams is less than 1 kHz in this direction, which is much smaller than the confinement provided by the SWT in this direction. Since the total trapping frequency is obtained by quadratically adding the different trapping frequencies, the contribution from the lattice is less than 3 % and can be neglected. Thus the trap frequency in z-direction is to a good approximation

[6] The quick ramp must not be to big as otherwise also the non-harmonic part of the confinement is probed. On the other hand if the rapid change is to small the amplitude of the oscillation is to small to detect.

given by the value obtained for the SWT.

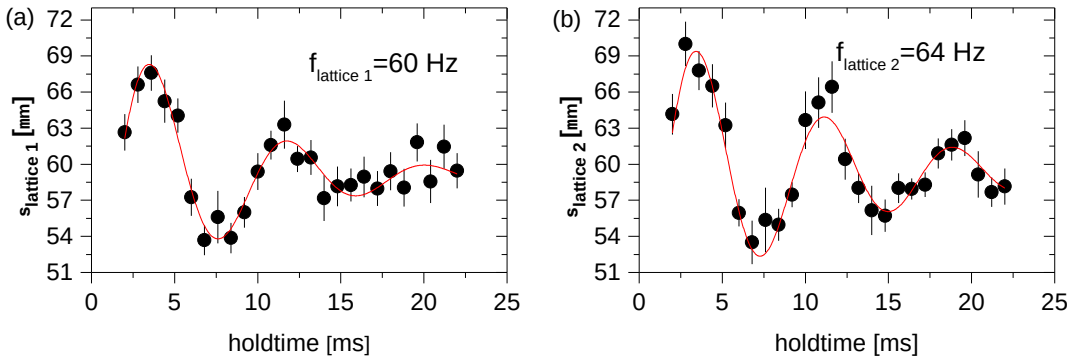

Figure 4.5: Gaussian size of the cloud for different hold times after quickly ramping the lattice power to a final depth of $V_{control} = 0.1$ V , which would correspond to a $V \approx 7.4\ E_r$ deep lattice. A damped oscillation of the cloud with twice the trapping frequency is visible. Each point is the average of approximately 20 measurements and error bars denote the standard error of the mean.

We have measured the trapping frequencies f for different control voltages (powers) $V_{control}$ of the lattice beams (see figure 4.6). The trapping frequencies show the expected behavior and are described by

$$f = \sqrt{const^2 \cdot (V_{control} - V_0) + f_{SWT}^2}\ . \tag{4.5}$$

They increase as the square root of the intensity (control voltage[7]) plus a quadratically added offset given by the trapping frequency of the SWT confinement f_{SWT} (compare to section 2.3).
The strong increase in radial trapping frequency at nearly constant vertical trapping frequency reduces the possible atom number in a quasi-2D system. This can seen from the Fermi energy of a non-interacting 2D gas in a harmonic trap (see equation 2.7),

$$E_F = \hbar\,(2N\omega_x\omega_y)^{1/2}\,. \tag{4.6}$$

In the quasi-2D, regime the Fermi-energy (chemical potential) must be smaller than the trapping frequency in the tightly confined direction. For increasing radial trapping frequency the particle number must thus be smaller in order to stay in the 2D regime. This means that even if we start with a quasi-2D sample in the SWT, excited levels in the z-direction can become populated, when the lattice is turned on and the aspect ratio of the trap changes. Thus we have to be careful that most particles

[7] The offset in the control voltage is needed since the photodiode used for feedback gives a non-zero voltage even without any light from the lattice beam.

stay in ground state of the confinement in z-direction, when doing experiments in a 2D lattice. Furthermore, these particles in the excited z-states will not contribute to the coherent part of the sample and only make the system more complicated.

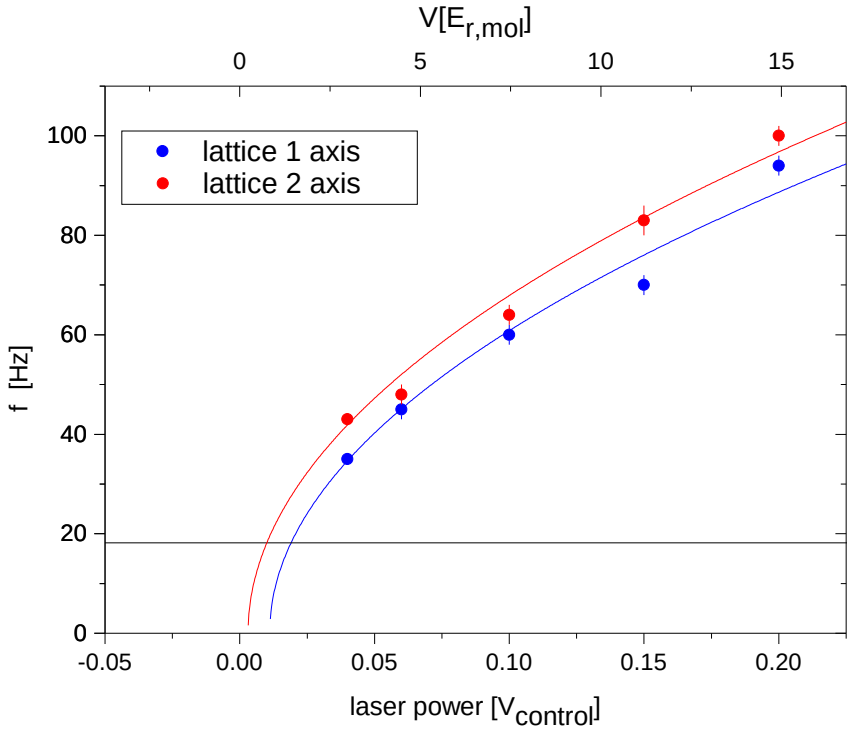

Figure 4.6: Trap frequency along the two lattice arms as a function of control voltage and lattice depth. The black line indicates a trap frequency of 18.2 Hz provided by the SWT and magnetic offset field. The data points show the expected behavior as discussed in the text. The different trapping frequencies in the two directions might be due to alignment problems or errors from the calibration of the lattice depth V.

4.3 Lifetime in the Lattice

Since low temperatures and high degeneracy are crucial for experiments, probing the ground state properties of a system (e.g. the superfluid to Mott-insulator transition), we need to know the heating rates and lifetime of the atoms in our lattice. To measure the lifetime of the atoms in the trap, we produced a single component Fermi gas in state $|2\rangle$ as described above. These particles are hold for up to 8 s at different lattice depths. The particle numbers as a function of the hold time are shown in figure (4.7). From the small change of roughly 10 percent in atom number over several seconds it is clear that the lifetime will not limit the experiments performed in the lattice, since these normally take less than 1 s of time. The number of atoms can be fitted by an exponential decay $N = N_0 \exp(-t/\tau)$, with a 1/e-lifetime of 24 s and 27 s for lattice depths of $V \approx 37$ E_r and $V \approx 22$ E_r, respectively. This functional shape suggests that the losses are due to single particles processes. Hence

processes like scattering non-resonant photons from the trapping beams, collisions with the background gas and heating due to trap noise [Geh98], do not lead to atom loss limiting the planed experiments in the lattice. As expected the lifetime is longer for lower light intensity.

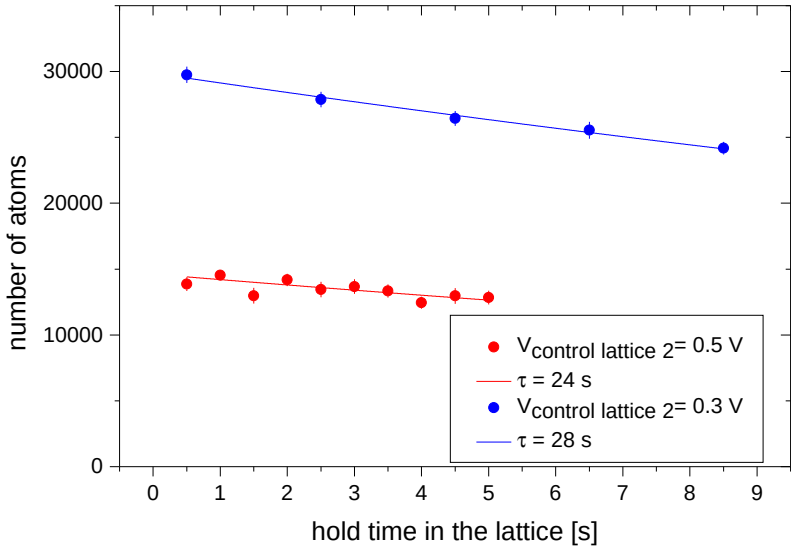

Figure 4.7: Particle number of a single component Fermi gas as function of hold time in our square lattice for lattice depths of $V \approx 37\ \mathrm{E}_r$ (red) and $V \approx 22\ \mathrm{E}_r$ (blue). The number of atoms is well described by an exponential decay with a single time constant.

5 Non-Interacting Fermions in a Lattice

The aim of this thesis is to study the superfluid to Mott-insulator transition for strongly interacting bosonic molecules in the 2D lattice. However, also ultracold fermions in optical lattices are interesting. Since these systems can be used as simplified toy models for electrons in solid-state systems. Thus in a first step and to get a better handle on our system, without the complications arising from strong interactions, we performed some measurements with non-interacting fermions. These are produced using the high-field evaporation scheme, described in the previous chapter. This allows us to load a single layer of the SWT, but as we shoot out one component in this scheme we cannot switch on interactions again in the single component Fermi gas, making thermalization impossible.
For (non-interacting) fermions at low temperatures[1] the properties strongly depend on the filling of the highest occupied band. From solid state physics it is well know that if the highest occupied band of a solid is completely filled the system is insulating, as excitation of the electrons to higher bands requires more energy than is (thermally) available and are thus gapped out. On the other hand if a band is only partially filled the electrons can easily be excited to other states inside the band and transport is possible. The system is then in a conducting metallic state. Changing continuously from a band insulator to a metallic state is impossible in a solid, but can be done with a fermionic quantum gas in an optical lattice [Köh05] by either changing the number of atoms in the trap or by tuning the overall lattice confinement.
Both methods allow for obtaining the right filling of one particle per spin and lattice side required for a band insulator. For non-interacting systems the occupation of the different bands can be probed using a so-called band mapping technique [Köh05, Gre01].

5.1 Band Structure

The occupation of different quasi momentum states in different bands is obtained by turning off the confining lattice potential slowly compared to the trapping frequencies of the single lattice sites[2]. Thereby the quasi-momentum states are adiabatically mapped to the free-particle momentum states and the occupation of the bands is conserved [Kas95]. Afterwards the particles expand freely to make the momentum

[1] The temperature must be smaller than the band gap.
[2] The ramp down must be fast enough that no redistribution of atoms inside the trap is possible, i.e. faster than the overall trapping frequency.

distribution visible and are imaged after time of flight. This allows for obtaining the quasi-momentum distribution. Hence, particles in the lowest band of the 2D lattice are mapped to states in the first Brillouin zone. The different Brillouin zones for a 2D square lattice are depicted in figure(5.1).

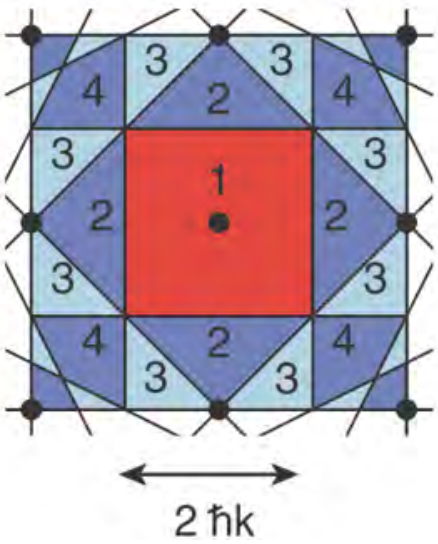

Figure 5.1: The first Brillouin zones of a 2D square lattice in momentum space. The different zones are separated by the Bragg planes. Take from [Gre01].

From this it is now clear that one would expect a round quasi-momentum distribution in the metallic state, if the chemical potential (Fermi energy) lies inside the (first) band. For the band insulator on the other hand, one would expect a squarish top hat quasi-momentum distribution, since all states within the Brillouin zone are occupied with exactly one particle and all other higher quasi-momentum states are unoccupied. This transition can be nicely seen in figure (5.2). Figure (5.2 a) shows the squarish quasi-momentum distribution of a band insulator, whereas in figure (5.2 b) a round Gaussian (Fermi) quasi-momentum distribution is visible. Here the time for the adiabatic ramping down (5 ms) and (free) expansion was chosen such that the best signal was obtained. However, this required short expansion times of only 2 ms and thus the initial cloud size has a significant influence on the imaged density distribution. Therefore, the size of the cloud released from the lattice is twice as big as expected from the momentum spread of the first Brillouin zone and the expansion time[3]. Surprisingly, still a top hat like density distribution is observed, where the rounding off at the edges might be due to the initial size of the cloud, which still matters for these short expansion times and non-adiabaticity at the end of the ramp. This squarish flat top distribution indicates that only the first band of the 2D square lattice is occupied[4] whereas all higher bands are unoccupied and the system is a band insulator, with only the lowest band occupied (compare to figure 5.1). The influence of the initial cloud size is even bigger for releasing from the SWT

[3]This is in relatively good agreement with the initial cloud size with is roughly half as big as the final size.

[4]Also the second Brillouin zone has a quadratic form, but its sides are oriented differently.

(figure 5.2c), due to the smaller trapping frequency and thus larger in-situ size.
Increasing the depth of the lattice potential tightens the overall confinement and decreases the width of the lowest band. Thus at a constant particle number a larger fraction of the system becomes a band insulator with (nearly) full filling of the lowest band. This implies that in the inhomogeneous system one can go from the metallic to the band insulating state for fixed particle number by only tuning the lattice depth, as done here.
The relatively small trapping frequency of the SWT in z-direction of only $\omega_{vert} \approx 2\pi\times$ 5.8 kHz makes it impossible to populate higher bands in the xy-plane of our 2D lattice. This is because of the fact that ω_z is much smaller than the on-site trapping frequency of the lattice in the xy-plane $\hbar\omega_{on-site} = 2\sqrt{VE_R}$, which roughly gives the energy gap between the lowest and the first excited band. As the cold fermions fill up the energy level from the bottom, loading more particles in the lattice only populates higher excited oscillator states in the z-direction orthogonal to the 2D lattice confinement while still all particles are in the lowest band in the xy-plane of the 2D lattice, as particles in the second band in xy-direction would have an additional energy on the order of several 100 kHz.
The band mapping technique is unfortunately not usable for strongly interacting two component Fermi gases. Thus we have no easy tool to probe the transition to a band insulating state of interacting fermions. These we can create by our high-field evaporation scheme and subsequent adiabatically transfer of the molecules into atoms by ramping across the Feshbach resonance. There the scattering length is still large $a \approx -2500\ a_0$ such that the interaction energy is on the order of the trapping frequency in z-direction (see chapter 6.3.2). Thus during the slow ramp down of the potential, scattering leads to redistribution of momenta and the density distribution after time of flight does not reflect the initial quasi-momentum distribution [Nat12].

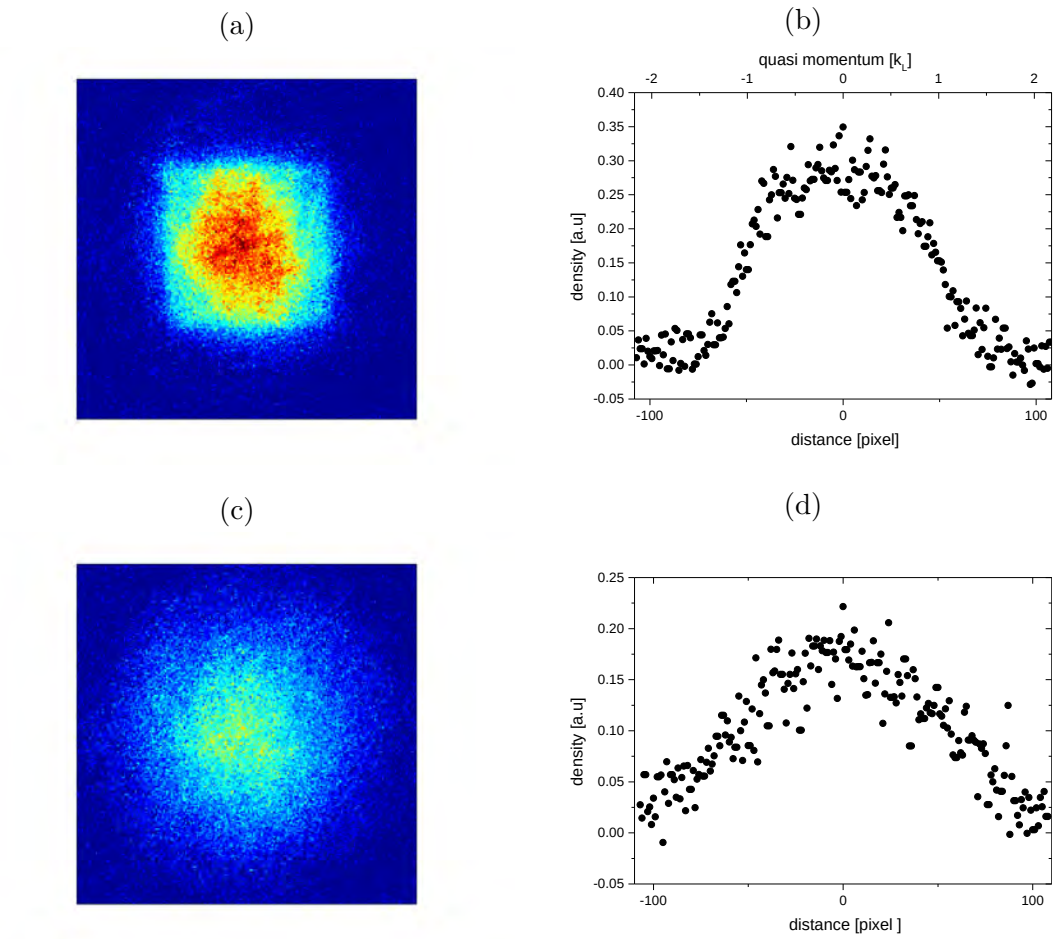

Figure 5.2: (a),(c) Atom distribution obtained from band mapping. The atoms were imaged after adiabatically ramping down the trapping potential for a $V \approx 44$ E_r deep lattice (a) and without lattice from the SWT (c) in 5 ms and subsequent free expansion for 2 ms, for a single component Fermi gas. When releasing the sample from the lattice one obtains a squarish top hat density distribution, reflecting the occupation of the quasi-momentum states in the first Brillouin zone for a band insulator. Note that the images were rotated by 45° such that the lattice 1 direction corresponds to the y-axis. (b) and (d) cuts parallel to the lattice 1 direction through the density distributions of (a) and (c), respectively. Also here a top hat occupation of states is seen when releasing from the lattice, while the sample released from the SWT (d) has a Gaussian shape. Each picture is the average of 13 measurements. The larger size of the cloud released from the SWT is due to its larger initial size, which is not much smaller than the final size and the atomic distribution only approximately reflects the momentum distribution.

6 Reaching the Quasi-2D Regime in the Lattice

In this chapter we investigate the occupation of excited states in the z-direction perpendicular to the 2D lattice (see figure 3.5 for the orientation of the different axes). This is important as in order to minimize complications arising from occupation of excited states in the direction orthogonal to the lattice, we want only a small occupation of the excited level in z-direction perpendicular to the lattice and the sample to be as quasi-2D as possible. Furthermore, the particles in the excited states will not contribute to the coherence and thus are of no interest for studying the superfluid to insulator transition. In the first part of this chapter the method to characterize the occupation of excited states is explained. Then the results obtained for the 2D bulk system, without the lattice are presented. In the last section the occupation of excited states in the tightly confined z-direction in the lattice is discussed.

6.1 Measuring the Occupation of Excited States and the Interaction Energy

Measuring the occupation of excited states in the z-direction and the interaction energy E_{int} is possible by investigating the expansion of the cloud after the release from the trap [Bou03]. The energy of a freely expanding cloud can be deduced from its velocity distribution and thus from its size after a given time of flight.
The energy of the expanding cloud, the so-called release energy E_{rel} is given by [Pit03]

$$E_{\mathrm{rel}} = E_{\mathrm{int}} + E_{\mathrm{kin}}, \tag{6.1}$$

where E_{kin} is the kinetic energy of the trapped system. For small interactions the release energy can be used to deduce the occupation of excited states in z-direction, as the kinetic energy is larger for excited states resulting in a faster expansion. For a particle in the harmonic oscillator ground state the kinetic energy is given by $E_{kin} = \frac{1}{4}\hbar\omega_z$. The potential energy does not contribute to the release energy as it is lost by quickly switching off the trap.
When the cloud flies apart the interaction energy gets converted into kinetic energy directly after the release, when the density is still high. The expansion of the sample released from our trap is very anisotropic and most of the interaction energy is converted in kinetic energy in the tightly confined z-direction, where the gradient of the density is highest. Thus in the following we will only investigate the expansion

in the initially tightly confined z-direction. Thus, the vertical width z of the cloud in the harmonic oscillator ground state after an expansion time τ is

$$z = \tau\sqrt{\frac{\hbar\omega_z}{2m} + \frac{2E_{\text{int}}}{m}}. \tag{6.2}$$

Here the initial size of the cloud of less than 1 μm was neglected. Furthermore, we neglected the acceleration of the atoms due to the anti-confinement produced by the magnetic offset field, as this results in an error of less than 1 μm for the short expansion time used.
Hence measuring the release energy and expansion of the cloud in z-direction allows to measure the occupation of excited z-states for a weakly or non-interacting system. If the system is prepared such that there is negligible occupation of excited states, the release energy can be used to measure the interaction energy.
In the experiment we load the sample in either the SWT or the combined potential of STW and the lattice and image the cloud after a short expansion time τ. Then the radial and vertical size of the cloud are obtained by fitting the atom distribution with a Gaussian. This gives a good estimate for the cloud size after the expansion.

First, we measured the expansion of a non-interacting fermionic sample, produced using the so-called low field evaporation scheme. In this scheme a sample of weakly interacting fermions is produced. During the evaporation in the ODT we ramp down the magnetic offset field to 300 G, where the scattering length is negative. This is done before molecules are created. By continuing evaporation with the weakly interacting Fermi gas at a magnetic field, where the scattering length is negative no molecules are created.
This low-field evaporation scheme is less effective than evaporation with bosonic molecules because of the smaller scattering length and Pauli blocking of the Fermions, which limit thermalization during evaporation and thus the achievable temperatures [DeM99].
A second more important problem arises because of the Fermi pressure, which limits the size of the cloud and makes it impossible to load a single layer of the SWT. At reasonable particle number to have sufficient signal to noise at least 3 layers of the SWT are usually loaded [Nei13]. In principle it is possible to remove atoms from the non-central layer, by applying a magnetic field gradient in vertical direction and selectively transferring the population in the other layers in to high field seeking and collisional unstable states (e.g. $|6\rangle$) using a microwave pulse. But this is not fully implemented in our setup yet. Thus the possibility of tuning interactions in a weakly interacting Fermi gas comes at the expense of averaging over different layers. With the sample of free fermions it is possible to go to the zero crossing of the scattering length at magnetic field of 527 G without having any losses, which is not possible for the system in the molecular branch as discussed before.
To measure the release energy of a non-interacting Fermi gas in the ground state, the sample was prepared using low field evaporation. Then the magnetic field was ramped to the zero of the scattering length at 527 G before the release. The particle number and the temperature are such that only the ground state of the z-confinement is occupied. The atoms are released from the SWT and imaged after $\tau = 2$ ms of

expansion.
The expansion width of 24.3 μm of this non-interacting gas yields an trapping frequency of $\omega_z = 2\pi \times 4.4$ kHz, which is roughly 20 % smaller than the value of $\omega_z = 2\pi \times 5.3$ kHz obtained from a trap frequency measurement. This discrepancy is most likely due to a wrong calibration of the magnification, which results in a wrong value for the cloud size. Thus we used the trap frequency measurement to recalibrate the magnification of this camera. The new magnification M_{new} can be calculated from the old magnification M_{old} and the measured z_{old} and expected cloud $z_{new} = 26.4$ μm size as

$$M_{\text{new}} = M_{\text{old}} \frac{z_{\text{old}}}{z_{\text{new}}} = 1.9. \tag{6.3}$$

This is roughly 10 % smaller than the old value of $M_{old} = 2.0$. Note, that this deviation cannot stem from neglecting the anti-confinement or the initial cloud size or occupation of excited states of the vertical confinement due to temperature, as all these would result in an larger measured cloud size than expected from the free expansion of the ground state. Since the measured cloud size was smaller than the value expected from the calculation and all of these correction would result in a larger calculated cloud size, the deviation is most likely due to a error in the calibration of the magnification. For the following measurements we used this new value of the magnification.

6.2 The 2D Bulk System

In this section we discuss the results obtained for the expansion of a sample released from the SWT without a lattice. This is done as we later us the measurements for a sample released from the SWT to benchmark the measurements performed in the lattice. The measurements presented in this section were already used to show, that the bulk system in the SWT is in the quasi-2D regime for low enough particle numbers [Rie14, Rie15]. Thus we uses these measurements to validate the method of measuring the release energy to estimate the occupation of excited state in the tightly confined direction. This measurement is performed using a relatively weakly interacting two component Fermi gas, at a magnetic offset field of 1400 G, where the scattering length is $a = -2500\ a_0$ [Rie15]. This scattering length is small enough, that from the release energy the occupation of the states in z-direction can be deduced.
If the particle number is such, that the chemical potential μ is smaller than the axial trapping frequency $\hbar\omega_z$, the system should be in the ground state of the z-confinement and the width after expansion is independent of the particle number. If the chemical potential reaches the axial trapping frequency, particles start to occupy excited states and the size of the cloud after expansion increases with particle number[1]. This is nicely illustrated in figure (6.1), where we see that the cloud size is independent of the particle number for up to 60000 atoms. Hence the bulk gas is in the quasi-2D regime for a experimentally feasible particle number.

[1]Note that this argument requires the temperature to be much smaller than the axial trapping frequency.

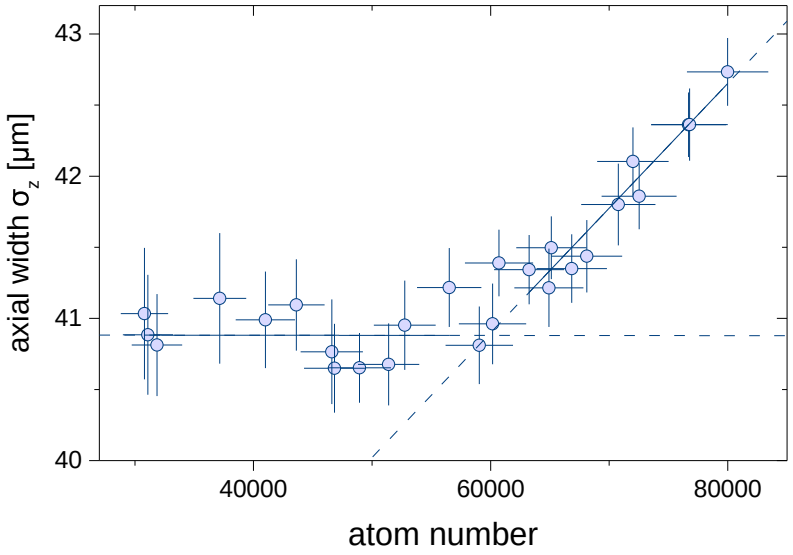

Figure 6.1: Gaussian width of a weakly interacting fermionic cloud, after releasing the sample from the SWT and $\tau = 3$ ms expansion as a function of the particle number. For low atom numbers the system is in the axial ground state and the width after expansion is independent of the particle number, whereas the width increases with the number of particles once the chemical potential is larger than the axial trapping frequency. This allows us to estimate the maximal particle number of approximately 60000 in the quasi-2D regime for the bulk system. Taken from [Rie15].

6.3 The 2D Lattice

As explained in the last chapter increasing the particle number in the lattice populates excited states in the z-direction of the SWT, while all particles stay in the lowest band in the xy-directions of the 2D lattice. This is due to the fact that the on-site trapping frequency $\omega_{\text{on-site}}$ in the radial xy-plane is much larger than the trapping frequency in the z-direction ω_z, which is given by the SWT[2]. Thus it is energetically much more costly to populate the second band in xy-direction of the lattice, than occupying excited states in the z-direction. Furthermore the overall radial confinement is larger in the lattice than in the SWT. In combination with the constant trapping frequency in the z-direction, this decrease the maximal particle number in the quasi-2D regime. Thus it is possible to start with a sample in the quasi-2D regime in the SWT and leave this regime, while ramping on the lattice.
Therefore, we will now examine in more detail how to the lattice confinement influences the occupation of excited states in the tightly confined z-direction. These measurements are compared to similar measurements performed in the SWT without the lattice confinement. First, we will investigate the expansion for non-interacting samples.

[2]The confinement in the z-direction is mainly given by the SWT whereas the contribution from the lattice beams in this direction is neglected, as it changes the trapping frequency ω_z by less than 2 %.

6.3.1 Non-Interacting Gas

In the lattice, the experiment at 1400 G performed in the SWT gives no useful information about the vertical ground state occupation. This is due to the fact, that in the lattice the expansion of the cloud is dominated by the release of interaction energy, already for very small scattering lengths. Thus measuring the release energy does not give us information about the occupation of the trap levels at this magnetic field. This strong effect of the interactions results in an increase of the cloud size with particle number for all particle numbers and no plateau of the expansion is observed. The effect of interactions in the lattice is discussed in more detail in the next section.
Thus interactions have to be completely switched off, when we want to test the increased 'geometric' occupation of the higher excited states due to the additional lattice potential and increase in overall confinement in the radial plane compared to the SWT. The non-interacting sample can be produced in the two different sample already mentioned in the last chapters:

- **Low-field evaporation: two component non-interacting gas** Evaporative cooling is done at a magnetic field of 300 G at negative scattering lengths. This produces a sample of weakly interacting fermions. The interactions can be switched off by ramping the magnetic field to the zero crossing of the scattering length at 527 G. The drawback of this method is, that at least 3 different layers of the SWT are loaded during the transfer. Thus the atom number in a single layer cannot be determined.

- **High-field evaporation: single component non-interacting gas** During the evaporation strongly interacting molecules are created. These are dissociated by ramping to the BCS side of the resonance. Then the atoms in state $|1\rangle$ are removed by a resonant light pulse. This produces a single and thus non-interacting Fermi gas. However, this leads to significant heating of the remaining atom, but allows to load a single layer of the SWT, and therefore to determine the particle number in this layer.

Since this 'geometric' occupation of excited states of the SWT in the non-interacting case depends — for low temperature — only on the particle number, we have to exactly know the particle number in a single layer of the SWT. Thus it is important that only a single layer of the SWT is occupied. Hence we have to use high-field evaporation scheme. However, the removal of the second state considerably heats the remaining atoms. As a result we never observe a plateau of the vertical width as function of the particle number (see figure 6.2). This is true for both the measurement with and without the lattice and the single component gas.
Nevertheless, the expansion from the SWT with and without the lattice confinement can be compared, to obtain an estimate for the additional occupation of excited z-levels due to the lattice confinement. Here, one sees that the sizes after releasing the atoms from the SWT with and without lattice only differ significantly for particle numbers larger than 50000 atoms. This is somewhat surprising as one would expect a deviation to occur for smaller particle number when considering only the radial trapping frequencies of $\omega_{lattice} \approx 60$ Hz for a lattice depth of $V = 7$ E_r and

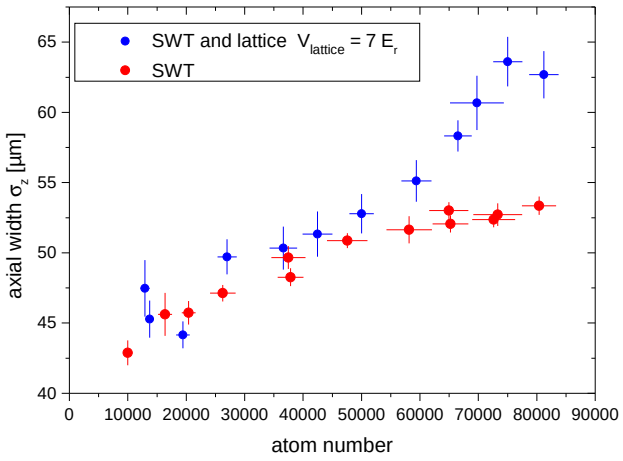

Figure 6.2: Gaussian width of a single component Fermi gas, after releasing from the SWT (red) or the SWT and lattice (blue) as a function of the particle number. For low atom numbers the expansion widths are the same for both systems. However the system is never in the axial ground state due to heating during the removal of the second component. It seems as the heating is increasing with particle number. At higher atom numbers ($\geqq$ 50000) the width increases strongly for the sample released from the SWT and the lattice, whereas it stays nearly constant for the gas trapped only in the SWT.

$\omega_{SWT} \approx 18$ Hz of the system and applying equation (2.7). This, however, is not correct as the additional periodic potential modifies the density of states (in the limit of tight binding each lattice well can be filled with one atom per state). This leads to a higher density in the lattice compared to the bulk gas and more particles fit into the lattice at the same chemical potential.
Also temperature plays a significant role. The removal of component $|1\rangle$ heats the remaining atoms so much, that there are always excited states occupied and the width after the expansion is always larger than expected from theory for a gas in the ground state. Note, that this was not a problem for the band mapping measurements discussed in the last chapter, as the excitation to a higher band of the 2D lattice requires much more energy than excitation of vertical trap levels and thus there is no measurable occupation of these level due to temperature.
As already discussed, producing a non-interacting Fermi gas via low-field evaporation and ramping the magnetic field to 527 G to solve the heating problem would not help us for this measurement as we then load several layers of the SWT and cannot determine the particle number in a single layer.
More generally, also the radial size of the cloud can be used to estimate, whether axial states are occupied. Here we follow the reasoning of the supplementary material of [Rie15]. The energy of a particle sitting at a radial distance r from the trap center has an additional potential energy of

$$E = \frac{1}{2} m \omega_r^2 r^2 \tag{6.4}$$

compared to a particle at the trap center. To have no significant occupation of excited states in the vertical direction (assuming equipartition) the energy of a particle sitting at the edge of the cloud must be smaller than the excitation energy in axial direction (in a local density picture this estimates the chemical potential μ). Thus, from the requirement that the chemical potential is smaller than the axial trapping frequency, one can estimate the maximal cloud radius for a system to be in the quasi-2D regime as

$$r^2 \leq \frac{2\hbar}{m}\frac{\omega_z}{\omega_r^2}. \tag{6.5}$$

For the lattice it is possible to translate this radius to a maximal particle number as the density is limited by one fermion per state and lattice site. Assuming this maximal density, i.e. unity filling of each lattice site inside this radius and no particles outside (which is of course unrealistic as one would expect a smooth density distribution) this gives a upper bound for the particle number of

$$N \leq \pi\frac{r^2}{d^2} = \pi\frac{1}{d^2}\frac{2\hbar}{m}\frac{\omega_z}{\omega_r^2}, \tag{6.6}$$

where $d = 536$ nm is the lattice spacing and the density for unity filling is $\rho = \frac{1}{d^2} = 3.48\ \mu\text{m}^{-2}$. For the parameters of the lattice used for the measurement in figure (6.2), this yields a maximum number of roughly 60000 particles before higher vertical levels get occupied. Which is — considering that these assumptions are not completely justified — surprisingly close to the atom number, where the expansion from the lattice begins to differ from the expansion without the lattice.
The strong increase in radial trapping frequency when turning on the lattice beams limits the possible particle number in the quasi-2D regime, to roughly 50000 atoms. This is on the same order of the value estimated for the bulk gas (see figure 6.1), which has a much weaker radial confinement. This is due to the much larger density of fermions in the lattice compared to the bulk gas.

6.3.2 Interaction Effects

In the last section we have investigated the occupation of excited states in the tightly confined z-direction for non-interacting fermions in the lattice. There we have seen that despite the increased radial confinement of the atoms in the lattice, the system of non-interacting fermions can still be in the quasi-2D regime at reasonable particle numbers, as also the maximal possible density increases. However, having no significant occupation of excited states in the tightly confined z-direction limits the particle number to below 50000.
So far we only considered non-interacting particles, but our main experiments are performed close to a Feshbach resonance with an interacting sample. The interactions between particles can not only change the state of the system, but can also result in the occupation of excited states and as a result of this the atoms can leave the quasi-2D regime. Thus we will have a closer look at interacting systems in the optical square lattice and how the presence of interactions influences the occupation

of excited states.
As a first naive guess for the strength of interactions, the on-site interaction energy U can be calculated using equation (2.42). Furthermore, we approximate the ground state Wannier wave function with a product of Gaussians in each direction, i.e. we assume that the atoms are tightly bound to a single site and the ground state of an atom localized on a lattice site can be approximated by that of a harmonic oscillator. In the xy-plane, the on-site trapping frequency for deep lattices is well approximated by $\hbar\omega_{on-site} = 2\sqrt{VE_r}$, whereas the confinement in z-direction is given by the SWT as the additional confinement provided by the lattice beams is negligible in this direction. This yield an on-site interaction energy of

$$U = \sqrt{\frac{8}{\pi}}\ \frac{a}{a_z}\ h\ \sqrt{E_r V}, \tag{6.7}$$

where $a_z = \sqrt{\frac{\hbar}{m\omega_z}}$ is the harmonic oscillator length in z-direction given by the confinement of the SWT. Even though the approximation of taking the ground state to be Gaussian is not correct and in principle the full Wannier functions have to be used this should give a reasonable result for deep lattices and small scattering lengths [Zwe03]. For our main experiments, described in the next chapter, neither of these two assumptions is true. There, we investigate the transition from a superfluid to an insulating state close to the Feshbach-resonance. Thus for these experiments the scattering length is large and the interesting physics of a transition to the insulating state happens at relatively low lattice depths.
However, to gain better understanding of our setup, we first performed some experiments with weakly interacting fermions in the lattice, where this approximation should give a good estimate of the interaction energy.
To probe the interaction energy in this regime, we load a non-interacting Fermi gas produced by low-field evaporation in a $V = 5.6\ \mathrm{E}_{r,mol}$ deep lattice. The particle number of roughly 30000 is such that only the ground state in z-direction is occupied. At the final lattice depth we turn on interactions by ramping the magnetic field from the zero of the scattering length at 527 G to its final value. Then the atoms are released from the trap and imaged after $\tau = 2$ ms of expansion.
Here we observe that the radial size is independent of the scattering length in the investigated region, whereas the vertical size strongly changes with the scattering length (see figure 6.3). This confirms, that the interaction energy is predominantly released in the tightly confined z-direction, where the density gradient is highest.
Now, assuming that each lattice site is filled with one atom per spin state, the on-site interaction energy can be determined from the release energy. This assumption of one atom per state and site is reasonable as shown below. First, there can be more than one atom per state on only very few sides, as the expansion of the non-interacting cloud is well described by the expansion of a non-interacting gas in the ground state. Thus only a small fraction of atoms can occupy excited state of the vertical confinement. Hence, there cannot be a considerable fraction of sites with more than one atom per state, as the second atom would be in the first excited state of the z-confinement (Pauli principle). Second, we load a balanced non-interacting sample of the same temperature for both spin states. Thus the occupation of the different states in the trap should be approximately the same for both spin states.

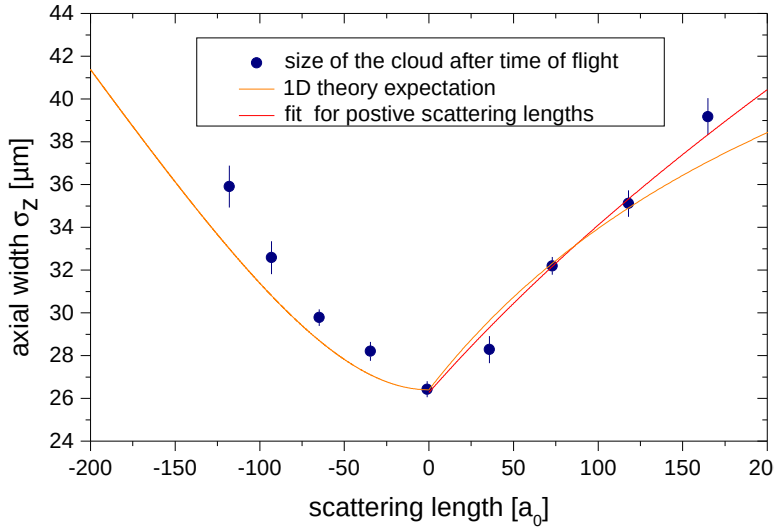

Figure 6.3: Measurement of the release energy. Shown is the Gaussian width in z-direction of a fermionic cloud after releasing from a $V = 5.6\ E_{r,mol}$ deep lattice and $\tau = 2$ ms time of flight for different scattering lengths. For positive scattering lengths the width is fitted to obtain the on-site interaction energy U (red curve). The orange curve gives the expected expansion if one assumes the lattice to consist out of quasi-1D tubes and the interactions are quasi-1D. For negative scattering lengths the expansion of the cloud is well described by taking into account the dissociation of molecules bound in this quasi-1D tubes.

As the filling in the trap center is reasonably high a considerable fraction of sites should be occupied with two particles.
Hence, measuring the release energy should give a good approximation for the on-site interaction energy. For small positive scattering lengths a, the on-site interaction energy U can be approximated by the result from equation (6.7). The size of the cloud after expansion should then be given by

$$z(a,\tau) = \frac{\tau}{\sqrt{m}}\sqrt{\frac{\hbar\omega_z}{2} + 2h\gamma a}, \tag{6.8}$$

where m is the mass of the fermions and $h\gamma = \sqrt{\frac{8}{\pi}}\,\frac{1}{a_z}\,h\,\sqrt{E_r V} = \frac{U}{a}$ gives the on-site interaction energy per scattering length as calculated from equation(6.7). From the fit of this function to the data points for positive scattering length in figure (6.3) the following values of $\omega_z = 2\pi \times 5.2 \pm 0.2$ kHz and $\gamma = 9.1 \pm 0.6$ Hz/a$_0$ are obtained. These are in reasonable agreement, but slightly smaller than the values of $\omega_z = 2\pi \times 5.3$ kHz and $\gamma = 10.3$ Hz/a$_0$ obtained from the trap frequency and lattice depth measurements described in chapter 4.
The smaller measured value of the interaction energy γ for a given scattering length can be partly attributed to our calculation of the on-site energy. Calculating the energy using the Gaussian ground state overestimates the interaction energy U, as the real ground state (Wannier) wave function in the lattice is more extended than

a Gaussian. Another reason for this deviation could be an error in the very rough calibration of the lattice depth.
Due to the large ratio of the on-site trapping frequencies, with a large on-site trapping frequency $\omega_{on-site}$ in the xy-plane and small trapping frequency ω_z in the vertical direction, the system can also be viewed as an array of coupled quasi-1D tubes with weak confinement in the z-direction. For these measurements, viewing the atoms confined on a single lattice sites to be in the quasi-1D regime is a good approximation, as the ratio of the trapping frequencies is $\omega_{on-site}/\omega_z \approx 25$. Thus a quasi-1D theory can be applied to calculate the interaction energy of two particles occupying the same lattice site. For a large aspect ratio of the trap and positive scattering lengths the interaction energy can be calculated via [Idz06]

$$\frac{1}{a} = -\frac{a_z}{a_{on-site}^2}\left(\frac{\Gamma(-\epsilon/2)}{\Gamma(1/2-\epsilon/2)} + \frac{a_{on-site}}{a_z}\zeta(1/2)\right), \tag{6.9}$$

where $\zeta(1/2) \approx 1.46$, Γ is the gamma function and ϵ is the interaction energy in units of the trap energy of the weakly confined direction, i.e. $\hbar\omega_z$ and $a_{on-site}$ is the harmonic oscillator length of a single lattice well in the xy-plane. The calculated values for the cloud size after expansion are shown in figure (6.3) as orange curve for positive scattering lengths and show fair agreement with the measured data. The deviation from the measured values could be due to the fact that our system is more complicated than a single quasi-1D tube. First, the different lattice sites at this depth are still coupled in the xy-plane, with a tunneling rate of several hundred Hz, thus the on-site wave function in the radial plane is not that of a particle trapped in a harmonic potential, for which this theory is developed. This coupling results in a broader wave function in the xy-plane than for a harmonic trap of this trapping frequency. This smaller confinement results in a different interaction energy. Also the large tunneling rate in the xy-plane leads to a more complex system, where the interaction dynamics of two atoms on a single site are mainly along the weak confined z-direction, whereas tunneling and coupling between the sites is along the xy-directions, where the on-site confinement is stronger.
Second, the used theory is developed for harmonic traps, which is not exactly true for our system.
Another possible explanation for the deviation could be errors from the calibration of the lattice depth, which would result in a different on-site trapping frequency and thus interaction energy in these quasi-1D tubes.

The increasing expansion width for negative scattering lengths show that also for negative scattering lengths the released interaction energy is positive. This can again be explained by the fact, that the lattice can be thought of as an array of coupled quasi-1D tubes with weak confinement in the z-direction. In these quasi-1D systems there exists a bound state for negative scattering lengths. Its binding energy ϵ_B is determined by [Idz06]

$$\frac{1}{a} = a_{on-site}\zeta_H(\frac{1}{2}, \frac{\epsilon_B}{2\hbar\omega_{on-site}}), \tag{6.10}$$

where ζ_H is the Hurwitz zeta function. When the trap is switched off, the molecules dissociate, since for negative scattering lengths there exists no bound state in three

dimensions and the system is projected onto the free momentum states. Thus the binding energy is released as kinetic energy. The expected cloud size after expansion for negative scattering length are shown in figure (6.3) in orange and show reasonable agreement with the measured value for negative scattering lengths. However, the calculated cloud sizes lie systematically lower, than the measured values. Again this systematic deviations form the measured values could be due to problems of applying this quasi-1D theory to our more complicated system, as already mentioned above.

Now we will consider a strongly interacting Bose gas of molecules close to the Feshbach-resonance produced via high field evaporation. In the following, we will only consider positive scattering lengths, as our current experiments with the superfluid Bose gas are done with repulsive interactions. From the above discussion it is clear that for small positive scattering lengths $a \approx 100\ a_0$ the on-site interaction energy can be calculated using the simplified ansatz of equation (6.7).
However, this naive picture does not hold for our experiments on the molecular branch. In this regime our system is more complicated due to the combination of the relatively weak confinement in vertical direction and the large scattering length close to the resonance. The on-site interaction energy U for a scattering length $a \approx 1500\ a_0$ (corresponding to the molecule-molecule scattering length[3] at a magnetic field of 732 G where we perform most experiments) is depicted in figure (6.4).

Already for a lattice depth of $V = 3E_r$ one would expect an interaction energy of $U = h \times 8.4$ kHz, which is larger than the vertical trapping frequency. This simple calculation gives not the correct result, since if the interaction energy becomes too large, the wave function should be deformed from the ground state and the approximation of using a non-interacting wave function becomes poor. In this case it is more appropriate to calculate the interaction energy using the quasi-1D theory described above. The so obtained values for a molecule–molecule scattering length of $a = 1500\ a_0$ are depicted in figure (6.4) in orange and are lower than the interaction energy calculated in the naive approach and the vertical trapping frequency.
The above mentioned deformation of the wave function reduces the interaction energy at the cost of increasing the kinetic energy. The energy gained from this admixture of excited trap levels should be on the order of the energy scale of the trap, i.e. the trapping frequency in the weakly confined direction and thus limiting the gained energy to the same scale. Busch et al. [Bus98] analytically calculated the energy and wave function of two particles with contact interaction in a harmonic trap and indeed observe that turning on interactions results in admixture of excited trap levels. The maximum change in energy when going from zero to infinite strong interaction is given by the trap energy in the weakly confined direction, which in our case is $\hbar\omega_z$ [Bus98, Idz06].
However, also the so calculated values have to be taken with caution, as these calculations are done for harmonic potentials with constant level spacing, which is not

[3] The scattering length was obtained from the atom-atom scattering length and equation (2.19). However, this might not give the correct result for the deformed molecules in the elongated tubes.

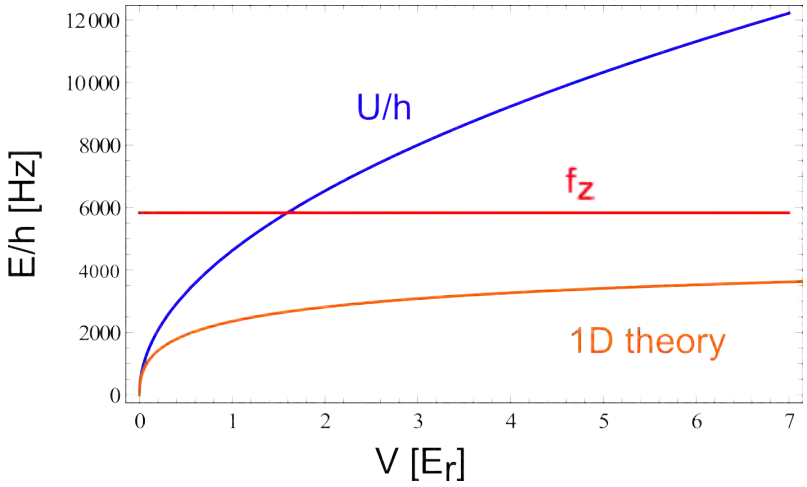

Figure 6.4: Interaction energy U calculated from equation (6.7) (blue) and from a quasi-1D theory (orange) as function of the lattice depth V, for a scattering length of $a = 1500\ a_0$. The trapping frequency in z-direction (red) is independent of the lattice depth as it is mainly given by the SWT confinement. Already for a small lattice depth of $V = 1.5\ E_r$ the interaction energy calculated this way becomes larger than the vertical trapping frequency and thus does not describe the interaction correctly. Furthermore, the calculated interaction energies should give a good estimate only in deep lattices, at least deeper than $3\ E_r$. Thus the naively calculated interaction energy U using equation (6.7) completely fails to describe the system.

true for our potential given by the interference of laser beams. Since the potential has a sinusoidal shape, the level spacing is decreasing for the excited states, especially when considering the small depth of the potential of the SWT of roughly $V_{SWT} \approx h$ 50 kHz [Nei13]. Thus the used quasi-1D description does not give a good estimate, when many excited levels are expected to be occupied.
As mentioned above our system is even more complicated as the lattice sites are coupled due to the tunneling in the 2D lattice. Thus, the dynamics are mainly taking place in the 2D plane, and not along the weakly confined direction of the tubes. Furthermore, the molecules consist of two fermions and it is unclear, whether the interaction can be described by the interaction of the two molecules or if also the internal structure of these molecules has to be taken into account.
However, the effect that these strong interactions in the lattice lead to occupation of excited vertical trap levels can nicely be seen in figure (6.5). Here, we performed the same measurement as for the non-interacting system and looked at the vertical expansion of the cloud as a function of atom number for releasing from the SWT and from the SWT plus the lattice at a magnetic offset field of 732 G. The vertical cloud size after 3 ms expansion is significantly larger when releasing from the lattice for all particle numbers. This indicates an increased occupation of excited trap levels due to the additional lattice confinement, where in double occupied sites the large interaction leads to occupation of excited states of the vertical confinement. The

fact that the expansion width follows the lattice depth very quickly compared to the overall radial confinement on a time scale of less than 1 ms indicates that this occupation of excited states is local few body physics and does not require transport in the trap.
The expansion width is nearly the same for both shown depths of the lattice potential. It is only slightly larger for the sample released from the deeper lattice. This is in agreement with the on-site interaction energy obtained from the quasi-1D calculations, as at this lattice depth the interaction energy only weakly depends on the potential depth (compare figure 6.4). This interaction induced occupation of excited states in the direction of weakest confinement has already been observed for fermions in a lattice [Köh05].

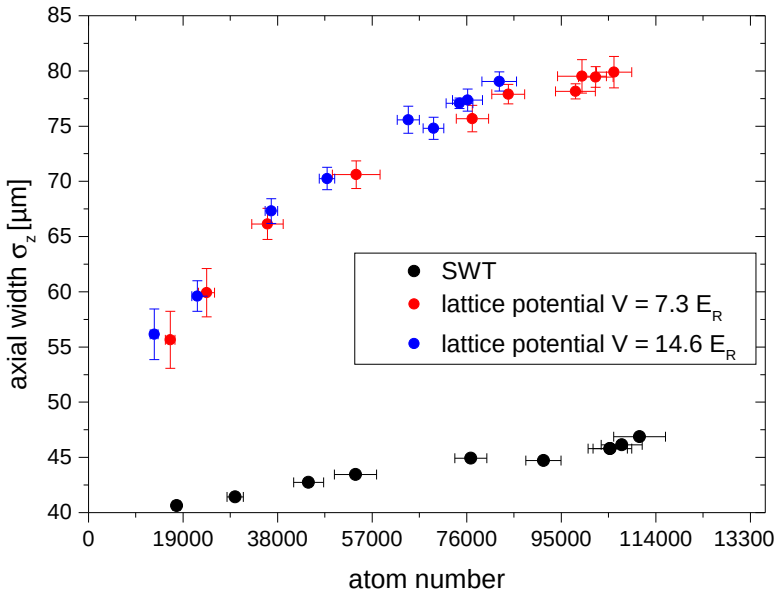

Figure 6.5: Gaussian width of a Bose gas at 732 G, after releasing from the SWT (black) or lattice (blue,red) and subsequent expansion for 3 ms as a function of the particle number. Due to the release of interaction energy the size of the clouds is much larger than the size expected for the expansion of the non-interacting ground state of the potential. Even for low atom numbers the width for releasing from the lattice and the SWT significantly differ. This indicates the increased role of interactions and the interaction induced occupation of higher vertical trap levels in the lattice.

These results have two main implications for our goal of creating a Mott-insulator of molecules. First, the on-site interaction energy can be relatively well described by a quasi-1D theory. However, due to the complicated nature of the system precise calculations to determine the interaction energy are very hard. Thus a good experimental method to precisely determine the interaction energy has to be found. This is crucial as the state of the system in the lattice depends on the ratio of interaction and kinetic energy.
Second, the interaction energy U is on the order the vertical trapping frequency of

the SWT, which can cause occupation of excited states in the z-direction. Thus our system is more complicated than the single band Bose-Hubbard model discussed in the theory section and the system has to be described by a multi band model. Nevertheless the atoms always stay in the lowest band in the xy-direction of the 2D lattice. This makes the system unusual, as the occupation of excited states in z-direction is orthogonal to the xy-directions, where the dynamics take place.

7 Superfluidity in a 2D Lattice

The first experiments investigating the superfluid to Mott-insulator transition in three dimensional systems have been done using weakly interacting rubidium [Gre01]. There the disappearance of sharp peaks in the momentum distribution of the sample was used to determine the transition to the insulating state. In a two dimensional lattice the direct observation of incompressible Mott shells was used to determine the phase transition to the insulating state [Gem09]. The first experiment showing the transition from a superfluid to insulating state in a 3D lattice in the BEC–BCS crossover were done using lithium [Chi06].
In our setup we now want to extend this study of the superfluid to insulating transition for lithium in the vicinity of a Feshbach resonance to a 2D square lattice. Our current progress on loading a superfluid from the SWT in the lattice and reaching a Mott type insulating state is summarized in this chapter. In a first step, the experimental constraints on the loading procedure arising from our setup are discussed. In the second part the superfluid in the lattice is characterized and preliminary results on a transition to an insulating state are presented.

7.1 Constraints on the Loading Procedure

Loading only a single layer of the SWT makes it possible to access the total particle number and density distribution in this layer without averaging. This makes it, in principle, possible to observe Mott shells of constant density [Gem09], when averaging over several 2D systems with different densities and thus degeneracies is avoided.
For our experiment this comes at the expense of a small vertical trapping frequency, which is linked to the large distance of the different layers of the SWT. Since with our current scheme the loading of a single layer is only possible for bosonic molecules close to the Feshbach resonance, also the scattering length is large. Tuning to smaller scattering lengths is not possible, as there the molecules become collisionally unstable, if the scattering length becomes too small as discussed in chapter 2.2.
For the 2D bulk system this is not a problem, but in the lattice this combination leads to excitations in the vertical direction, making our system more complicated than a simple single band Hubbard model. As a compromise between not too large scattering lengths and not too big heating rate due to loss at small scattering lengths, we decided to load the lattice at a magnetic field of 730 G. There the molecule–molecule scattering length is approximately 1500 Bohr radii and the system is still sufficiently long lived. Later, we want to extend this measurement over the whole crossover to the fermionic side as done for a 3D lattice in [Chi06].
The problem of the strong interactions and small trapping frequency vertical to the

lattice potential could be solved by increasing the vertical confinement using a different setup for the interfering beams or a light sheet to produce the 2D confinement. This would require a major change of the setup and has therefore not been done so far.
The problem of the strong curvature of the overall confinement due to the lattice beams, as discussed in section 6.3.1, was (partly) solved by increasing the focal spot size, which decreases the curvature of the trapping potential created by the lattice beams. This was achieved by replacing the last f = 300 mm lenses which focus down the ingoing lattice beams onto the atoms with f = 500 mm lenses. The new lenses were shifted in a way that the focus position did not change. This increases the focal spot size by a factor of 5/3 and thus reduces the overall confinement trapping frequency by a factor of $(5/3)^2$. As the retro-reflected beam is imaged back onto the atoms by the two lenses after the chamber (see figure 3.4), only the lenses in the ingoing beam path had to be changed while leaving everything else untouched. The results of the calibration of the lattice depth and the overall confinement, which were done in the same way as discussed in chapter 4, are summarized in table 7.1 and figure (7.1). The calibration factor for the power between the two lattice arms needed to create potential of the same depth in both directions is $V_{lattice1} : V_{lattice2} = 2.36 : 1$. This is larger than the value obtained in the previous measurement. Partly this is due to slight misalignment of lattice beam 1. As lattice beam 1 was not perfectly aligned with the atoms the Kapitza–Dirac scattering probed only the lower intensity wing of the laser beam. Thus the central depth of the lattice potential should be higher than the value obtained from this calibration. For the data presented in this chapter, this has not been fixed, since we also had issues with the transfer of atoms from the MOT to the ODT. These have been solved while this thesis was written and we will hopefully be able to perform more experiments with a well aligned lattice and obtain a better understanding of the system soon.

lattice	control voltage [mV]	lattice depth V [kHz]	lattice depth V [E_r]
1	1320	153	10.5
2	650	178	12.2

Table 7.1: Calibration of the lattice depth V as function of control voltage for the new setup after changing the lenses. The lattice potential is roughly a factor of 4 smaller for the same power, which is more than the factor of $(5/3)^2 \approx 2.8$ expected from the different spot sizes. Part of this deviation might be due to non-perfect alignment. Again the lattice depth is just a rough estimate, as for a more reliable calibration, data at different intensities has to be taken.

As expected the depth of the lattice potential is smaller with the new setup and thus limits the maximally achievable lattice depth. However, with our experimental setup we can put up to roughly 7 W of power in each beam. This yields a lattice depth of up to $V \approx 50\ E_r$. This is sufficient for most of the planned purposes, as this

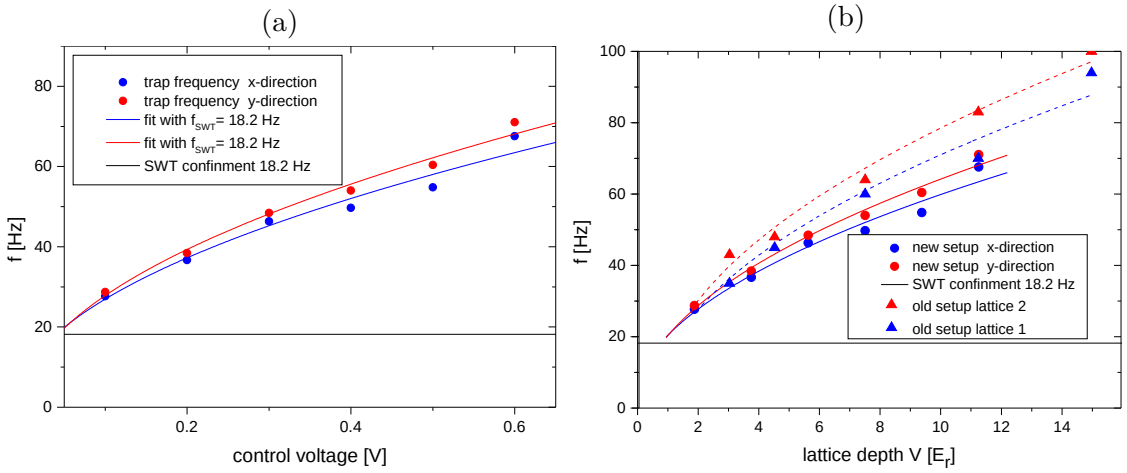

Figure 7.1: Overall confinement trap frequency as function of the lattice depth. (a) For the new setup as function of the control voltage. (b) Trap frequencies of the new (dots) and old (triangles) setup as function of the lattice depth. The power was set such that the central lattice depth is the same in both directions. The black line indicates a trap frequency of 18.2 Hz provided by the SWT and magnetic offset field saddle. The lines are fits to the data, as described in chapter 4. At the same lattice depth, the trapping frequencies of the new setup are smaller than in the old setup. The different trapping frequencies in both directions might partly be due to a wrong relative calibration from the Kapitza–Dirac scattering and non-perfect alignment.

allows to freeze particles on single sites with a tunneling rate of less than 1 Hz. The new lenses make the lattice potential more homogeneous, i.e the change in the depth of the periodic potential between different lattice sites is smaller. Also the overall confinement is smaller at the same central lattice depth. Thus, at the same lattice depth the maximal possible particle number in the quasi-2D regime is larger, which enhances the signal-to-noise ratio. In the next step we loaded a strongly interacting superfluid of bosonic molecules into this lattice and studied its properties.

7.2 Superfluidity in an Optical Lattice

7.2.1 Probing the Momentum Distribution

Our main observable to probe the state of the system is the momentum distribution, which is obtained using the T/4-imaging which was described in chapter 3.8.1 and in [Mur14]. The transition to the superfluid is signaled by a peak in the momentum distribution [Rie15]. This peak originates from the macroscopic occupation of the low momentum states in the condensed phase.
For a superfluid in a lattice, the observed momentum distribution shows additional peaks at distances corresponding to the lattice momentum k_L from the central peak, as can be seen nicely in figure (7.2). This can easily be explained by the fact that the

low quasi-momentum states of the lowest band are macroscopically occupied in the superfluid phase. These states are a superposition of plane waves, whose momentum differs by a multiple of the lattice momentum (see equation 2.33). When the trap is now switched off the wave function is projected on these free momentum states, which then after time of flight are visible as distinct peaks at positions corresponding to the lattice momentum.

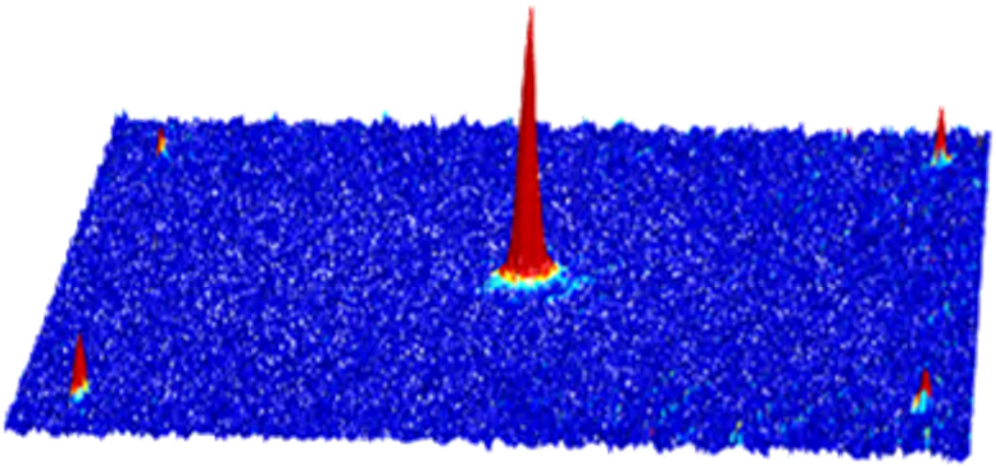

Figure 7.2: Momentum distribution of the atoms as obtained from T/4-image of a superfluid in a V = 4.5 E_r deep lattice. In the momentum distribution additional peaks at the lattice momenta are visible. The different visibilities of the four peaks are most probably due to inhomogeneities of the imaging light beam at these large distances of roughly 1 mm from the beam center. Furthermore, the peaks along different lattice axes have different visibilities due to different lattice depths along the two directions. They stem from the previously mentioned systematics in the calibration of the lattice depth. The picture is the average of 17 single images.

Experimentally it is hard to detect these additional peaks at the lattice momenta, due to the relatively small number of less than 1000 atoms per peak. The signal is further reduced by scattering at the beginning of the time of flight expansion, as the fast particles with lattice momentum have a large transverse velocity and thus scattering rate. This problem of scattering particles out of the peaks was solved by quickly ramping the magnetic field to 527 G, close to the zero of the scattering length before releasing the cloud from the lattice[1]. Furthermore, we turn off the SWT 50 μs before the lattice is turned off. Thus the atoms expand in vertical direction, which drastically reduces the density and scattering rate, while the lattice confinement is still on. The initial tight vertical confinement leads to a fast expansion and a quick drop of the density. This quenches the interactions much more

[1]Note that this magnetic field ramp is to significantly smaller fields than the ramp for the measurements in the 2D bulk gas.

efficiently than in a 3D lattice, where the same scheme was used [Chi06]. The less efficient quench of interactions in the 3D system is due to the much slower decrease of the density, after the release of the atoms from a 3D trap. For shallow lattices the particles are delocalized over several lattice sites and the expansion after the release is determined by the weak overall 3D confinement. For deep lattices the particles localized on a single site have large momentum and quickly expand after the release, but this does not lead to a quick drop in density, as they cross particles released from the other layers of the lattice.
Since the enhanced role of interactions in the lattice leads to population of vertically excited states of the SWT, it also increases the vertical cloud size after time of flight. This causes — due to the limited depth of focus — a worse signal compared to a sample released from the SWT without the additional lattice potential. To solve this problem a stopping pulse was applied as described in chapter 3.8.2. Without this the additional peaks at the lattice momenta are very difficult to resolve.
In principle, there should also be peaks corresponding to multiples of the lattice momenta visible. But, with the used matter-wave focusing technique they are outside the field of view of our camera. One could use a shorter expansion time, but still they would be hard to detect, as their relative weight is much smaller. This is because of their smaller admixture to the lowest band quasi-momentum states. Furthermore, the signal would be even worse, as for shorter time of flights the width of the peaks is larger. This is due to the much larger size of the in situ density distribution compared to the momentum spread of the superfluid (see figure 4.3).

From the momentum distribution we extract three quantities to characterize our system. The number of condensed/superfluid atoms in the central peak N_c, the thermal atoms in the central peak $N_{thermal}$ and the number of atoms in the side peak N_p as depicted in figure (7.3).
The atom number is determined by first summing up the signal of the image along the x-axis. The obtained integrated density profile is then fitted. To account for the bimodal structure of the central peak with a thermal and superfluid part (see figure 7.3 c), it was fitted with a sum of two Gaussian distributions. The number of atoms in a side-peak N_p is extracted fitting a single Gaussian distribution to the integrated density profile. This is done because, the thermal atoms around the side peaks are not distinguishable from the background. Thus we assume that all the atoms in the side peak are superfluid.
Due to imaging imperfections the visibility of the side peaks is different. Only the best visible upper-right side peak was fitted, as it is often the only one which can be clearly distinguished from the noise. As we believe that the observed differences in the particle numbers in the peaks are due to the imaging process, we assume the number of particles to be the same in all side peaks.
We choose fitting instead of summing up different pixels to extract the particle number due to the noise and fringes on the images. We fit the peaks in the direction orthogonal to the fringes to reduce their influence on the extracted values. In the future, the effect of technical noise and fringes could be reduced by applying a fringe removal algorithm [Ock10]. The signal-to-noise ratio is further improved by averaging several pictures before fitting.

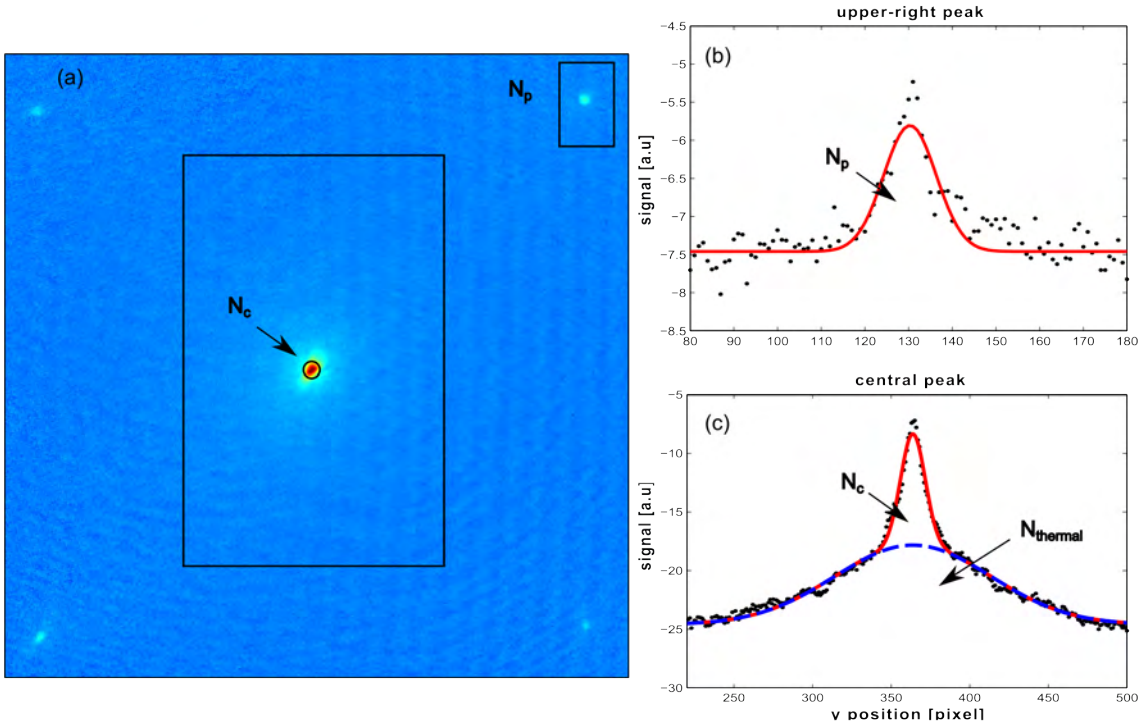

Figure 7.3: (a) Momentum distribution of a superfluid released from a V $\approx 3.8\ E_r$ deep lattice. It was obtained using T/4-imaging. (b) Optical density summed along the x-axis around the upper right peak, which is fitted with a Gaussian to obtain the number in the side peak N_p. (c) Optical density summed along the x-axis around the central peak, which is fitted with a double Gaussian to obtain the atoms in the condensed N_c and thermal part $N_{thermal}$. The image is the average of 130 single images.

7.2.2 Optimization of the Loading Scheme

In a first step, we optimized the speed at which the lattice potential is turned on. On one hand the ramp speed should be as large as possible, because a short loading time reduces heating of the sample due to technical noise and photon scattering. On the other hand the ramp speed has to be small enough such that it is adiabatic with respect to excitation of higher oscillator states and bands. For our system, this means the ramp time of the lattice must be adiabatic with respect to the vertical trapping frequency of the SWT.
For the current setup the more important problem limiting the ramp speed is the difference in the initial and final density distribution, shown in figure (7.4). This difference leads to significant redistribution of particles during the lattice loading, which has been identified as the major source of heating during the loading of an inhomogeneous lattice [Dol15]. Hence, the ramp must be slow enough to allow for

transport during the loading of the lattice. The time scale for transport is difficult to estimate in a lattice, since tunneling and transport are hindered by the lattice. Most probably, this limits the maximal possible speed for ramping on the lattice.

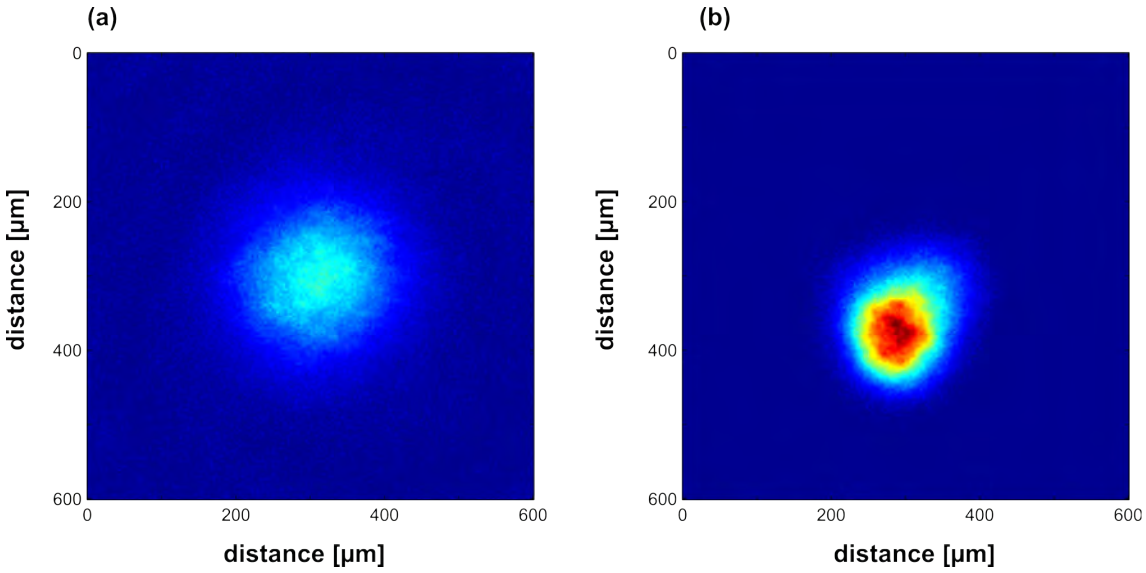

Figure 7.4: Density distribution of bosons in the SWT (a) and in a V $\approx$ 4.5 E_r deep lattice (b). The cloud in the lattice is significant smaller due to the increased overall confinement in the lattice. The different positions of the cloud and the halo visible in the upper-right part of the cloud in the lattice are due to the discussed slight misalignment of the lattice beams. Also the density in the lattice is much higher. Each picture is the average of 30 measurements.

Experimentally, finding the best ramp speed was done by ramping to the same lattice depth with different speeds and looking at the number of condensed atoms in the central peak N_c and in (upper-right) side peak N_p. As we always start with the same initial system and ramp to the same final lattice depth, these atom numbers give a measure for the coherence. Hence, we can use them as a measure for degeneracy and thus temperature.

Starting from a condensed sample in the SWT, we linearly ramp the power in the lattice beam to the same final depth with a variable speed. Afterwards we give the system 10 ms to equilibrate and then probe its momentum distribution.
The thus obtained number of condensed particles in the central and upper-right side peak for a V $\approx$ 3.8 E_r deep lattice are depicted in figure (7.5) as a function of lattice ramp speed. The number of condensed atoms is relatively insensitive to the ramp speeds at moderate values. For low ramp speeds ($\leq$ 0.04 E_r/ms) the number of condensed atoms quickly drops. Because of the long time required to load the lattice at this ramp speeds technical noise and photon scattering lead to significant heating and loss of coherence. For all further experiments, we chose a ramp speed of $dV/dt = 0.08\ E_r$/ms, which also gave the largest number of condensed atoms, when

ramping to different final lattice depths. In order to further optimize the loading of the lattice one can try different functional forms. However, this will not solve the problem of the different initial and final density distributions, which we believe to be the main source of heating [Dol15].

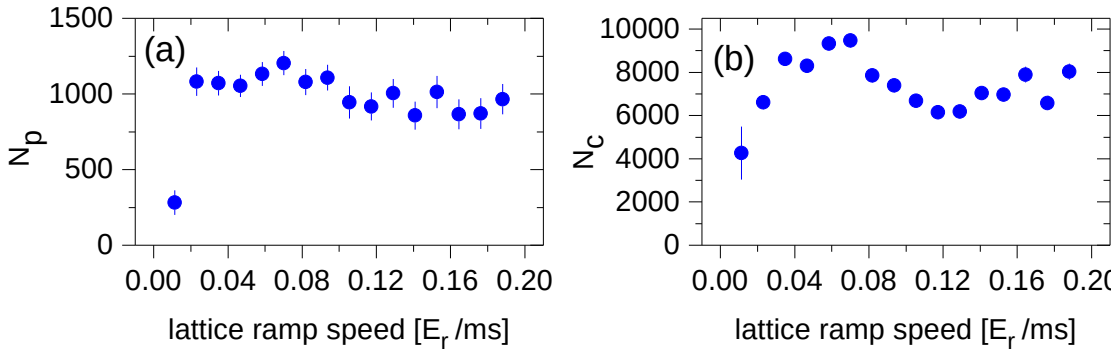

Figure 7.5: Number of condensed particles in central N_c (b) and upper right side-peak N_p (a) for a final lattice depth of V $\approx$ 3.8 E_r as a function of the ramp speed. For all further experiments we chose a ramp speed of $dV/dt = 0.08\ E_r$/ms, where the number of condensed atoms is maximal. Each data point is the average of 130 single runs and the errors are the errors of the fit.

To make sure the heating rates in the lattice are low enough to perform experiments in the superfluid phase, we tested the lifetime of the coherence for different depths of the lattice potential. For this we loaded a superfluid into the lattice and looked at the number of atoms N_p in the side peak after a variable hold time. This is shown in figure (7.6) for different depths of the lattice potential. The lifetime of the coherence is only on the order of tens of ms and limits the time available for experiments before heating out of the superfluid into the normal phase. Nevertheless, it should still be possible to perform experiments due to the large tunneling rates[2] of several hundred Hz at these lattice depths, before the coherence is lost. The lifetime of the coherence is decreasing for deeper lattices indicating larger heating rates. Another explanation for this could be the increased occupation of excited states in z-direction for deeper lattices, as discussed in section 6.3.2. This might also lead to loss of coherence. Note that the lifetime of the coherence is roughly a factor 100 smaller than the lifetime of non-interacting particles (see chapter 4.3). This indicates that the heating rate is higher for these strongly interacting particles and the interactions in our anisotropic lattice lead to a loss of coherence.

[2]The tunneling rates are calculated for the non-interacting system and might be strongly affected by the strong interactions in our system.

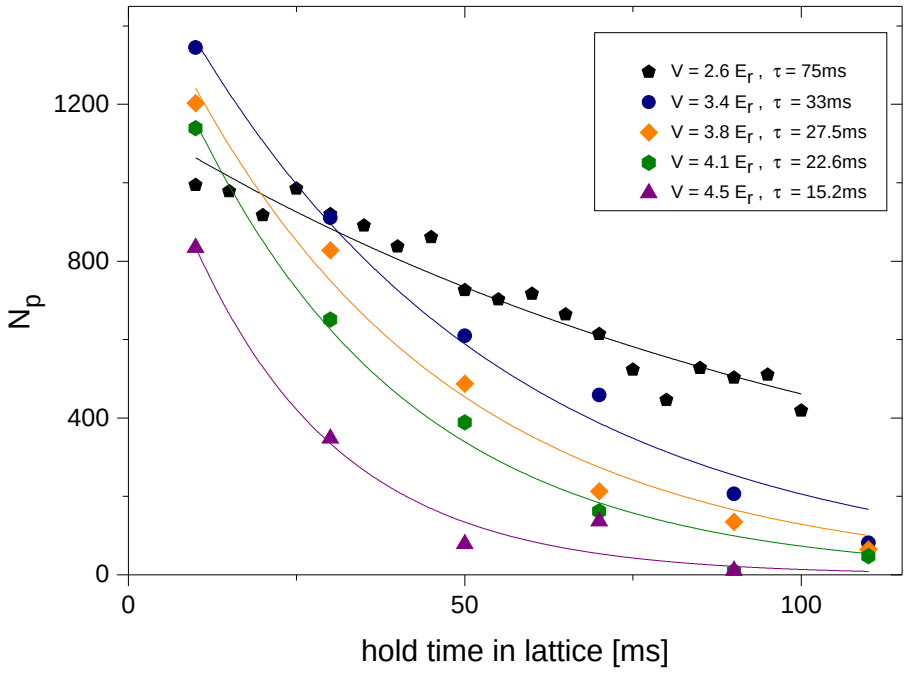

Figure 7.6: To determine the lifetime of the coherence, we measured the number of (superfluid) particles in the upper-right side peak as a function of the hold time in the lattice for different depths of the lattice potential. The half-life time τ of the coherence is strongly dependent on the depth of the lattice. The atom number as a function of the hold time is well described by an exponential decay, which we used to determine the lifetime of the superfluid.

7.2.3 Observation of a Transition to an Insulating State

As our main measurement, we started to characterize the superfluid in the lattice. For this we measured the momentum distribution of the molecules as function of the depth of the lattice potential. First, we investigated the number of atoms (visibility) in the upper-right peak N_p as a function of the depth of the lattice potential. To obtain the best signal we ramped to the final lattice depth and immediately released the sample, in order to not be limited by the finite coherence lifetime. In figure (7.7 a), it can be nicely seen, that at moderate potential depths the particle number in the peak is increasing with the potential depth.
This initial increase of the particle number in the side peaks can be understood by looking at the admixture of the different free space plane waves to the Bloch states with low quasi-momentum (equation 2.33). The admixture of states with lattice momenta to the Bloch states with zero quasi-momentum is increasing with the lattice depth. Thus, the number of particles visible in the side peak is increasing. This is nicely seen, when considering the fraction of superfluid atoms in the side peaks (again taking all atoms in the side peaks to be superfluid) on the total number of

superfluid atoms, which is given by

$$f_{\text{peaks}} = \frac{4 \cdot N_p}{4 \cdot N_p + N_c}. \tag{7.1}$$

Here, we assume that the number of particles in the other side peaks is equal to the number in the upper-right peak. The fraction of atoms in the side peaks f_{peaks} is depicted in figure (7.7 b) and monotonically increases with the depth of the lattice potential up to a lattice depth of V $\approx 6\ E_r$, where N_p quickly drops and the atoms in the side peak cannot be distinguished from the background, signaling a loss of superfluidity.

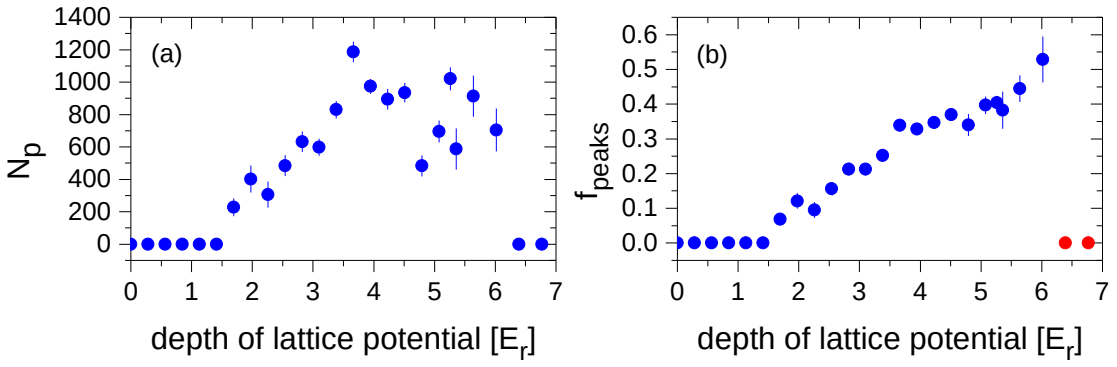

Figure 7.7: (a) Number of (superfluid) particles in the upper right side-peak N_p as a function of the depth of the lattice potential. For potentials smaller than V $\approx 1.5\ E_r$ or larger than V $\approx 6\ E_r$ no signal above the background is visible. The fluctuations in N_p at large lattice depths are due to fluctuations in atom number and temperature and are not present when looking at f_{peaks}. (b) Fraction f_{peaks} of condensed atoms in the side peaks as defined in equation (7.1). The fraction of superfluid atoms in the side peaks increases with the depth of the lattice potential up to a depth of V $\approx 6\ E_r$, where the superfluid fraction quickly drops and no more side peaks can be observed (red points).

For deeper lattices, the side peaks (Fig. 7.7 a) quickly disappear. To investigate this in more detail we look at the and the fraction of condensed atoms

$$f_{\text{coherent}} = \frac{N_c + 4N_p}{N_{\text{total}}} = \frac{N_c + 4N_p}{N_c + 4N_p + N_{\text{thermal}}}, \tag{7.2}$$

shown in figure (7.8). For deeper lattices f_{coherent} decreases and becomes zero at a central lattice depth of V $\approx 6.5\ E_r$. This we interpret as the transition from a superfluid state, with long range coherence and thus visible interference peaks in the momentum distribution, to an insulating state, with no phase coherence between atoms on different lattice sites. However, the disappearance of the interference peaks

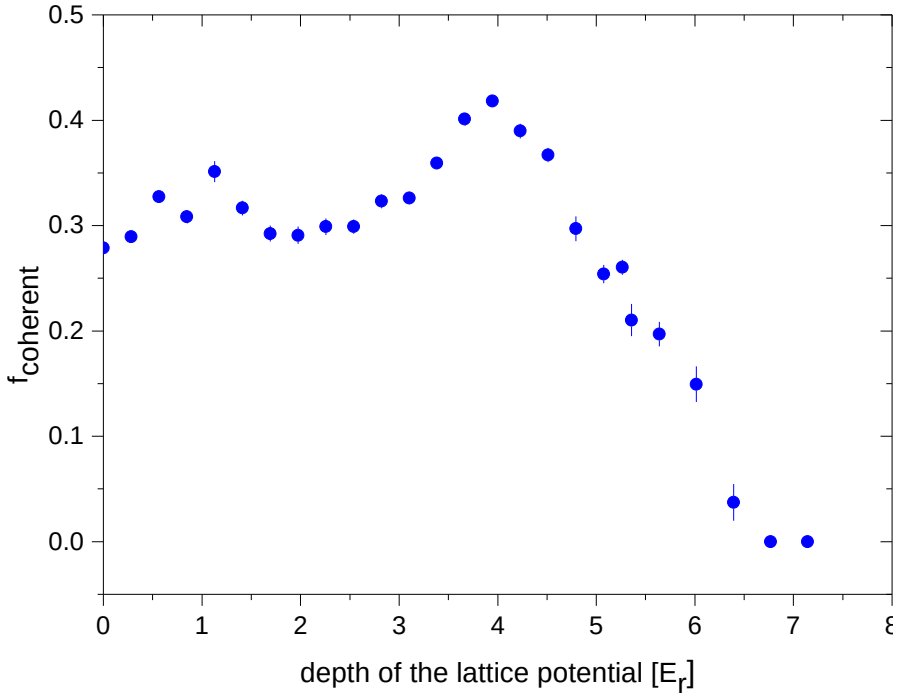

Figure 7.8: Coherence in the lattice. Depicted is the fraction of superfluid atoms f_{coherent} as a function of the depth of the lattice potential. f_{coherent} increases with the depth of the lattice up to a potential depth of V $\approx 4.5\ E_r$, where the superfluid fraction quickly drops and reaches zero at a lattice depth of V $\approx 6\ E_r$. The data points are obtained from the average of 130 single experimental realizations.

could also be due to heating in the lattice, especially when considering the short lifetime of the coherence. Furthermore, loss of coherence could be caused by the occupation of excited states in vertical direction. These states do not contribute to the coherence, but get populated when increasing the depth of the lattice potential, as the overall radial confinement also increases.
The finite width of the decrease of the superfluid fraction f_{coherent} is most likely due to the inhomogeneity of the lattice. As the depth of the lattice potential is decreasing with distance from the center (for a sketch see figure 4.1) the sample becomes first insulating in the center, while still being superfluid in an outer ring. By increasing the central lattice depth, this ring shrinks until the whole sample is inside the insulating regime. Then one would place the critical central lattice depth rather at a lower value of V $\approx 5\ E_r$, where the superfluid fraction begins to decrease. To clarify the cause for the complete loss of coherence at a lattice depth of V $\approx 6.5\ E_r$ we performed the measurements described in the following.
One method to elucidate the type of phase transition is to investigate the reoccurrence of coherence when ramping down the lattice potential from a depth, where no coherence is present to a depth, where initially coherence was present. This was done in the first experiments observing the superfluid to Mott-insulator transition [Gre01] and for the experiments in the BEC–BCS crossover in a 3D lattice

[Chi06]. If the loss of coherence is due to a quantum phase transition, i.e. because of a transition to a Mott-insulator type state and not due to heating out of the superfluid phase or loss of coherence due to occupation of excited states, the coherence and the interference peaks in the momentum distribution reappear on a very short time scale on the order of the tunneling rate [Gre01, Chi06], when ramping down the lattice.
To perform this measurement, we ramp into a $V = 6.8$ E_r deep lattice, where no coherence is visible and hold the system there for 5 ms. Afterwards, we quickly ramp down the lattice in 1 ms to its final depth V_{probe}, where the system can equilibrate for another 4 ms and then probe the momentum distribution via T/4-imaging (see figure 7.9 for a sketch).

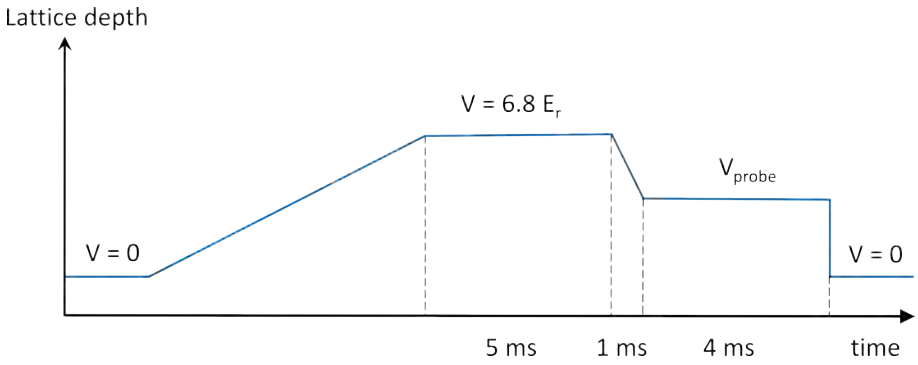

Figure 7.9: Illustration of the timing graph used to probe the reappearance of coherence when ramping down from a deep lattice to a variable final lattice depth V_{probe}.

When releasing the atoms directly from the $V = 6.8$ E_r deep lattice, no peak can be distinguished from the background in the momentum distribution (see figure 7.10 a), whereas if the lattice is ramped down to $V_{probe} = 3.1$ E_r a peak in the momentum distribution can be observed (figure 7.10 c).
To obtain a more quantitative understanding, we investigated the integrated momentum distribution. There, for the sample released from the $V = 6.8$ E_r deep lattice a very broad distribution is observed (7.10 b). This is most likely due to the localization of the particles on the lattice sites. Then the momentum spread corresponding to this localization would be larger than the momentum difference of the peaks in the superfluid regime. Thus the cloud would be larger than the distance of the different momentum peaks visible in the superfluid regime. This would lead to the observed effect, that the distribution is extremely broad and the width of the cloud in T/4-imaging is larger than the imaging region. Furthermore this broad momentum distribution of the sample shows that there is no phase coherence between the particles on different sites and the system cannot be superfluid.
When ramping down the lattice to $V_{probe} = 3.1$ E_r before releasing the sample, the integrated momentum distribution is bimodal (see figure 7.10 d). This quick reappearance of coherence when ramping down indicates that the loss of coherence is not due to heating out of the superfluid phase, but due to a transition to an insulating state, when the lattice depth exceeds $V \approx 6.5$ E_r.
Despite the reappearance of a bimodal structure after ramping to a shallow lattice,

the fraction of coherent atoms in the a $V = 3.1$ E_r deep lattice, when first ramping into the deep lattice is only $N_c/N_{tot} = 0.17 \pm 0.02$ and thus much lower than the fraction of superfluid particles of $N_c/N_{tot} = 0.33 \pm 0.01$ observed when directly ramping to the final potential depth, without going through the insulating phase. This reduction of the coherent fraction is due to the faster loss of coherence in deeper lattices. This results in the observed smaller degeneracy and superfluid fraction of the sample after the ramp down of the lattice. Partly, this loss of coherence might be caused by the excitation of particles to vertical excited states in the deeper lattice.

Nevertheless, these results hint towards a transition to a Mott-insulator like state. However, further studies have to be performed to unambiguously clarify the nature of the phase transition. For example one could probe the in situ density distribution and look for the appearance of a plateau of constant density, indicating a incompressible and insulating Mott-insulator type phase, as it was done with Cs in a 2D lattice [Gem09]. In a preliminary measurement probing the in situ density, we could not clearly observe a plateau of constant density, but the average densities close to the trap center were higher than expected for unity filling. This indicates that vertically excited states where occupied and the data should be retaken with smaller atom numbers once the experiment is running again.
Even though the reason for the loss of coherence is not fully clear yet, one can compare the potential depth of $V \approx 6.5$ E_r, where no more coherence is visible to the theoretical prediction for the superfluid to Mott-insulator transition in a Bose–Hubbard model. As a first crude approximation, one can take the tunneling rates J calculated in chapter 2.4 and assume that the on-site interaction U between to molecules is given by the quasi-1D theory discussed in section 6.3.2. Then the critical $(U/J)_c$ of 16.2 for the transition to a Mott-insulator for the Bose–Hubbard Hamiltonian [Wes04] would be reached for a lattice depth of $V_{theo} = 10.5$ E_r, which is roughly 40 % higher than the measured value above which no coherence is visible. This deviation is larger than the estimated value of approximately 20 % for the calibration of the lattice depth. However, this calculation is only valid for a weakly interacting single band model, which does not properly describe our system as the scattering length is large and excitations to higher vertical trap levels are possible. Also a previous experiment in the BEC-BCS crossover in a 3D lattice has observed the transition to an insulating state at smaller lattice depths than expected [Chi06]. For this experiment of fermions close to a Feshbach resonance in a 3D lattice a simple multi-band model predicts a transition to an insulating state at lower lattice depths [Zha07] than expected from a simple single band Hubbard model. This is in agreement with our observation. However, there are currently no theoretical predictions describing the anisotropic 2D lattice, such that a quantitative comparison of our system to theory is not possible at the moment.
In the last weeks we fixed the already mentioned stability issues of the experiment, so now we will hopefully be able to unambiguously clarify the nature of the observed transition and further study the condensate and insulator in the lattice.
Another question is whether the fermionic nature of the atoms forming the Feshbach molecules influences our lattice system and affects the phase transition. The influence of this effect will be tested by tuning the magnetic offset field across the

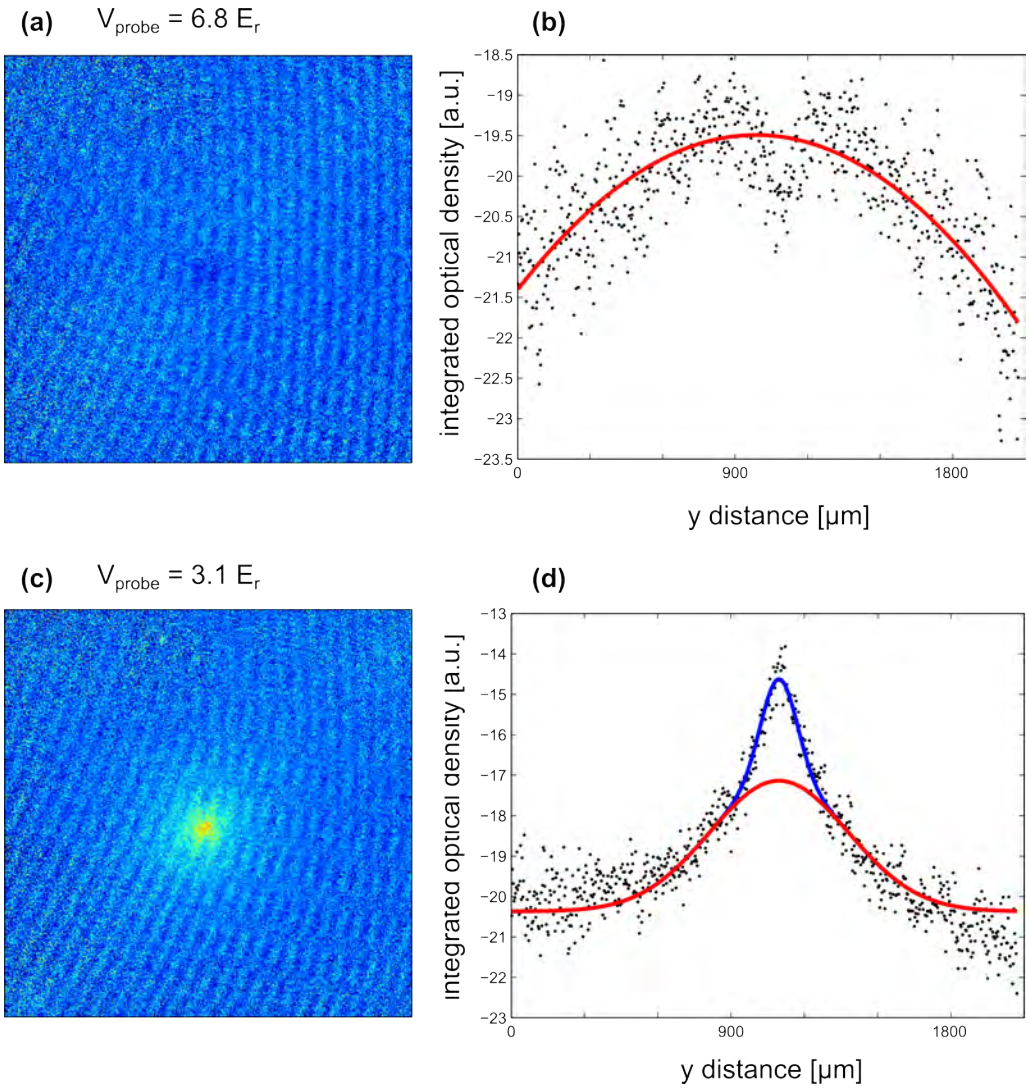

Figure 7.10: Momentum distribution of the atoms released from a $V = 6.8\ E_r$ (a) and a $V = 3.1\ E_r$ (c) deep lattice. The atoms were first loaded into a $V = 6.8\ E_r$ deep lattice. Before the release the lattice depth was ramped down to the final depths of $V = 6.8\ E_r$ (a) and $V = 3.1\ E_r$ (c). (b) and (d) show the corresponding integrated optical densities. After the ramp down to a shallow lattice a bimodal momentum distribution is visible in the integrated momentum distribution (d), whereas the integrated momentum distribution for the $V = 6.8\ E_r$ (b) is a broad Gaussian. This indicates that the loss of coherence in the $V = 6.8\ E_r$ deep lattice is not due to heating. Each picture is the average of 40 measurements.

Feshbach resonance to the fermionic side. This will extend the current measurements of the superfluid to insulator transition over the whole BEC–BCS crossover, where the type of the insulator changes from a Moot insulator (BEC side) to a band insulator (BCS side).

8 Conclusion and Outlook

During the course of this master thesis we combined a two-dimensional optical lattice potential with an existing two-dimensional trapping potential. The square lattice is created by two retro-reflected laser beams. This setup was used to study the physics of strongly interacting particles in a single layer of a 2D square lattice.
To characterize the setup, the depth of the lattice potential was calibrated using Kapitza–Dirac scattering.
Then, starting form a degenerate quasi-2D gas in an anisotropic trap, the particles were loaded into the 2D square lattice. To obtain a better understanding of the single particle processes and heating rates, the first experiments were performed with non-interacting fermions. By applying a band mapping technique, the occupation of quasi-momentum states in the lattice was obtained. We were thus able to observe indications for a transition from a metallic to a band insulating state, when the filling of the lattice was tuned. This was done by increasing the overall confinement such that the density in the trap center increases.
In the next step, the effect of interactions in the lattice was investigated. Because of the large anisotropy of the single lattice wells, where the trapping frequency in the direction orthogonal to the lattice is much smaller than the on-site trapping frequency in the radial plane, the system can be thought of as coupled one-dimensional tubes. Strong interactions in these tubes result in the occupation of excited states in the direction orthogonal to the lattice. Thus our system is not in the usually investigated regime of a simple single band Hubbard model and a multi band theory is necessary to describe our system.
Our main findings were obtained by loading a strongly interacting superfluid of molecules into a 2D square lattice. Using a matter wave focusing technique, the momentum distribution of the sample was measured [Mur14, Rie15]. Here, in addition to the central coherent peak, peaks at the lattice momenta were observed as can nicely seen in figure (8.1). This indicates that the system shows long range coherence over several lattice sites. Thus the system is superfluid, like the bulk gas [Mur15].
Increasing the depth of the lattice potential decreases the kinetic energy compared to the interaction energy. Above a critical value of the lattice depth of roughly $V \approx 6.5\ E_r$, both the central and side peaks in the momentum distribution disappeared, as shown in figure (8.1 c). Thus indicating that phase coherence between different lattice sites and superfluidity are lost at this lattice depth. When ramping down the lattice potential, the coherence partly reappeared on a short time scale, compared to the radial trapping frequency. This hints that the loss of coherence was due to a change of the ground state of the system at this lattice depth and not due to heating. We attribute this change to a transition from the superfluid to a Mott type insulating state, where the particles become localized due to interactions.

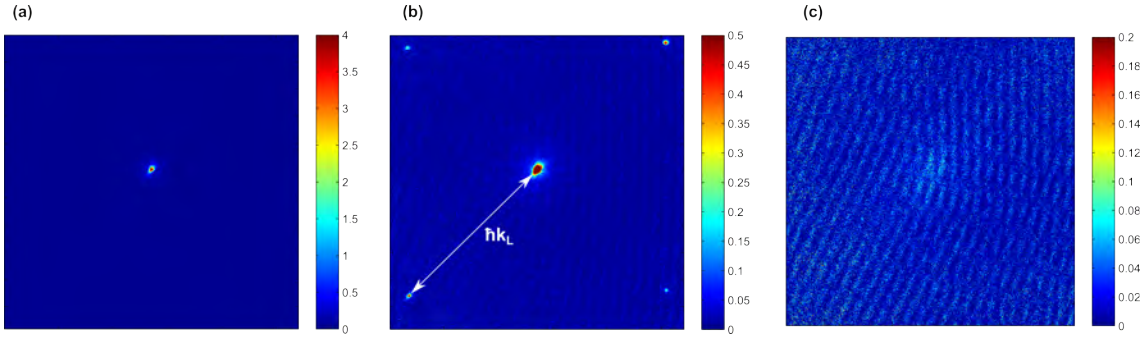

Figure 8.1: Momentum distribution of a superfluid released from the SWT (a) and from a shallow lattice (b) as obtained via t/4-imaging. The sharp peaks indicate long range coherence. The superfluid released from a lattice shows additional peaks at the lattice momenta. The momentum distribution of a sample released from a deep lattice (c) is broad and shows no coherence.

The transition was observed at a lower lattice depth than expected from Bose-Hubbard theory. However, as mentioned above this single band theory is not expected to properly describe our setup.
After these first studies of the system, a further characterization has to be done in the next steps. These experiments are currently performed after we solved some minor stability problems of the experimental setup. With these experiments on the way, we hope to obtain an unambiguous and clear signature of the phase transition to the insulating state soon. Furthermore, the properties of this insulating phase have to be investigated, as they could be different from the predictions for a simple Mott-insulator, as several bands are involved. For example, the compressibility of the insulating phase could be tested using in-situ imaging [Gem09]. For our 2D system this is easily possible, since we have access to the complete density distribution, without averaging over several layers. This would allow to check whether the insulating phase is incompressible as expected if the insulating behavior occurs due to interactions. Additionally the excitation spectrum and the on-site interaction energy have to be investigated in more detail, to obtain a full and clear understanding of this system. Then these studies can be extended over the whole BEC-BCS crossover to observe the transition from a Mott type insulator of molecules to a band insulator of free fermions on the BCS side of the resonance.

For the near future, this insulating state with exactly one molecule per site is also a perfect starting point to explore more interesting physics and accessing systems with a richer phase diagram. Two examples for these systems and possible directions for the experiment are:

- Transferring the molecules into free fermions and tuning the system to repulsive interactions would allow for realizing a Fermi–Hubbard model at very low temperatures and entropy. Then, by changing the filling in a smart way (i.e. lowering the overall confinement or removing part of the atoms), the system can be tuned from a band insulator to a metallic state to a fermionic Mott-

insulator at half filling and potentially low enough temperatures to realize anti-ferromagnetic order. This would be a starting point to investigate the still not completely understood phase diagram of the Fermi–Hubbard model.

- Another interesting system that can be accessed from this insulating state is a three component mixture. This should be possible to realize by starting from an insulator and driving some of the atoms to a third internal spin state using an rf pulse. This technique has already been used in our group to produce three component gases [Ott08]. Theses systems are not stable in a bulk gas. However, in a lattice this system is predicted to be stable towards three-body loss due to the quantum Zeno effect [Kan09]. This effect prevents tunneling of a third fermion on a site already occupied by two other fermions and has been demonstrated for bosons [Sya08]. In our system, this would allow for studying three component physics, with BCS pairing and atomic color superfluity [Kan09, Pri11].

After studying the above mentioned systems, we plan to implement a spatial light modulator (SLM) together with a high resolution objective (see figure 8.2). This is currently being tested in an external setup [Kri13, Hol14]. The objective is designed for 671 nm and 1064 nm light and thus would not only allow to project nearly arbitrary potentials onto our 2D confinement, but also offers the possibility of high resolution imaging. This upgrade will allow us to probe the transition from microscopic to mesoscopic physics in lattices. Alternatively, also different potentials, like a box potential or more complicated lattice geometries could be realized. The combination of a larger lattice spacing of roughly 1 μm for potentials created with the SLM together with the high resolution objective should allow to perform single site resolved imaging.

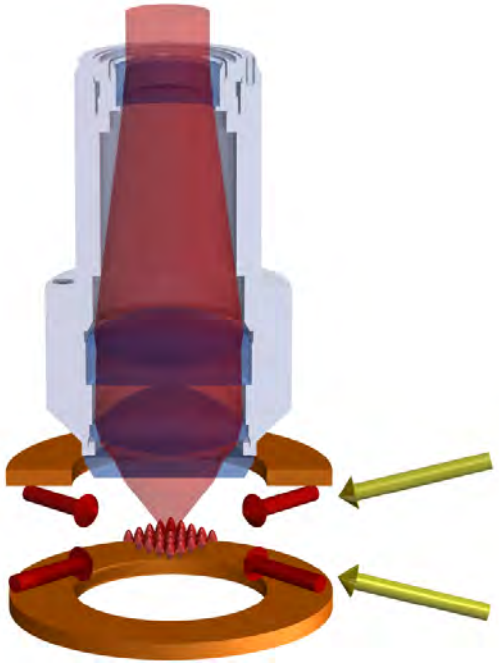

Figure 8.2: Illustration of the high resolution objective together with the Feshbach coils (brown), lattice beams (red) and SWT beams (yellow). The objective is designed for 671 nm and 1064 nm light. Thus it can not only be used for high resolution imaging, but also, together with a spatial light modulator, to project arbitrary potentials onto the 2D confinement of the SWT. Taken from [Rie10].

Bibliography

[Ash76] N. Ashcroft, N. Mermin, *Solid state physics*, Science: Physics (Saunders College, 1976).

[Bec13] J. H. Becher, *A two dimensional optical lattice for ultracold fermions*, bachelor thesis (2013).

[Blo08] I. Bloch, J. Dalibard, W. Zwerger, *Many-body physics with ultracold gases*, Rev. Mod. Phys. **80**(3) (Jul 2008).

[Boe37] J. H. de Boer, E. J. Verwey, *Semi-conductors with partially and with completely filled 3d-lattice bands*, Proceedings of the Physical Society **49**(4S), 59 (1937).

[Boh12] A. Bohn, *Towards an ultracold three-component Fermi Gas in a two-dimensional optical lattice*, Diploma thesis (2012).

[Bou03] T. Bourdel, J. Cubizolles, L. Khaykovich, K. Magalhaes, S. Kokkelmans, G. V. Shlyapnikov, C. Salomon, *Measurement of the Interaction Energy near a Feshbach Resonance in a L i 6 Fermi Gas*, Physical review letters **91**(2), 020402 (2003).

[Bus98] T. Busch, B.-G. Englert, K. Rzażewski, M. Wilkens, *Two cold atoms in a harmonic trap*, Foundations of Physics **28**(4), 549–559 (1998).

[Chi06] J. K. Chin, D. Miller, Y. Liu, C. Stan, W. Setiawan, C. Sanner, K. Xu, W. Ketterle, *Evidence for superfluidity of ultracold fermions in an optical lattice*, Nature **443**(7114), 961–964 (2006).

[Chi10] C. Chin, R. Grimm, P. Julienne, E. Tiesinga, *Feshbach resonances in ultracold gases*, Reviews of Modern Physics **82**(2), 1225 (2010).

[Dal99] J. Dalibard, *Collisional dynamics of ultra-cold atomic gases*, in *Proceedings of the International School of Physics-Enrico Fermi*, Vol. 321 (1999).

[Day05] A. J. Dayle, *Manipulation and Simulation of Cold Atoms in Optical Lattices*, Dissertation, Leopold-Franzens-Universität Innsbruck (2005).

[DeM99] B. DeMarco, D. S. Jin, *Onset of Fermi degeneracy in a trapped atomic gas*, Science **285**(5434), 1703–1706 (1999).

[Dol15] M. Dolfi, A. Kantian, B. Bauer, M. Troyer, *Minimizing nonadiabaticities in optical-lattice loading*, Physical Review A **91**(3), 033407 (2015).

[Foo04] C. J. Foot, *Atomic physics* (Oxford University Press, 2004).

[Fre01] D. L. Freimund, K. Aflatooni, H. Batelaan, *Observation of the Kapitza–Dirac effect*, Nature **413** (2001).

[Fre02] D. L. Freimund, H. Batelaan, *Bragg scattering of free electrons using the Kapitza-Dirac effect*, Physical review letters **89**(28), 283602 (2002).

[Gad09] B. Gadway, D. Pertot, R. Reimann, M. G. Cohen, D. Schneble, *Analysis of Kapitza-Dirac diffraction patterns beyond the Raman-Nath regime*, Optics Express **17**(21), 19173 (2009).

[Geh98] M. Gehm, K. O'hara, T. Savard, J. Thomas, *Dynamics of noise-induced heating in atom traps*, Physical Review A **58**(5), 3914 (1998).

[Geh03] M. Gehm, *Properties of* ^{6}*Lithium* (2003).

[Gem09] N. Gemelke, X. Zhang, C.-L. Hung, C. Chin, *In situ observation of incompressible Mott-insulating domains in ultracold atomic gases*, Nature **460**(7258), 995–998 (2009).

[Gou86] P. L. Gould, G. A. Ruff, D. E. Pritchard, *Diffraction of atoms by light: The near-resonant Kapitza-Dirac effect*, Physical Review Letters **56**(8), 827–830 (Feb 1986).

[Gre01] M. Greiner, I. Bloch, O. Mandel, T. W. Hänsch, T. Esslinger, *Exploring phase coherence in a 2D lattice of Bose-Einstein condensates*, Physical Review Letters **87**(16), 160405 (2001).

[Gre03] M. Greiner, C. A. Regal, D. S. Jin, *Emergence of a molecular Bose–Einstein condensate from a Fermi gas*, Nature **426**(6966), 537–540 (2003).

[Gre13] D. Greif, T. Uehlinger, G. Jotzu, L. Tarruell, T. Esslinger, *Short-range quantum magnetism of ultracold fermions in an optical lattice*, Science **340**(6138), 1307–1310 (2013).

[Gri00] R. Grimm, M. Weidemüller, Y. B. Ovchinnikov, *Optical dipole traps for neutral atoms*, Advances in Atomic, Molecular and Optical Physics (2000).

[Gün07] K. J. Günter, *Interacting Fermi gases and Bose-Fermi mixtures in optical lattices*, Dissertation, Swiss Federal Institute of Technology (2007).

[Har15] R. A. Hart, P. M. Duarte, T.-L. Yang, X. Liu, T. Paiva, E. Khatami, R. T. Scalettar, N. Trivedi, D. A. Huse, R. G. Hulet, *Observation of antiferromagnetic correlations in the Hubbard model with ultracold atoms*, Nature **519**(7542), 211–214 (2015).

[Heu11] S. Heupts, *A new radio frequency setup to manipulate spin mixtures of fermionic atoms*, Bachelor thesis (2011).

[Hol14] M. Holten, *Hamiltonian Engineering in Ultracold Atom Experiments using a Spatial Light Modulator*, bachelor thesis (2014).

[Idz06] Z. Idziaszek, T. Calarco, *Analytical solutions for the dynamics of two trapped interacting ultracold atoms*, Physical Review A **74**(2), 022712 (2006).

[Ino98] S. Inouye, M. Andrews, J. Stenger, H.-J. Miesner, D. Stamper-Kurn, W. Ketterle, *Observation of Feshbach resonances in a Bose–Einstein condensate*, Nature **392**(6672), 151–154 (1998).

[Jak99] D. Jaksch, *Bose-Einstein Condensation and Applications*, Dissertation, Leopold-Franzens-Universität Innsbruck (1999).

[Joc03] S. Jochim, M. Bartenstein, A. Altmeyer, G. Hendl, S. Riedl, C. Chin, J. H. Denschlag, R. Grimm, *Bose-Einstein condensation of molecules*, Science **302**(5653), 2101–2103 (2003).

[Jör08] R. Jördens, N. Strohmaier, K. Günter, H. Moritz, T. Esslinger, *A Mott insulator of fermionic atoms in an optical lattice*, Nature **455**(7210), 204–207 (2008).

[Kan09] A. Kantian, M. Dalmonte, S. Diehl, W. Hofstetter, P. Zoller, A. Daley, *Atomic color superfluid via three-body loss*, Physical review letters **103**(24), 240401 (2009).

[Kap33] P. L. Kapitza, P. A. M. Dirac, *The reflection of electrons from standing light waves*, Proceedings of the Cambridge Philosophical Society **29**, 297 (1933).

[Kas95] A. Kastberg, W. D. Phillips, S. Rolston, R. Spreeuw, P. Jessen, *Adiabatic cooling of cesium to 700 nK in an optical lattice*, Physical review letters **74**(9), 1542 (1995).

[Ket08] W. Ketterle, M. W. Zwierlein, *Making, probing and understanding ultracold Fermi gases*, arXiv preprint arXiv:0801.2500 (2008).

[Ket09] W. Ketterle, D. S. Durfee, D. M. Stamper-Kurn, *Making, probing and understanding Bose-Einstein condensates* (2009).

[Köh05] M. Köhl, H. Moritz, T. Stöferle, K. Günter, T. Esslinger, *Fermionic atoms in a three dimensional optical lattice: Observing Fermi surfaces, dynamics, and interactions*, Physical review letters **94**(8), 080403 (2005).

[Kri13] S. Krippendorf, *An optical setup for high-resolution imaging and manipulating of ultracold atoms*, bachelor thesis (2013).

[Lew12] A. . A. V. Lewenstein, Maciej ; Sanpera Trigueros, *Ultracold atoms in optical lattices : simulating quantum many-body systems* (Oxford Univ. Press, Oxford, 2012).

[Lom08] T. Lompe, *An apparatus for the production of molecular Bose-Einstein condensates*, Diploma thesis (2008).

[Mot37] N. Mott, R. Peierls, *Discussion of the paper by de Boer and Verwey*, Proceedings of the Physical Society **49**(4S), 72 (1937).

[Mot49] N. F. Mott, *The basis of the electron theory of metals, with special reference to the transition metals*, Proceedings of the Physical Society. Section A **62**(7), 416 (1949).

[Mur14] P. A. Murthy, D. Kedar, T. Lompe, M. Neidig, M. G. Ries, A. N. Wenz, G. Zürn, S. Jochim, *Matter-wave Fourier optics with a strongly interacting two-dimensional Fermi gas*, Phys. Rev. A **90** (2014).

[Mur15] P. Murthy, I. Boettcher, L. Bayha, M. Holzmann, D. Kedar, M. Neidig, M. Ries, A. Wenz, G. Zürn, S. Jochim, *Observation of the Berezinskii-Kosterlitz-Thouless phase transition in an ultracold Fermi gas*, arXiv preprint arXiv:1505.02123 (2015).

[Nat12] S. S. Natu, D. C. McKay, B. DeMarco, E. J. Mueller, *Evolution of condensate fraction during rapid lattice ramps*, Physical Review A **85**(6), 061601 (2012).

[Nei13] M. Neidig, *A realization of a two-dimensional Fermi gas in a standing wave trap*, Diploma thesis (2013).

[Ock10] C. F. Ockeloen, A. F. Tauschinsky, R. J. C. Spreeuw, S. Whitlock, *Detection of small atom numbers through image processing*, Phys. Rev. A **82**(6) (Dec 2010).

[Ott08] T. B. Ottenstein, T. Lompe, M. Kohnen, A. Wenz, S. Jochim, *Collisional stability of a three-component degenerate Fermi gas*, Physical review letters **101**(20), 203202 (2008).

[Pet04] D. Petrov, C. Salomon, G. V. Shlyapnikov, *Weakly bound dimers of fermionic atoms*, Physical review letters **93**(9), 090404 (2004).

[Pit03] L. P. Pitaevskii, S. Stringari, *Bose-Einstein condensation*, No. 116 (Oxford University Press, 2003).

[Pri11] A. Privitera, I. Titvinidze, S.-Y. Chang, S. Diehl, A. J. Daley, W. Hofstetter, *Loss-induced phase separation and pairing for three-species atomic lattice fermions*, Physical Review A **84**(2), 021601 (2011).

[Rie10] M. Ries, *A magneto-optical trap for the preparation of a three-component Fermi gas in an optical lattice*, Diploma thesis (2010).

[Rie14] M. Ries, *A Two-Dimensional Fermi Gas in the BEC-BCS Crossover*, Dissertation (2014).

[Rie15] M. Ries, A. Wenz, G. Zürn, L. Bayha, I. Boettcher, D. Kedar, P. Murthy, M. Neidig, T. Lompe, S. Jochim, *Observation of Pair Condensation in the Quasi-2D BEC-BCS Crossover*, Physical Review Letters **114**(23), 230401 (2015).

[Sak94] J. J. Sakurai, *San Fu Tuan, Modern Quantum Mechanics* (Reading, Mass.: Addison-Wesley Pub. Co, 1994).

[Sch08] U. Schneider, L. Hackermüller, S. Will, T. Best, I. Bloch, T. Costi, R. Helmes, D. Rasch, A. Rosch, *Metallic and insulating phases of repulsively interacting fermions in a 3D optical lattice*, Science **322**(5907), 1520–1525 (2008).

[Sim10] P. Simon, *Apparatus for the preparation of ultracold Fermi gases*, Diploma thesis (2010).

[Sya08] N. Syassen, D. M. Bauer, M. Lettner, T. Volz, D. Dietze, J. J. Garcia-Ripoll, J. I. Cirac, G. Rempe, S. Dürr, *Strong dissipation inhibits losses and induces correlations in cold molecular gases*, Science **320**(5881), 1329–1331 (2008).

[Wan37] G. H. Wannier, *The structure of electronic excitation levels in insulating crystals*, Physical Review **52**(3), 191 (1937).

[Wei09] M. Weidemüller, C. Zimmermann, *Cold atoms and molecules* (2009).

[Wen08] A. N. Wenz, *Few-Body Physics in a Three-Component Fermi Gas*, Diploma thesis (2008).

[Wen13] A. Wenz, *From Few to Many: Ultracold Atoms in Reduced Dimensions*, Dissertation (2013).

[Wes04] S. Wessel, F. Alet, M. Troyer, G. G. Batrouni, *Quantum Monte Carlo simulations of confined bosonic atoms in optical lattices*, Phys. Rev. A **70**(5) (Nov 2004).

[Zha07] H. Zhai, T.-L. Ho, *Superfluid-insulator transition of strongly interacting fermi gases in optical lattices*, Physical review letters **99**(10), 100402 (2007).

[Zür12] G. Zürn, T. Lompe, A. N. Wenz, S. Jochim, P. S. Julienne, J. M. Hutson, *Precise characterization of ^{6}Li Feshbach resonances using trap-sideband resolved RF spectroscopy of weakly bound molecules*, Phys. Rev. Lett. (2012).

[Zwe03] W. Zwerger, *Mott-Hubbard transition of cold atoms in optical lattices*, Journal of Optics B: Quantum and Semiclassical Optics **5**(2) (2003).

[Zwi03] M. W. Zwierlein, C. A. Stan, C. H. Schunck, S. M. Raupach, S. Gupta, Z. Hadzibabic, W. Ketterle, *Observation of Bose-Einstein condensation of molecules*, Physical Review Letters **91**(25), 250401 (2003).

[Zwi05] M. W. Zwierlein, J. R. Abo-Shaeer, A. Schirotzek, C. H. Schunck, W. Ketterle, *Vortices and superfluidity in a strongly interacting Fermi gas*, Nature **435**(7045), 1047–1051 (2005).

Danksagung

Hier möchte ich mich bei allen bedanken, die diese Arbeit möglich gemacht haben:

Zuerst bei Selim, dass er mich in seine Gruppe aufgenommen hat und ür die gute Betreuung während des Jahres.

Bei der ganzen Ultracold Gruppe für die Zeit im Labor, beim Mittagessen, Kickern und all den anderen gemeinsamen Aktivitäten. Besonderer Dank geht an alle, die dieser Arbeit Korrektur gelesen haben und die Rechtschreibfehler beseitigt haben.

Bei Prof. Dr. Markus Oberthaler für die Übernahme der Zweitkorrektur dieser Arbeit.

Auch vielen Dank an all meine Freunde, meine Familie und Caro für die tollen Zeit und die gemeinsamen Aktivitäten während der letzten 25 Jahre.

Erklärung

Ich versichere, dass ich diese Arbeit selbstständig verfasst und keine anderen als die angegebenen Quellen und Hilfsmittel benutzt habe.

Heidelberg, den 09.07.2015

.....
(Unterschrift)